Characterizing the Performance of a New Infiltrometer and Hydraulic Properties of Roadside Swales

A Dissertation

SUBMITTED TO THE FACULTY OF

UNIVERSITY OF MINNESOTA

BY

Farzana Ahmed

IN PARTIAL FULFILLMENT OF THE REQUIREMENTS

FOR THE DEGREE OF

DOCTOR OF PHILOSOPHY

Dr. John S. Gulliver and Dr. John L. Nieber

September, 2014

Acknowledgements

I would like to thank the three funding agency of this research project: Minnesota Pollution Control Agency (MPCA), Minnesota Department of Transportation (MnDOT), Minnesota Local Road Research Board (LRRB) for their monetary support. Guidance on this project from experienced technical advisory panel (TAP) members is greatly appreciated.

A special thanks to my advisors John Gulliver and John Nieber for their technical counsel, for their thoughts and comments on the earlier draft of this thesis, Ray Hozalski and Bruce Wilson for serving in my final defense committee and Kimberly Hill for serving in my preliminary oral exam committee. Without their many revisions this thesis would not be in its current form. I am also grateful to Bruce Wilson for his valuable suggestions in the statistical analysis of my data. I am greatly thankful to the members of the project research team including Graduate students Nick Olson, undergraduate student Anne Haws, Anthony Vecchi, Bradley Weiss, John Farmer, Lanre Adekola and Ugonna Ojiaku. The undergraduate researchers helped to take around 800 infiltration measurements in the field and they did soil texture analysis of around 120 samples in the lab. I am grateful for all the hours they put into this project. I am also grateful to St. Anthony Fall laboratory for their facilities provided during my field work and for their technical support.

Dedication

I would like to dedicate my thesis to my husband, Shafayat; my daughter Nabiha; my parents and my in laws for supporting and encouraging in pursuing a higher level degree.

ABSTRACT

A roadside swale is an infiltration practice that removes water during rainfall-runoff, infiltrate water into the soil and filter the soil and associate pollutant from the water. Infiltration rate is an important factor affecting the performance of a swale. Though roadside swales convey and treat road runoff, data on the performance of swales with regards to infiltration is relatively sparse. Therefore, the objective of this study is to, 1) Modify the optimization technique of the new Modified Philip Dunne (MPD) infiltrometer, 2) Verify the results obtained from this MPD infiltrometer for uniform soil, layered soil and uniform soil with macopores by numerical simulation, 3) Utilize the MPD infiltrometer to characterize the field-saturated hydraulic conductivity (K_{fs}) of five roadside swales located in Twin-Cities, MN and one swale located in Madison, WI and 4) Analyze the derived results obtained from the measurements taken by the MPD infiltrometer. From numerical simulations it was found that MPD Infiltrometer overestimates K_{fs} value by 10 to 36% for the uniform soil, 12% to 63% for layered soil and 4% to 29% for uniform soil containing macropores.

MPD infiltrometer allows collecting multiple infiltration measurements simultaneously to capture the spatial variation of infiltration rate of an infiltration practice. In this study a total of 720 infiltration measurements were collected in swales located in Twin-Cities, MN and in Madison, WI. Statistical analysis was performed on the K_{fs} values to analyze the effect of initial soil moisture content, season, soil texture class and distance in downstream direction on the geometric mean K_{fs} value of a swale. Because of high spatial

variation of K_{fs} value in the same swale no effect of initial soil moisture content, season and soil texture class was observed on the geometric mean K_{fs} value. But the distance in downstream direction may have positive or negative effect on the K_{fs} value.

Table of Contents

List of Tables

List of Figures

1. Overview

This thesis is based on a collaborative project funded by Minnesota Pollution Control Agency (MPCA), Minnesota Department of Transportation (MnDOT) and the Local Road Research Board (LRRB) to develop a method to measure the infiltration rate of roadside swales and to analyze the data. The title of the project funded by MPCA is "Performance of Low Impact Development Practices on Stormwater Pollutant Load Abatement" and the title of the project funded by MnDOT and LRRB is "Assessing and Improving Pollution Prevention by Swales". The principal investigators (PIs) from the University of Minnesota were Dr. John S. Gulliver from the Department of Civil Engineering, and Dr. John L. Nieber from the Department of Bioproducts and Biosystems Engineering.

The field-saturated hydraulic conductivity (K_{fs}) of the media in infiltration practice can vary spatially, up to two orders of magnitude (*Asleson, et al. 2009; Olsen et al. 2013*). Thus, a large number of measurements are required to capture the spatial variability of K_{fs} and to determine a representative infiltration capacity. A new infiltrometer, the Modified Philip Dunne (MPD) infiltrometer has been developed which requires a lower amount of water, is relatively easy to set up and a single practitioner can collect the measurements simultaneously at multiple locations. However, The MPD Infiltrometer analysis based on the Green-Ampt assumptions assumes that the soil is homogeneous and macropore free, and a spherical wetting front is developed due to infiltration. But in reality soil is usually non-homogeneous (layered soil or soil with macropores) in the field and can develop a non-spherical wetting front. In a fully developed soil profile, top soil often has a loose

texture containing macropores, cracks and preferential paths which can also lead to develop a non-spherical wetting front. Therefore one would expect some inaccuracy in the prediction of the true field saturated hydraulic conductivity of the soil. Therefore, the first two objectives of this study are to, 1) Modify the optimization technique of the new Modified Philip Dunne (MPD) infiltrometer, 2) Verify the results obtained from this MPD infiltrometer for uniform soil, layered soil and uniform soil with macopores by numerical simulation.

The other objective of this study relates to the characterization of the hydraulic properties of roadside swales. A roadside swale is an infiltration practice that removes water during rainfall-runoff, infiltrate water into the soil and filter the soil and associate pollutant from the water. Infiltration rate is an important factor affecting the performance of a swale. Though roadside swales convey and treat road runoff, data on the performance of swales with regards to infiltration is relatively sparse. So the third and fourth objectives of this study are to 3) Utilize the MPD infiltrometer to characterize the infiltration rate of five roadside swales located in Twin-Cities, MN and one swale located in Madison, WI and 4) Analyze the derived results obtained from the measurements taken by the MPD infiltrometer.

The first manuscript (chapter 2) has been accepted by Vadose Zone Journal. The main component of this manuscript include the background and theory behind the MPD infiltrometer, The modification of the optimization technique of MPD infiltrometer analysis, the verification of the MPD analysis with the numerical simulation of Richards' equation for uniform soil and with falling head lab test, analysis on the shape of the

wetting front for different soil type and the outlier removal of lab data. Rebecca Nestingen was responsible for the background and theory of the infiltrometer, as well as the falling head lab tests. My responsibility was the remainder of the chapter.

The second manuscript (chapter 3) has been prepared for submission to Vadose Zone Journal, and is a continuation of the first manuscript. The main component of this manuscript include the verification of the MPD analysis with the numerical simulation of Richards' equation for layered soil and uniform soil containing macropore, analysis on the shape of the wetting front for uniform soil containing macropore and a discussion about how stratification or presence of macropore effect soil hydraulic property based on the moisture content distribution in the soil matrix of the numerical simulations.

The third manuscript (chapter 4) has been prepared for submission to the Water Resources Research Journal. This manuscript depicts how the MPD infiltrometer was utilized in roadside swales to characterize the infiltration rate which include site selection criteria and procedure, infiltration measurement method, uncertainty analysis and analysis of the data obtained from MPD analysis to observe the effect of initial soil moisture content, season, soil texture class and distance from downstream on the soil hydraulic property of swales.

2. A Modified Philip-Dunne Infiltrometer for Measuring the Field-Saturated Hydraulic Conductivity of Surface Soil

F. Ahmed, Department of Civil, Environmental and Geo-Engineering, University of Minnesota, Minneapolis, MN 55414; R. Nestingen, Short Eliott Hendrickson, Inc, 3535 Vadnais Center Drive, St. Paul, MN 55110; J. L. Nieber, Department of Bioproduct and Biosystem Engineering, University of Minnesota, St. Paul, MN 55108**;** J. S. Gulliver, Department of Civil, Environmental and Geo-Engineering, University of Minnesota, Minneapolis, MN 55414; R. M. Hozalski, Department of Civil, Environmental and Geo-Engineering, University of Minnesota, Minneapolis, MN 55414

EXECUTIVE SUMMARY

There is a current and expanding need to measure surface infiltration rate parameters for stormwater infiltration practices used to mitigate the detrimental effects of land development activities on watershed hydrology. Herein, we discuss the development of a falling-head soil surface infiltrometer, termed the Modified Philip-Dunne (MPD) infiltrometer that is inexpensive to construct, easy to use, and requires minimal water volume per test. Because of these characteristics, many MPD devices can be deployed simultaneously to obtain infiltration rate data at multiple locations within a given infiltration practice. Green-Ampt theory was used to derive the expressions needed for analyzing the falling head data to solve for the field-saturated hydraulic conductivity (K_{fs}) and Green-Ampt wetting front suction (ψ). The accuracy of the analysis was determined using numerical experiments in which falling head data were generated from

a computational solution of the axisymmetric form of the three-dimensional Richards' equation for homogeneous and isotropic porous media with specified input parameters. The falling head data were then analyzed using a quasi-analytical procedure and the resulting values of K_{fs} and ψ were compared with the input values. The accuracy of the K_{fs} and ψ derived from data acquired using the MPD device was then assessed using physical experiments involving three large barrels packed with different types of sand. The K_{fs} values obtained for the media in the barrels using an MPD infiltrometer were, on average, 82 % of the values obtained from whole barrel falling head tests. The resulting uncertainty in field-saturated hydraulic conductivity values from the MPD infiltrometer is considered to be small compared to the orders of magnitude of variability commonly observed for K_{fs} values in the field.

Key words: Infiltration, Stormwater, Rain garden, Field-Saturate Hydraulic Conductivity, Infiltrometer, van Genuchten parameters, Green-Ampt model, Falling head method.

INTRODUCTION

Infiltration basins, rain gardens, swales, and other infiltration practices are stormwater control measures that reduce runoff volume through means of infiltration and evapotranspiration; of which infiltration is the most significant. If infiltration is not occurring at a sufficient rate, the capacity to reduce runoff volume is decreased, potentially leading to increased pollutant discharge, increased degradation of stream channels, and increased potential for flooding of downstream areas. The surfaces of

infiltration practices are prone to compaction (*Olson et al., 2013*) due to foot and equipment traffic as well as clogging from the fine particles typically transported in stormwater runoff. To evaluate the impacts of compaction and particle accumulation, it is important to measure the field-saturated hydraulic conductivity of the media at the surface since it is the main determinant of infiltration capacity of a particular soil.

Field-saturated hydraulic conductivity (K_{fs}) is the most important soil property that controls water infiltration and consequently surface runoff. Methods to determine this soil property can be placed into two main categories, one using methods based on steady-state infiltration, and the other using methods based on unsteady infiltration. Within these categories there are subcategories that relate to the type of geometric and pressure boundary conditions imposed. The common types of geometries include boreholes, surface disks and surface rings. Pressures applied at the soil boundary can be positive, zero, or negative. Of interest in this manuscript is a type of measurement that will yield the hydraulic properties of the soil surface. For this several methods have been developed, with water application geometries that include disk infiltrometers, single ring infiltrometers or double ring infiltrometers (*ASTM, 2003*), applied for steady-state flow or for unsteady flow (*Parr and Bertrand, 1960; Reynolds and Elrick, 1990; Bagarello et al., 2004; Lassabatere et al. 2006; Reynolds, 2008; Nimmo et al., 2009*).

It has been found that, for both field soils and for infiltration practices, the field-saturated hydraulic conductivity of the media can vary spatially, up to two orders of magnitude (*Asleson, et al. 2009; Olsen et al. 2013*). To capture the spatial variability of K_{fs} and to determine a representative infiltration capacity, a large number of measurements are

required to represent field conditions. This situation calls for measurement methods that are quick, require the least amount of water, and relatively easy to set up. To meet time constraints on projects it is also desirable if the measurements can be made simultaneously at multiple sites by a single practitioner. This almost certainly requires that the methods involve measurement of short term unsteady infiltration. To meet this data collection requirement for our own needs of data collection, we developed and tested a modified version of the Philip-Dunne borehole permeameter (referred to as the Modified Philip-Dunne infiltrometer or MPD infiltrometer). The device is simple, inexpensive to construct, and has low water volume requirements per test; hence, twenty or more devices can be deployed to measure the soil hydraulic parameters at as many different locations simultaneously. The MPD Infiltrometer requires ~0.003 m^3 of water per test while the most commonly used device, the double ring infiltrometer, requires ~0.028 m^3 of water (*Ahmed et al., 2011*).

The falling-head Philip-Dunne permeameter is inserted into a borehole to a given depth and is used to obtain the field-saturated hydraulic conductivity (K_{fs}) and Green-Ampt wetting front suction (ψ) of the soil at that depth. It cannot be used to measure K_{fs} and ψ at the soil surface of an infiltration practices. In contrast, the MPD infiltrometer is not inserted into a borehole, but is driven into the soil surface to a specified depth without removing any soil. Because this modification changes the boundary conditions applied to the infiltrating flow, compared to the conditions associated with the Philip-Dunne borehole permeameter, it is not possible to use the approximate borehole infiltration analysis of *Philip (1993)* to derive the hydraulic properties of the soil. Philip's analysis,

however, can be modified to arrive at a similar approach for analyzing the head versus time data collected from the MPD infiltrometer.

Three fairly recent publications that describe alternative approaches to the one we present in this paper are those by *Bagarello et al. (2004), Lassabatere et al. (2006), and Nimmo et al. (2009).* The approach by *Bagarello et al.* applies the one-dimensional Green-Ampt formulation of *Philip (1992)* to analyze infiltration into an inserted ring infiltrometer. The approach by *Lassabatere et al*. fits a two-term infiltration formula to cumulative infiltration measurements to derive soil hydraulic property scale parameters and also a pedo-transfer function approach with particle size distribution to derive shape parameters to describe the porous media water retention and unsaturated hydraulic conductivity functions. The approach by *Nimmo et al.* uses a single ring infiltrometer inserted into the soil and measures the time required for ponded water to infiltrate into the soil. The data analysis with this approach involves a single simple formula for field-saturated hydraulic conductivity. The formula contains a capillarity parameter, but this is assumed to be known or can be estimated for a particular soil type. Of these three methods the one by Nimmo et al. appears to be the closest, in terms of simplicity and ease of use, to the MPD presented in this paper.

In this paper the accuracy of the MPD Infiltrometer, which is used to measure K_{fs} and ψ, was verified using numerical experiments and physical laboratory experiments.

THEORY

In our application the MPD infiltrometer is a 0.1 m diameter cylinder that is driven 0.05 m into the soil, although these dimensions are free to be selected by a user. The initial moisture content of the soil near the surface is measured, and this initial moisture content is assumed to represent the initial moisture content of the underlying soil profile. The infiltrometer is then filled with water to a specified level and the water level in the cylinder is monitored over time. The test continues until sufficient measurements of water surface elevation versus time have been taken to estimate K_{fs}, usually until the water has completely emptied out of the infiltrometer cylinder.

Philip's (1993) analysis is based on the assumptions of the Green-Ampt model. Thus he assumed the soil to be an isotropic and homogeneous porous medium, the wetting front to be sharp, and to represent the three-dimensional flow he assumed an ideal spherical geometry for the wetting front by considering symmetrical pressure-capillarity flow and superimposing a symmetrical gravity flow. He found that having spherical source geometry had little influence on estimates of K_{fs} and the ψ, which are of primary concern in our analysis.

A similar approach is taken for the analysis of the MPD infiltrometer. However, due to the application of the device at the surface rather than in a borehole, the no-flow boundary at the soil surface outside of the cylinder is taken into account by representing the wetted soil as a capped sphere as illustrated in Figure 2-1. In addition to modifying the geometry of flow, the pressure loss along the soil encased within the inserted portion of the device needs to be added into the analysis.

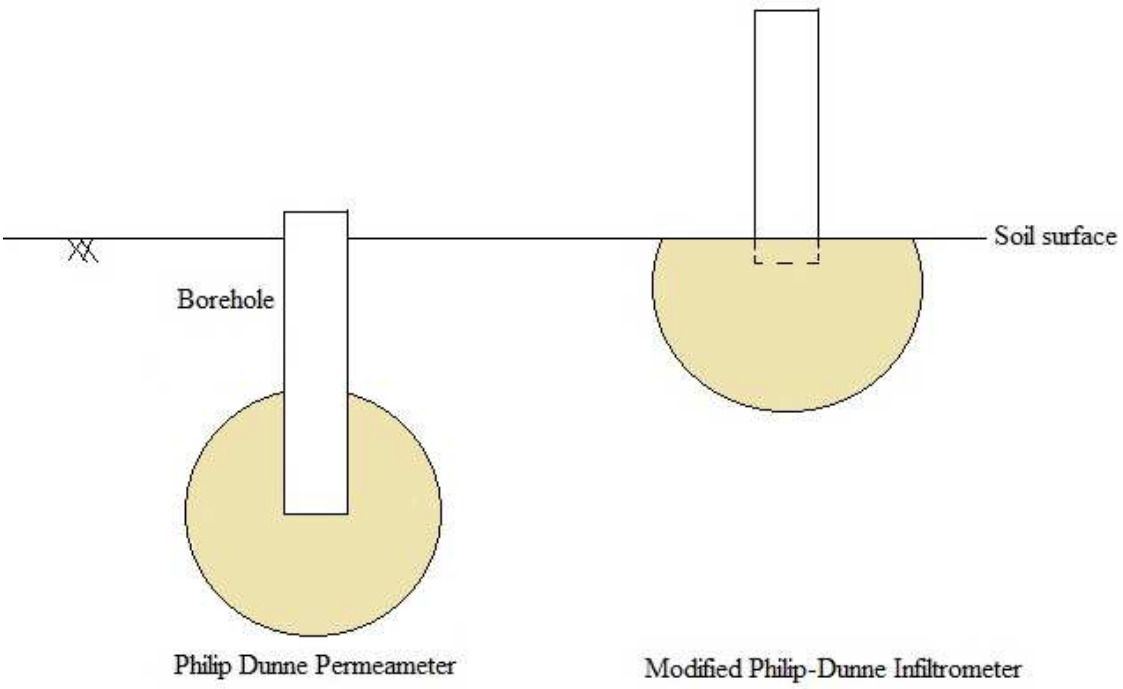

Figure 2-1: Comparison of assumed wetted cross-sections for the Philip-Dunne permeameter and the MPD infiltrometer

EQUATION MODIFICATIONS

The derivation of the governing equations for the MPD infiltrometer is based on the work of *Nestingen (2007)*. The notation used in the derivation is illustrated in Figure 2-2.

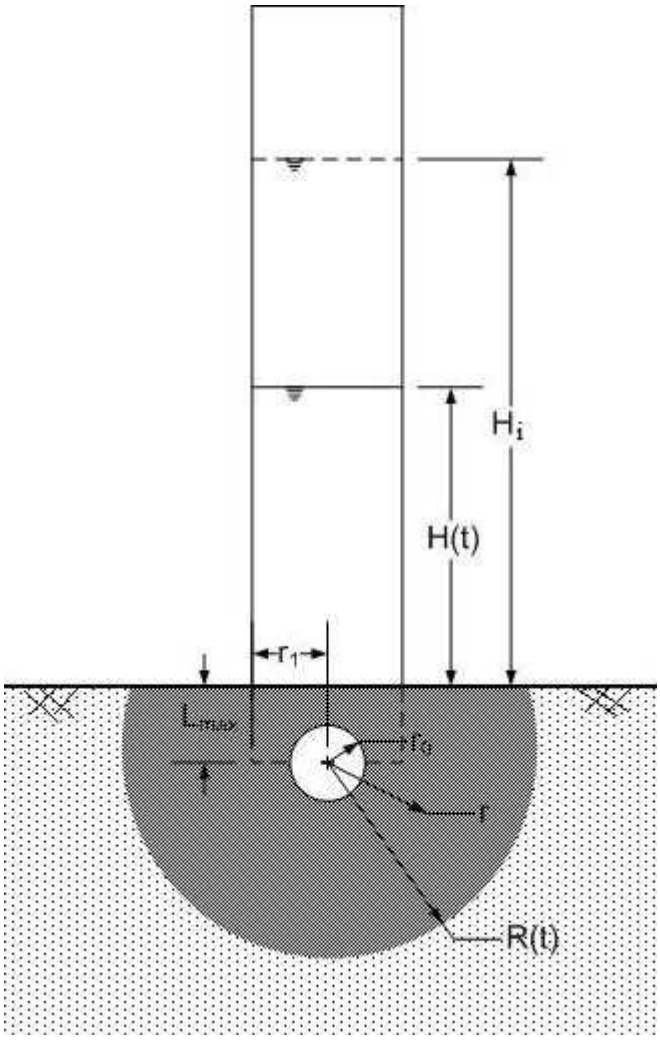

Figure 2-2: Important parameters of the Modified Philip-Dunne infiltrometer. H_i is the initial height of water, $H(t)$ is the height of water at time t, L_{max} is the depth of insertion into the soil, r_0 is the equivalent source radius, r_1 is the radius of the cylinder, r is any radius within the wetted front and $R(t)$ is the radius to the sharp wetted front at time t.

Using similar assumptions as *Philip (1993)*, the equation for cumulative infiltration $i(t)$, is expressed by an equation using the geometry of the wetting front, which is a capped sphere with a radius of $R(t)$ and centroid at a vertical distance of $L_{\max}$ from the soil surface at the center of the cylinder $R(t)+L_{\max}$. The soil within the capped sphere has an

initial and field saturated moisture content of θ_i and θ_s, respectively. The total volume of the wetted soil matrix is calculated by subtracting the volume of the equivalent spherical source $\frac{4}{3}\pi r_o^3$, where $r_o = \frac{r_1}{2}$ is the radius of equivalent spherical source, from the volume of the capped sphere defined by the advancing wetting front. The volume of the capped sphere bounded by the wetting front is $\frac{\pi}{3}\{R(t)+L_{\max}\}^2\left\{3R^2(t)-\left(R(t)+L_{\max}\right)\right\}$, where $R(t)$ is the sphere radius to the wetting front and $L_{\max}$ is the distance that the infiltrometer penetrates the soil. Thus the equation for temporal cumulative infiltration is:

$$i(t) = \frac{\pi}{3}\left(\theta_s - \theta_i\right)\left\{2R^3(t) + 3R^2(t)L_{\max} - L_{\max}^3 - 4r_o^3\right\} \qquad (1)$$

A mass balance on the water remaining in the infiltrometer and the water that has infiltrated into the soil at a given time is used to compute $R(t)$ as a function of $H(t)$ for use in the analysis, replacing $i(t)$ by $\left(H_i - H(t)\right)\pi r_1^2$ where H_i is the initial height and $H(t)$ is the depth of water in the cylinder above the soil surface over time. With this we can now write equation (1) as follows to establish a relation between $H(t)$ and $R(t)$:

$$\left(H_i - H(t)\right)\pi r_1^2 = \frac{\pi}{3}\left(\theta_s - \theta_i\right)\left\{2R^3(t) + 3R^2(t)L_{\max} - L_{\max}^3 - 4r_o^3\right\} \qquad (2)$$

Equations (1) and (2) are applicable only after $R(t)$ is greater than the value $\sqrt{r_1^2 + L_{\max}^2}$. The head versus time data before the wetted zone reaches this minimal radius are neglected from the analysis because this is a point where the geometric shape for the problem becomes constant for the remainder of the experiment. Up to that point the geometry changes from one-dimensional flow along the encased cylinder of soil, and

then to a sphere that grows until the top part of the sphere intersects with the soil surface and the geometry becomes that of a capped sphere. It would be possible to account for these intermediate changing geometries within the analysis if the equation set were expanded, but for the present the analysis we limit ourselves to the formulation using equation (2).

Following the analysis procedure as *Philip (1993)*, which involves differentiating equation (2) with respect to time, then separating the velocity into two components, a pressure-capillary driven flow and a gravity driven flow, the pressure-capillary flow velocity component, $v_c(r)$ at r between r_o and $R(t)$ becomes

$$v_c(r) = v_{c_o}\left[\frac{2r_o^2}{r^2 + rL_{\max}}\right] = \left[\left(\theta_s - \theta_i\right)\left(R^2(t) + R(t)L_{\max}\right)\frac{dR}{dt} - 2r_o^2 K_{fs}\right]\left[\frac{1}{r^2 + rL_{\max}}\right] \qquad (3)$$

where the gravity driven flow term is given by $2r_o^2 K_{fs}$. Applying Darcy's law, the pressure-capillarity potential drop, ΔP, from the spherical source to the wetted front is given by $\Delta P = \beta \int_{r_o}^{R(t)} \frac{v_c(r)}{K_{fs}} dr$, which can be evaluated to give

$$\Delta P = \beta \int_{r_o}^{R(t)} \frac{v_c(r)}{K_{fs}} dr = \beta\left\{\left(\theta_s - \theta_i\right)\frac{R^2(t) + R(t)L_{\max}}{K_{fs}}\frac{dR}{dt}B - G\right\} \qquad (4)$$

where: β is a coefficient that takes into account the hydraulic inefficiency of the actual flow path of infiltrated water into the soil, $B = \frac{1}{L_{\max}}\left\{\ln\frac{R(t)\left(r_o + L_{\max}\right)}{r_o\left(R(t) + L_{\max}\right)}\right\}$,

and $G = \left(2r_o^2 B\right)$ is the term arising from the gravity driven component of the flow. Through an exploratory analysis *Philip (1993)* estimated the β coefficient to be $\frac{\pi^2}{8}$, which will be used herein.

The use of the uppercase G for the gravity term follows from the analysis by *Reynolds (2011)*. As shown by Reynolds, at $t = 0$, for the Philip-Dunne borehole permeameter the gravity term is equal to zero, while at large time (if the volume of water in the permeameter tube is unlimited) the gravity term converges on r_o. For the MPD, the gravity term is zero at $t = 0$ while at large time the term converges on $\frac{2r_o^2}{L_{\max}} \ln\left(1 + \frac{L_{\max}}{r_o}\right)$.

To calculate the pressure $P_o(t)$, at the surface of the spherical source it is necessary to account for the pressure loss due to the flow in cylinder of soil encased within the infiltometer. This loss is represented with *Darcy's* law for which the flux along the cylinder of soil is

$$q = -K_{fs} \frac{d\Phi}{dz} = -K_{fs} \left[\frac{dP}{dz} + 1\right] \tag{5a}$$

where Φ is the total potential within the cylinder of soil, and z is the coordinate along the length of the cylinder, positive upward with the origin at the soil surface. This flux is also known from the rate of drop of water level in the infiltrometer reservoir, that is,

$$q = -\frac{dH(t)}{dt} \tag{5b}$$

Equating these two and integrating with z, the pressure at the spherical source is

$$P(t) = H(t) + L_{\max} - \frac{L_{\max}}{K_{fs}} \frac{dH(t)}{dt} \qquad (5c)$$

Equation (5c) is altered from Philip's analysis to account for the one-dimensional movement of water through the distance $L_{\max}$ of the MPD infiltrometer, and to account for the geometry of the capped sphere of wetted soil. The total pressure-capillarity potential drop from the spherical source to the wetted front can thus be described by the equation

$$\Delta P = \psi - H(t) - L_{\max} + \frac{L_{\max}}{K_{fs}} \frac{dH(t)}{dt} \qquad (6)$$

where: ψ is the Green-Ampt wetting front suction for the unsaturated soil. The Green-Ampt wetting front suction is defined as

$$\psi = \int_{h_i}^{0} \frac{K(h)}{K_{fs}} dh \qquad (7)$$

where, h_i is the initial pressure head and $K(h)$ is the unsaturated hydraulic conductivity which is a function of pressure head h.

By equating equations (4) and (6) we get the following two equations that can be used to simulate the temporal variations of ponding depth in the infiltrometer for a given combination of the infiltrometer geometry and soil properties (K_{fs} and ψ),

$$dH = \frac{K_{fs}}{L_{\max}} \left\{ \beta \left[\left(\theta_s - \theta_i \right) \frac{R^2(t) + R(t) L_{\max}}{K_{fs}} \frac{dR}{dt} B - G \right] - \psi + H(t) + L_{\max} \right\} dt \qquad (8)$$

$$dt = \frac{\beta\left(\theta_s - \theta_i\right)\dfrac{R^2(t) + R(t)L_{\max}}{K_{fs}L_{\max}}B \cdot dR - \dfrac{L_{\max}}{K_{fs}}\Delta H}{\psi - H(t) - L_{\max} + \beta\dfrac{2r_o^2}{L_{\max}}B} \tag{9}$$

Equations (8) and (9) are just different rearrangements of the equation resulting from equating equations (4) and (6), and each can be used in a numerical scheme to optimize for the K_{fs} and ψ given a time series of ponding depth measurements. Equations (8) and (9) are discretized in an implicit formulation along H and t, respectively, to facilitate the calculation of measurements of head at given times, or the calculation of time at given heads. The discretized forms of the equations are as follows:

$$H^n - H^{n-1} = \frac{K_{fs}}{L_{\max}}\left\{\beta\left[\left(\theta_s - \theta_i\right)\frac{\left(R^2(t)\right)^n + R^n(t)L_{\max}}{K_{fs}}\left(\frac{R^n - R^{n-1}}{\Delta t}\right)B^n - G\right] - \psi + H^{n-1} + L_{\max}\right\}\Delta t \tag{10}$$

$$t^n - t^{n-1} = \frac{\beta\left(\theta_s - \theta_i\right)\dfrac{\left(R^2(t)\right)^n + R^n(t)L_{\max}}{K_{fs}L_{\max}}B^n \cdot \left(R^n - R^{n-1}\right) - \dfrac{L_{\max}}{K_{fs}}\Delta H}{\psi - H^n - L_{\max} + \beta\dfrac{2r_o^2}{L_{\max}}B^n} \tag{11}$$

where n and $n-1$ represent the present and previous time step respectively, Δt is the time increment, and ΔH is the difference between the previous and present water level. In the computational procedure $R(t)$ in equation (10) and (11) is computed using equation (2) and the measured head in the infiltrometer versus time data. Equations (10) and (11) can each be applied to simulate observed time series of ponding depth vs. time data and do this in an iterative manner to find the optimum combination of K_{fs} and

ψ that yields the best agreement between the observed and simulated ponding depth time series.

The formulation leading to equations (8) and (9) are based on the approach presented by *Philip (1993)* in which it is assumed that the flow from the infiltrometer is driven by a combination of pressure (H) and capillarity (ψ), perturbed by a symmetric gravity flow. The symmetry of the gravity flow does not mean that the gravity component is zero. It is zero at the beginning but then approaches the full downward gravity flow described above ($2\beta r_o^2 \ln\left(1+\frac{L_{\max}}{r_o}\right)$). This type of behavior is well-known from infiltration theory (*Philip, 1969*). With that explanation we point out that *Cheng et al. (2011)* presented a formulation of the MPD, which they referred to as the Modified Nestingen (MN) method since they derived their analysis starting from the work of *Nestingen (2007)* for the MPD. In deriving their cumulative infiltration equation, they did not use the *Philip (1993)* formulation with the perturbed flow, but rather they accounted for gravity flow by adding constant flow given by $K_{fs}\left(t-t_o\right)$, where t_o is the time at which the wetting front reaches the base of the infiltrometer tube and the three-dimensional flow begins. The addition of this term is not consistent with the original *Philip (1993)* formulation based on the Green-Ampt equation. The effect of incorporating gravity in such an ad hoc manner on the accuracy of their resulting formulation remains to be determined. *Cheng et al.* also stated that the mass balance equation for the Nestingen formulation neglected the volume of water infiltrated into the encased cylindrical soil section, given by $L_{\max}\Delta\theta$. This claim is

not correct though because that volume of water is fully accounted in our equation for the capped sphere.

MATERIALS AND METHODS

To determine the accuracy of the derived equations for the MPD infiltrometer, falling head data were generated by solving the axisymmetric form of the Richards' equation for a series of simulated infiltration experiments for different soils. The MPD infiltrometer equations (2), (10) and (11) were then applied to estimate the hydraulic properties of the soils from the simulated falling head data. Comparison of the soil hydraulic parameters used in the Richards' equation simulations with the optimized parameters from the fitting with equations (2), (10) and (11) was then used to assess the accuracy of the MPD analysis. The validity of the MPD device and associated analysis was assessed using laboratory experiments involving three large barrels packed with different types of sand.

Numerical simulations

A numerical solution of the Richards' equation was used to provide the falling head data for evaluation of the analytical method described above. Because the hydraulic parameters are inputs to the numerical solution, one then has an exact way of assessing the accuracy of the approximate method. In this study, the Richards' equation was solved with the commercial finite element equation solver contained within the COMSOL Multiphysics software package *(COMSOL 2013)*. One comparison of the MPD with the Philip-Dunne borehole permeameter was conducted to illustrate some differences in

response between the two, but most of the analysis to follow focuses on the MPD configuration.

Boundary Conditions

Constraints on the solution of Richards' equation are the initial condition, which is initial pressure or initial saturation, and boundary conditions, either specified pressure or specified flux. For the borehole (Philip-Dunne borehole permeameter) domain illustrated in Figure 2-3a, the initial condition is one of uniform initial pressure, and the boundary conditions for the individual boundary segments are given by the following. AB: h =water depth(t) inside the permeameter; BC, CD: $\frac{\partial(h+z)}{\partial n}=0$; DE: h_i =initial soil water pressure; EF: $\frac{\partial(h+z)}{\partial n}=-1$; AF= $\frac{\partial(h+z)}{\partial r}=0$ due to axial symmetry, where **n** is the unit normal vector to the boundary, r and z represent radial and vertical direction respectively. For the infiltrometer (MPD infiltrometer) domain illustrated in Figure 2-3b the initial conditions are the same as for the borehole domain. The boundary conditions for the infiltrometer domain are the following. AB: h=water depth(t) inside the infiltrometer, BB" = B"C = CD: $\frac{\partial(h+z)}{\partial n}=0$; DE: h_i=initial soil water pressure ; EF: $\frac{\partial(h+z)}{\partial n}=-1$; AF: $\frac{\partial(h+z)}{\partial r}=0$ due to axial symmetry. For the two domains, the condition for boundary EF is for the assumption that a unit hydraulic gradient exists at the bottom boundary. The conditions for boundaries DE and EF are sufficient as long as the wetting front does not reach the boundaries during the infiltration event. Details concerning the solution domain and the COMSOL solver are presented in Appendix A.

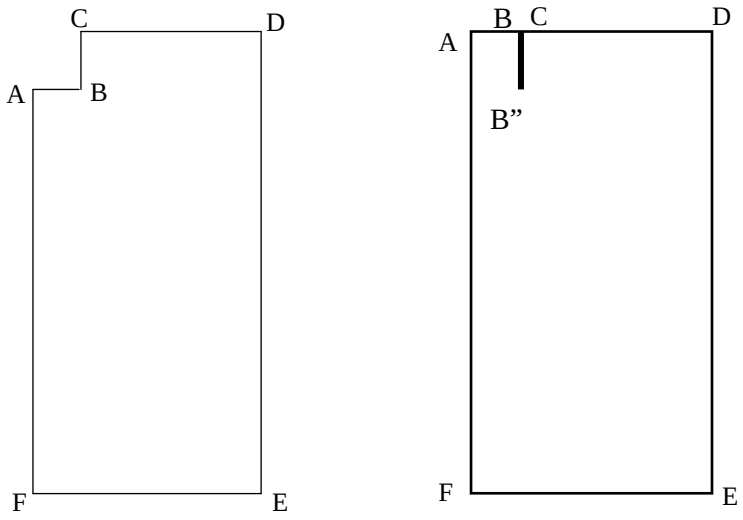

Figure 2-3.a) Illustration of the axisymmetric domain for the Philip-Dunne permeameter. b) Illustration of the axisymmetric domain for the MPD infiltrometer.

Description of Input Parameters

For the numerical simulations, five types of soil that are among the most common types of soil found in infiltration practices were chosen. The soil types are loamy sand, sandy clay loam, silty loam, sandy clay and silty clay. The hydraulic properties of the soils were defined in terms of *van Genuchten (1980)* parameters. The value of H_i was kept constant at 0.43 m for all numerical simulations, while the hydraulic properties of the soil include the field saturated volumetric soil moisture content θ_s, saturated hydraulic conductivity K_{sat} and the van Genuchten parameters, α and n were within one standard deviation of their respective mean values for the five aforementioned soil types as described by *Carsel and Parrish (1988).* In these simulations the initial soil water pressure was set to yield moderate to full wetting front potential, as calculated from equation (7), for each type of soil. $\Delta\theta$ was limited to be relatively small for the finest soil (silty clay) because in the numerical simulations for fine soil a very low soil water

pressure needs to be set for high $\Delta\theta$ (dry condition) which sometimes can lead to making the numerical simulations difficult to complete due to nonconvergence of solutions.

Another set of simulations was also performed with the solution to the Richards' equation for the case where *n* was kept constant at 4.0 while α and K_{sat} were varied using linear scaling theory (*Vogel et al., 1991*). According to this theory, the value of α varies in direct proportion to the scaling factor γ: $\alpha = \alpha_{ref}\gamma$, while the value of K_{sat} varies with γ^2: $K_{sat} = K_{sat_{ref}}\gamma^2$; where $\alpha_{ref} = 4$ and $K_{sat_{ref}} = 1.65x10^{-4}$ m/s are reference value of α and K_{sat}, respectively. The initial water depth inside the infiltrometer was the same as the previous simulations. But the initial moisture content and saturated moisture content was set to be 0.055 and 0.375 respectively, thus making $\Delta\theta$ equal to 0.32 for all cases.

The procedure for each simulation was as follows for all of the soils described above. A set of values for θ_s, θ_r, α, K_{sat}, and h_i was defined (Table 1 and Table 2) for use as inputs to the COMSOL-MP solver. Richards' equation was then solved for the period when the water level in the MPD infiltrometer was above zero. Using the head versus time curve produced by the simulation, the defined change in moisture, and the geometry of the infiltrometer, the modified analytical equations were tested using the MPD analysis procedure described in the previous section to produce values of K_{fs} and ψ. These parameters were then compared to the values used as inputs for the simulation. The K_{sat} values used as input for the simulation and the K_{fs} values determined from the MPD analysis are termed K_{eff} and K_{MPD} respectively. The value of ψ determined using the selected values for the van Genuchten parameters in equation (7) and determined from

the MPD analysis are termed ψ_{eff} and ψ_{MPD}, respectively. ψ_{eff} is determined by applying equation (7).

Analysis Procedure

A computational spreadsheet procedure in MS Excel with the solver add-in and visual basic application was developed to find solutions to equations (2), (10) and (11) and obtain optimal values of K_{fs} and ψ. The general procedure for finding values of K_{fs} and ψ from the head versus time data is as follows:

1. Input all variables, including initial moisture content, field saturated moisture content, initial height, and the head versus time curve.
2. For each measurement of head use the relationship in Equation (2) to find the corresponding distance of the sharp wetting front (note: SOLVER in Microsoft Excel 2010 and a macro were used to automate this step).
3. Estimate the change in head with respect to time and the change in wetting front distance with respect to time by using the forward finite difference method for all values of $R(t)$ equal to or greater than the distance $\sqrt{r_1^2 + L_{\max}^2}$.
4. Make initial guesses for the values of K_{fs} and ψ. By default the initial guess for K_{fs} and ψ are set as $1\text{x}10^{-3}$cm/s and 100 cm, respectively. We found that for a finer soil that has a K_{fs} value of less than $1\text{x}10^{-5}$cm/s, the initial guess of ψ might need to be changed to improve the convergence rate.
5. Solve Equations (10) and (11) for ΔH and Δt at each incremental value of $R(t)$.

6. Minimize the absolute difference between ΔH found in step 5 and change in measured head; and between Δt and the measured time interval by iterating the values of K_{fs} and ψ. Between these two optimization procedures (ΔH and Δt), the one with the minimum RMS error between measured data and estimated data was chosen to calculate K_{fs} and ψ. Occasionally one of the two does not converge, which is the primary reason that the dual fitting procedure is recommended.

Experiments

Experiment Set-up

Three barrels with a diameter of 0.56 m, height of 0.91 m, and volume of 0.208 m^3 (Greif, Inc.) were chosen as vessels for the calibration media. Each barrel was fitted with a threaded PVC valve along the side near the bottom that allowed the water to drain. A thin coating of sand was attached to the inner walls of the barrels with a spray adhesive to roughen the surface and minimize the potential for preferential flow of water along the walls. A 0.076 m layer of pea gravel (median diameter = 0.006 m) was placed at the bottom of the barrel and covered with a coarse filter fabric to isolate the gravel from the media above. Sand media of three particle size distributions was added to the three barrels over the filter fabric to a height of 0.51 m, stopping (roughly) every 0.05 m to tamp down the sand to prevent large voids and non-uniform compaction.

The three sand media were used in the experimental testing were: 1) 100% ASTM C-33 sand (barrel 1), 2) 80% (by weight) ASTM C-33 sand with 20% US Silica F110 sand

(barrel 2), and 3) 100% US Silica F110 sand (barrel 3). The media were selected to represent a range of relatively high permeability engineered soils used in bioretention facilities and other infiltration practices. For example, the Prince George's County Bioretention Manual recommends using 50%-60% clean ASTM C-33 construction sand with 20%-30% sandy loam/loamy sand and 20%- 30% leaf compost material for a soil medium (*Winogradoff, 2002*). Other manuals recommend similar mixes. The compost was omitted from our media in order to achieve homogeneous mixtures that would not change over time due to dissolution or degradation of the organic material. The sand media was mixed in a portable mortar mixer before addition to the barrels. The particle size distribution for each sand mixture was determined by a sieve analysis (*ASTM, 2006*) and is given in Figure 2-4.

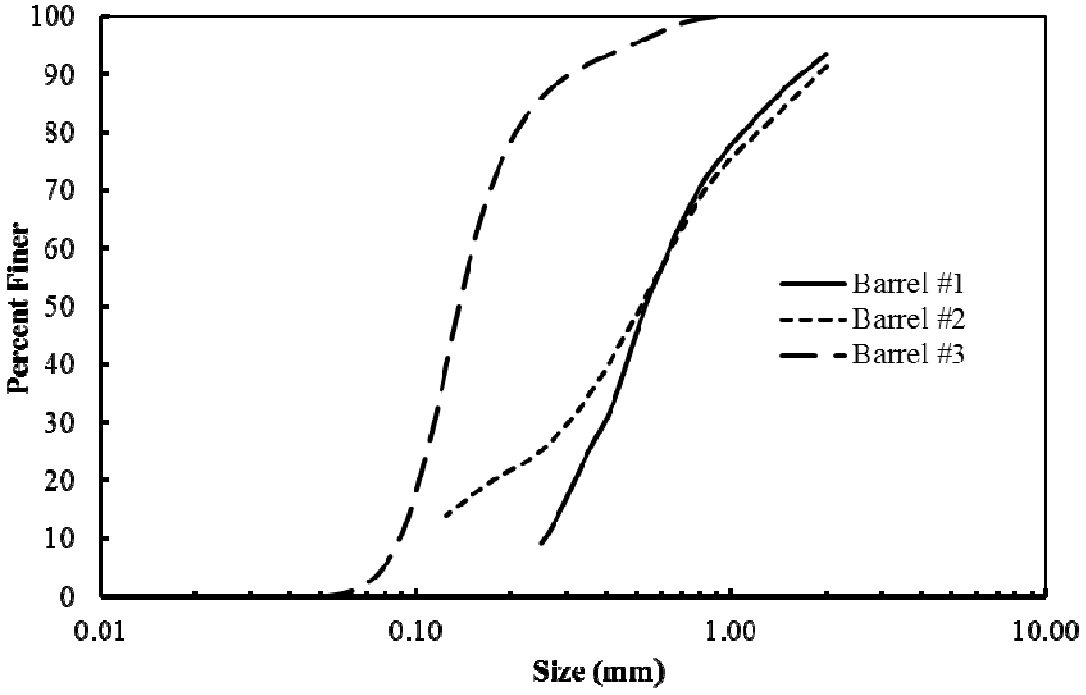

Figure 2-4. Particle size distribution of the three media used for infiltration testing.

MPD Infiltrometer Tests

The MPD infiltrometer was inserted 5cm into the surface of the soil near the center of the barrel. Initial soil moisture measurements were made from five locations around the outside edge of the infiltrometer at the soil surface. The initial soil moisture content was assumed to be uniform for the whole media. These measurements were made either gravimetrically (*Klute, 1986; ASTM, 2000, 2005*) or with a calibrated moisture probe (Theta Probe ®, ML2x). The temperature of the water used to fill the infiltrometer was measured. The MPD infiltrometer was then filled to a height of 0.43 m with the water. The head of water over time during the test was recorded at a rate of 6 readings per minute with an ultra-sonic sensor (MassaSonic, M-5000) mounted above the device. Immediately after the water had completely drained from the infiltrometer tube, the infiltrometer was removed from the barrel and five final moisture content measurements were made. Eleven (11), 17 and 19 independent tests were conducted with MPD Infiltrometer on barrels 1, 2 and 3 respectively.

Reference Falling Head Tests

To perform a reference falling head test the barrel was filled at an approximate flow rate of 0.005 L/s from a hose connected to a valve opened into the pea gravel layer at the bottom of the barrel. This method of filling the barrels from the bottom up at low flow was used to minimize the amount of entrapped air in the soil voids. The flow rate during filling was maintained below that required to fluidize the sand so as not to disturb the bed. When the water level was approximately 0.2 m above the sand surface the valve was closed and the hose was disconnected. An ultra-sonic sensor was then mounted to the top

of the barrel. The valve at the bottom was opened and the head versus time data were recorded. The analysis for the reference falling head test is similar to the analysis of a falling head lab permeameter. In the case of a falling head, the flow and hydraulic gradient are both time dependent. Darcy's law (*Klute, 1986*) is used to calculate the saturated hydraulic conductivity K_{sat} according to the following equation

$$K_{sat} = \frac{L}{\Delta t}\left[\frac{T_i + L}{T_{i+1} + L}\right] \tag{12}$$

where: L is the length of the soil column, and T_i and T_{i+1} are ponded head depths at the beginning and end of the time interval Δt. The barrels were conditioned for these tests by performing filling and draining in the same manner as described above approximately seven times before beginning the reference falling head tests. Twenty-five (25), 20 and 21 reference falling head tests were performed on barrel 1, 2 and 3 respectively.

Reference Falling Head Tests vs. MPD

The mean field-saturated hydraulic conductivity for each media determined by the MPD infiltrometer using the MPD analysis procedure ($\bar{K}_{MPD}$) was compared to the mean saturated hydraulic conductivity of the reference falling head tests for the same media ($\bar{K}_{ref}$). The uncertainty, U_r, of the ratio $K_R = \frac{\bar{K}_{MPD}}{\bar{K}_{ref}}$ is defined by following ASME standard technique (*Abernathy, et al. 1985*) which is as follows:

$$U_R = \sqrt{\left[\frac{\partial K_R}{\partial \bar{K}_{MPD}} U_{K_{MPD}}\right]^2 + \left[\frac{\partial K_R}{\partial \bar{K}_{ref}} U_{K_{ref}}\right]^2} = \sqrt{\left[\frac{1}{\bar{K}_{ref}} U_{K_{MPD}}\right]^2 + \left[\frac{\bar{K}_{MPD}}{\bar{K}_{ref}^2} U_{K_{ref}}\right]^2} \tag{13}$$

where: $U_{K_{MPD}}$ = uncertainty of K_{fs} value determined by the MPD analysis for each media,

$U_{K_{ref}}$ = uncertainty of K_{sat} value determined by reference falling head analysis for each media,

$\bar{K}_{MPD}$ = mean value of K_{fs} determined by the MPD for each media and

$\bar{K}_{ref}$ = mean value of K_{sat} determined by the reference falling head for each media.

$U_{K_{MPD}}$ and $U_{K_{ref}}$ are determined by the following equations:

$U_{K_{MPD}} = t_s \frac{\sigma_{K_{MPD}}}{\sqrt{N_{MPD}}}$ and $U_{K_{ref}} = t_s \frac{\sigma_{K_{ref}}}{\sqrt{N_{ref}}}$ where, $\sigma_{K_{MPD}}$ and $\sigma_{K_{ref}}$ represent the standard deviation of MPD measurements and reference falling head measurements, respectively, t_s is the student t value and N_{MPD} and N_{ref} represent the number of measurements for MPD analysis and reference falling head analysis, respectively.

RESULTS AND DISCUSSION

Richards' Equation Simulations

Borehole permeamter vs. MPD infiltrometer

It is instructive to compare computer simulation of infiltration into a homogeneous/isotropic soil for the two cases, one for the Philip-Dunne permeameter and one for the MPD infiltrometer, just to show the differences in infiltration characteristics. For this, a soil with the following soil moisture characteristics was used: θ_s = 0.375, $\theta_r = 0.05$, $\alpha = 4\ m^{-1}$, $n = 4$, and K_{sat} = 1.64x10^{-4} m/s. The initial water pressure was set to

-1.0 m, which gives a corresponding initial moisture content of 0.055. The simulation result for a 0.05 m deep, 0.05 m radius borehole (Philip-Dunne permeameter) is shown in Figure 2-5. The results for the MPD infiltrometer with 0.05 m radius penetrated to 0.05 m depth are shown in Figure 2-6. Both plots show the moisture distribution in the soil surrounding the infiltration surface at the moment that the ponding in the tube becomes zero. There are some similarities in the geometry of the flow for both cases, but there are also some differences. Primarily, the water in the MPD infiltrometer is forced to pass one-dimensionally through the 0.05 m long soil core before allowing for three-dimensional flow in the soil beneath and around the infiltrometer. This flow constraint for the MPD infiltrometer results in a reduced water pressure at the end of the tube compared to a Philip-Dunne permeameter due to the pressure loss within the soil core, and this then results in a longer time for the infiltrometer tube to empty, and a more diffusive wetting front than for the permeameter.

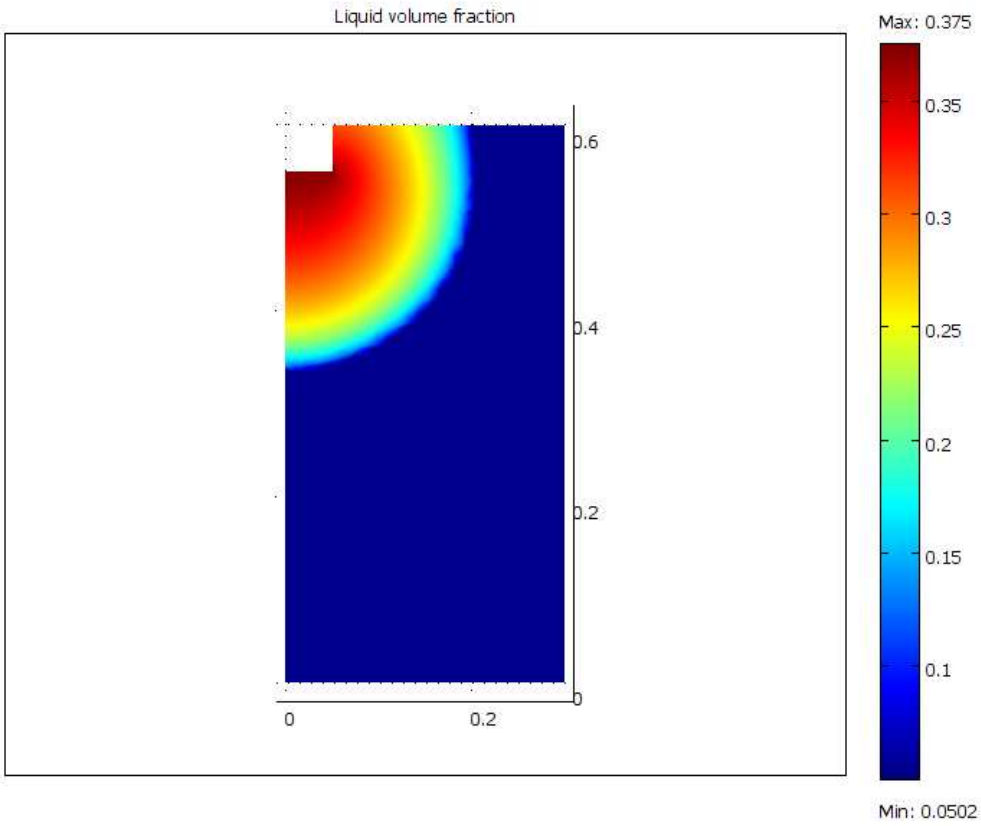

Figure 2-5. Soil moisture content at 380 seconds for the Philip-Dunne permeameter. The plot is for the end of the simulation period when the permeameter tube has emptied.

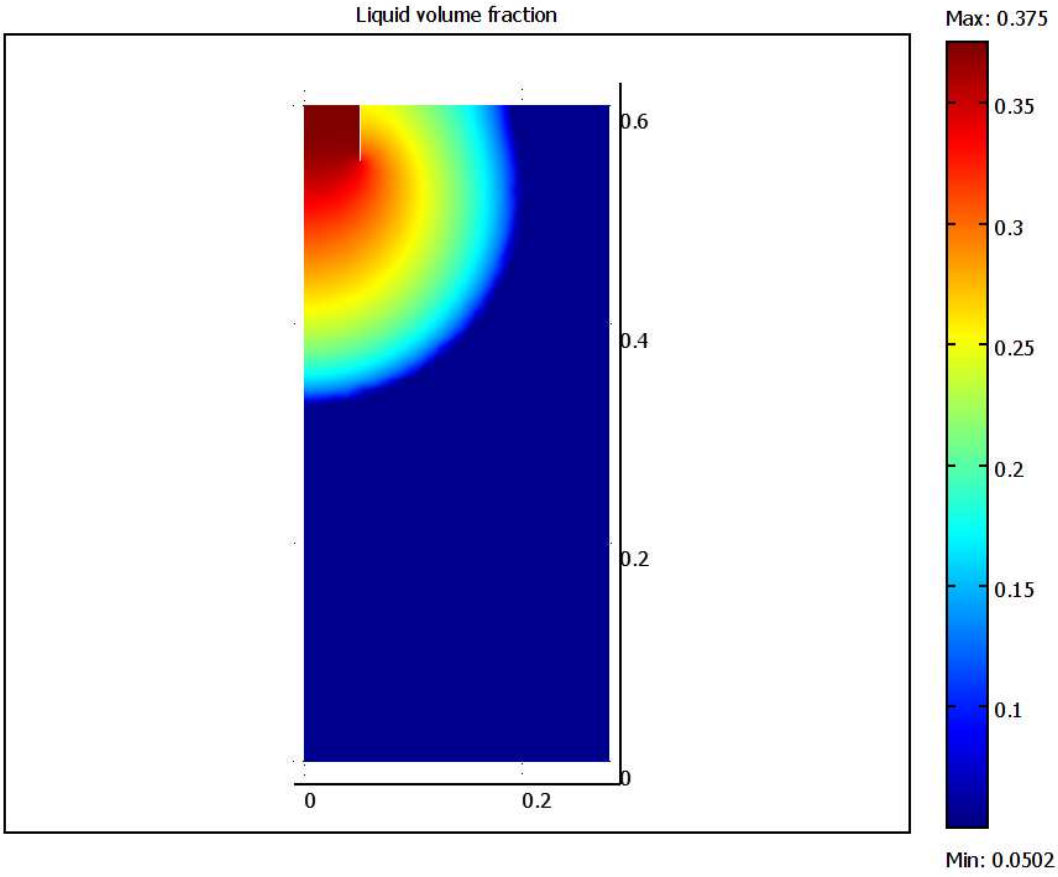

Figure 2-6. Soil moisture content at 1200 seconds for the MPD infiltrometer. The plot is for the end of the simulation period when the infiltrometer tube has emptied.

To illustrate the effect of borehole depth and infiltrometer penetration depth on the time variation of water height inside the permeameter and infiltrometer tubes, simulations for a few different penetration depths were conducted using Richards' equation for same initial condition as described in the previous paragraph and the results of these are presented in Figure 2-7. It is observed from the plots that the borehole depth for the permeameter does not affect the rate of water height decrease for borehole depths in the range between 0.15 m and 0.05 m. The depth of the borehole does begin to influence infiltration rate at 0.02 m and even more so for surface application. This influence of borehole depth results from the

fact that when the wetting front reaches the soil surface, which it would do for the shallower boreholes, the rate of infiltration is restricted because there is less volume of soil to be invaded by the advancing front.

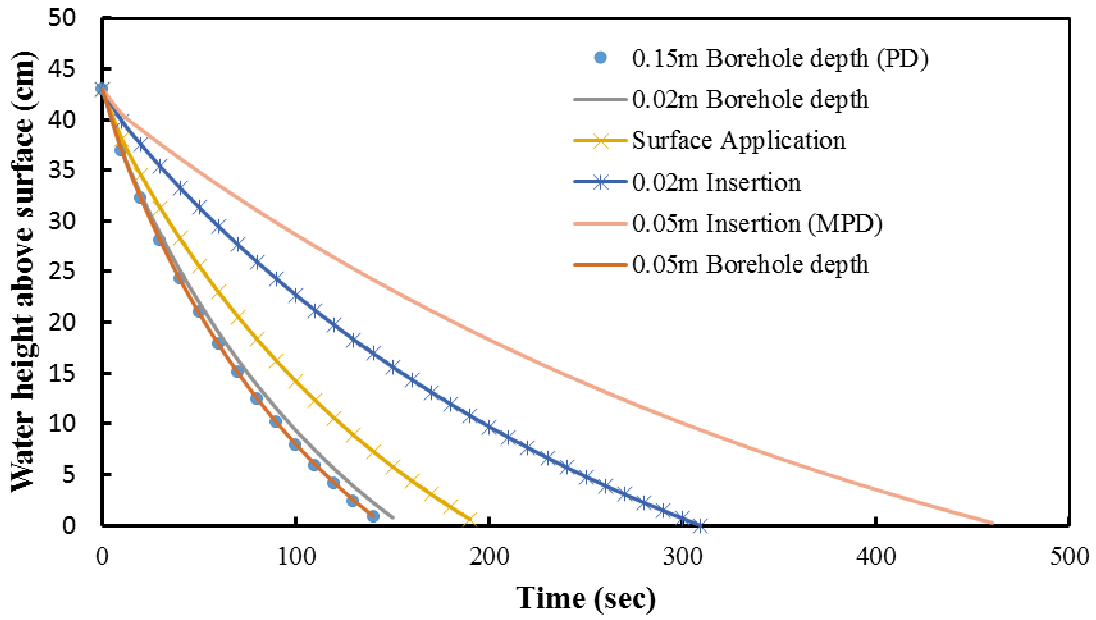

Figure 2-7. Water depth in Philip-Dunne permeameter or MPD infiltrometer versus time. Initial water depth = 0.43 m.

Infiltration rates for the MPD infiltrometer configuration are much slower than for the permeameter at equivalent borehole/ penetration depths. Also, it is observed that the time required for emptying of the initially filled volume for the case with a 0.05 m tube penetration is more than twice the time required for the case of surface application, and about 30% more time than for the case of 0.02 m penetration. This results from the pressure loss that occurs in transmitting the water through the encased soil volume as opposed to an open borehole.

Simulations of MPD infiltrometer for various soils

The input parameters for the soils where the value of the van Genuchten parameters (α and n) were reported by Carsel and Parrish for the five soil textures, loamy sand, sandy clay loam, silty loam, sandy clay and silty clay are presented in Table 2-1, along with the corresponding K_{fs} and ψ estimated from the MPD analysis procedure for each texture. The input parameters for the soils with parameters derived from linear scaling theory are presented in Table 2-2, and again the K_{fs} and ψ estimated from the MPD analysis procedure corresponding to each soil are also given in Table 2-1 and Table 2-2. Note for all the soils with the scaled parameters had the parameter n set equal to 4. The K_{sat} values that were input in the numerical simulations are termed as K_{eff} for both Table 2-1 and Table 2-2.

Table 2-1. Comparison of K_{fs} and ψ values determined from the MPD analysis of the simulated falling head data to the values used as inputs to the COMSOL simulations for the case of variable n. The pressure parameter h_s in the Vogel et al. (2001) modified van Genuchten equations was set to -0.04 m for all simulations given in this table.

Soil type	α (m^{-1})	n	h_i (m)	θ_r (%)	θ_o (%)	K_{MPD} (m/s)	K_{eff} (m/s)	$\frac{K_{MPD}}{K_{eff}}$	Ψ_{MPD} (m)	Ψ_{eff} (m)	$\frac{\psi_{MPD}}{\psi_{eff}}$
Loamy sand	10	2.3	-0.4	5.7	11.8	$4x10^{-05}$	$3.47x10^{-05}$	1.15	0.11	0.061	1.84
Sandy clay loam	4.5	1.5	-0.8	10	25	$8.66x10^{-06}$	$6.94x10^{-06}$	1.25	0.144	0.097	1.48
Silty loam	2	1.4	-2	6.7	28	$1.69x10^{-06}$	$1.39x10^{-06}$	1.22	0.197	0.173	1.13

Sandy clay	0.9	1.2	-10	10	27.9	$3.79x10^{-07}$	$2.78x10^{-07}$	1.36	0.26	0.28	0.94
Silty clay	0.4	1.1	-10	7	31.8	$6.12x10^{-08}$	$5.56x10^{-08}$	1.10	0.52	0.43	1.21

Table 2-2. Comparison of K_{fs} and ψ values determined from the MPD analysis of the simulated falling head data to the values used as inputs to the COMSOL simulations for the case of constant. The parameters α and n were derived from linear scaling theory.

Case	A (m^{-1})	n	h_i (m)	θ_r (%)	θ_o (%)	K_{MPD} (m/s)	K_{eff} (m/s)	$\frac{K_{MPD}}{K_{eff}}$	Ψ_{MPD} (m)	Ψ_{effL} (m)	$\frac{\psi_{MPD}}{\psi_{eff}}$
1	8	4	-0.50	5	5.5	$6.63x10^{-04}$	$6.60x10^{-04}$	1.00	0.14	0.087	1.57
2	4	4	-1	5	5.5	$1.63x10^{-04}$	$1.65x10^{-04}$	0.99	0.22	0.17	1.29
3	3	4	-1.33	5	5.5	$9.15x10^{-05}$	$9.28x10^{-05}$	0.99	0.28	0.23	1.19
4	2	4	-2	5	5.5	$4.11x10^{-05}$	$4.12x10^{-05}$	1.00	0.38	0.35	1.09
5	1.05	4	-3.82	5	5.5	$1.07x10^{-05}$	$1.14x10^{-05}$	0.94	0.73	0.66	1.10
6	0.61	4	-6.59	5	5.5	$3.84x10^{-06}$	$3.84x10^{-06}$	1.00	1.13	1.14	0.99
7	0.40	4	-10	5	5.5	$1.64x10^{-06}$	$1.65x10^{-06}$	0.99	1.71	1.74	0.98
8	0.27	4	-14.93	5	5.5	$7.79x10^{-07}$	$7.52x10^{-07}$	1.04	2.4	2.57	0.93
9	0.17	4	-23.57	5	5.5	$4x10^{-07}$	$2.98x10^{-07}$	1.34	2.87	4.09	0.70

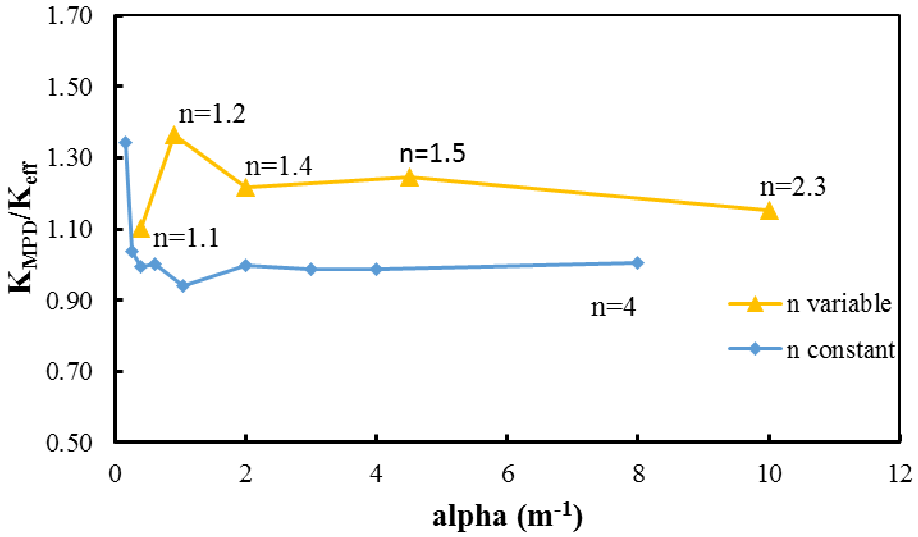

Figure 2-8. Variation of K_{MPD}/K_{eff} ratio for different values of alpha for variable and constant .

According to the results in Table 2-1 and Figure 2-8, the MPD analysis procedure overestimates K_{fs} from 10% (Silty clay, α =0.4, n =1.1) to 36% (Sandy clay, α =0.9, n=1.2) for the soil cases examined. The variation of $\frac{K_{MPD}}{K_{eff}}$ ratio with α is shown in Figure 2-8. Part of the overestimation of K_{fs} is believed to be due to the distortion of the actual flow path lines caused by the no-flow boundaries of the infiltrometer. This distortion effect should be accounted for in the value of β, and the distortion should increase with increasing capillarity. It is not clear that the constant value of β as assigned by *Philip (1993)* is correct, or whether it would be better to assign a value of β that accounts for capillarity. This effect should be examined further.

Reynolds (2011) used an ad hoc modified version of HYDRUS 2D to show that using $\beta = \frac{\pi^2}{8}$ in the Philip-Dunne permeamter analysis leads to overestimation of the K_{fs} ranging from few percent to about 23% for the different soils he examined. For the borehole permeameter he suggested this coefficient to be 1. In his analysis by using $\beta = 1$ the measured K_{fs} value was consistently more accurate ($\leq$20% difference).

A second possible reason for the overestimated K_{fs} value is that the MPD analysis assumes that the wetting front is sharp. But in the field and also in simulations of Richards' equation, the wetting front is not sharp, but will be diffuse to a degree determined by the capillarity of the soil. According to the results in Table 2-2 and Figure 2-8, where *n* was kept constant, the MPD analysis procedure in some cases overestimates K_{fs} (case 9, 34%) and in some cases underestimates K_{fs} (case 5, 6%). But overall in these cases the MPD analysis predicts K_{fs} better than the cases where n was variable (Figure 2-8). The reason is probably because a higher n value, such as $n = 4$, represents a narrower particle size distribution and a less diffuse wetting front, which corresponds more closely to the assumption of a sharp wetting front made in the Green-Ampt analysis.

From Table 2-1 and Table 2-2 we can also conclude that the MPD formulation overestimates the Green-Ampt wetting front suction in some cases (84% for loamy sand and 57% for case 1) and underestimates it in other cases (6% for sandy clay and 30% for case 9). A similar kind of trend, going from coarser textured materials to finer textured materials was shown by *Reynolds (2011)* for the borehole permeameter. He noted that

this inaccuracy seems to be associated with the gravity term G, in the Green-Ampt solution formulation, which was kept constant during the entire period of infiltration in his analysis and in the analysis of *Philip (1993).* The gravity term was kept constant in those two analyses because in both cases the governing equation was integrated analytically over time, which required that the gravity term be constant. In contrast, in our analysis the gravity terms was not kept constant because we integrated the governing equation (equation (8) or equation (9)) numerically, allowing the flexibility of a time-variant gravity term. *Reynolds (2011)* found that the detrimental effect of a constant gravity term on the estimated Green-Ampt wetting front suction is greatest for coarser soils, and demonstrated that a constant value of zero (rather than r_o) leads to improved estimates of the wetting front suction for the entire range of soil textures.

Another assumption made in the MPD formulation is that the wetting front will be hemispherical in shape. But in reality, because of the effect of gravity, the wetting front cannot be perfectly hemispherical after some period of infiltration. It will be more elongated in shape (i.e., bulged downward). This elongation may be another cause of deviation of parameter estimates from the input values. To illustrate this effect the moment of inertia about the axis of symmetry was calculated for each of the Richards' equation solutions. The moment of inertia (M) about the axis of symmetry is one way to quantitatively represent the shape of the wetting front. It was calculated as a function of time using the equation,

$$M(t) = \int_{o}^{t} 2\pi\theta(t) r^2 dr dz \tag{14}$$

Simulations of Richards' equation were performed with and without the presence of gravity for each type of soil and the values M were calculated from equation (14) for the instant in time that the infiltrometer just emptied. Results for these integrations are listed in Table 2-3, where the moment of inertia for cases without gravity (M_C) are given as a ratio with the moment of inertia for the cases with gravity (M_{C+G}). The amount of elongation depends on the ratio of capillary forces to gravitational forces. From the table it is seen that the coarser soils (i.e., loamy sand and sandy clay loam) have a larger ratio than the finer soils, indicating the importance of the gravitational component of flow for those soils. It also indicates that the wetting front will not be spherical as assumed in the Green-Ampt analysis and this could be a cause for some reduction in accuracy of parameter estimates with the MPD analysis.

Table 2-3. Comparison of the spread of the wetting front at the end of the simulation period, when the infiltrometer tube has emptied, for different types of soil.

Soil type	K_{eff}**(m/s)**	$\frac{M_C}{M_{C+G}}$
Loamy sand	3.47×10^{-05}	1.36
Sandy clay loam	6.94×10^{-06}	1.08
Silty loam	1.39×10^{-06}	1.01
Sandy clay	2.78×10^{-07}	1.0
Silty clay	5.56×10^{-08}	1.0

Illustration of the elongation of the wetted volume for the case of the loamy sand soil is presented in Figure 2-9. In Figure 2-9a is the wetted profile for the case with gravity, and

Figure 2-9b is for the case without gravity. There is a clear effect of gravity in the elongation of the wetting profile in this case.

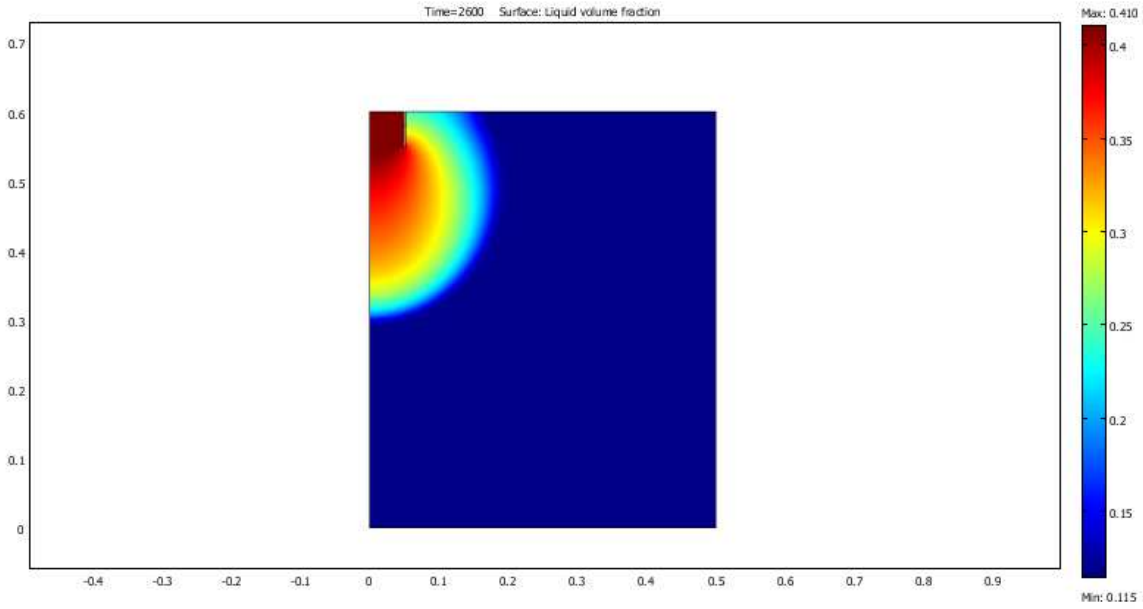

(a)

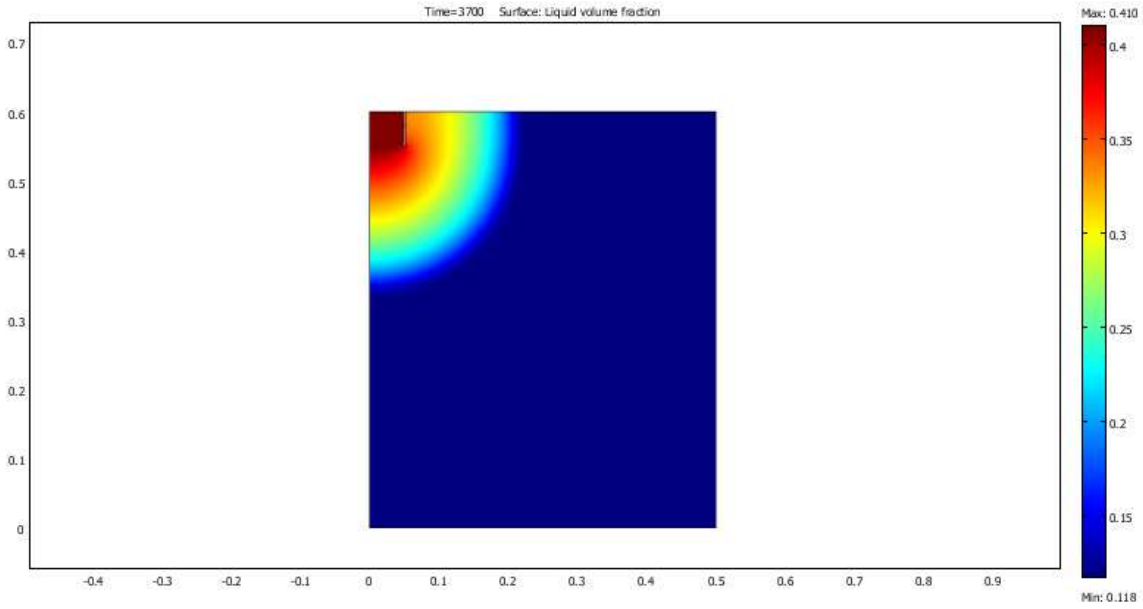

(b)

Figure 2-9. Illustration of the effect of gravity on downward distortion of the otherwise spherical shaped wetted domain. Loamy sand is compared with gravity (a) and without gravity (b).

Experimental Results

Treatment of Outliers

Though the flow rate during filling was maintained below that required to fluidize the sand, still in some cases the soil was slightly fluidized. This led to some unusually high K_{sat} values or outliers, which were not observed when the soil was freshly re-compacted. These outliers were removed to obtain a dataset free of erroneous measurements caused

by experimental error such as equipment malfunctions and operational issues. Outliers were identified (and removed from further consideration) using the median absolute difference method developed by *Rousseeuw (1990).* The technique incorporates an estimate of scale, S,

$$S = 1.483\left(\text{Median}\left|\text{K}_\text{i} - K_{med}\right|\right) \tag{15}$$

where K_i is the saturated hydraulic conductivity of test i and K_{med} is the median of the K_i values. Then a Z-score for each data point is determined from,

$$Z_i = \frac{K_i - K_{med}}{S} \tag{16}$$

Any data that has a Z-score above a critical value is considered an outlier. If the distribution is Gaussian, critical Z-scores of 2.5 and 1.5 correspond to the inclusion of 98.5% and 84% of the total data, respectively. A histogram of individual K_{ref} and K_{MPD} values (including outliers) of each media type is shown in Figure 2-10. For media 1 and 2, there is a wider range of K_{ref} than that of K_{MPD} and in media 3 the variation of K_{MPD} is wider. Because of this wide range of K_{ref} and K_{MPD} values which lead to difficulty in obtaining representative falling head tests, a low Z value of 1.5 was used to treat the outliers. Approximately 16% of the data were identified as outliers indicating that the measurements varied from a Gaussian distribution at the extremes. Outlier distribution among the different devices and barrels appeared to be random.

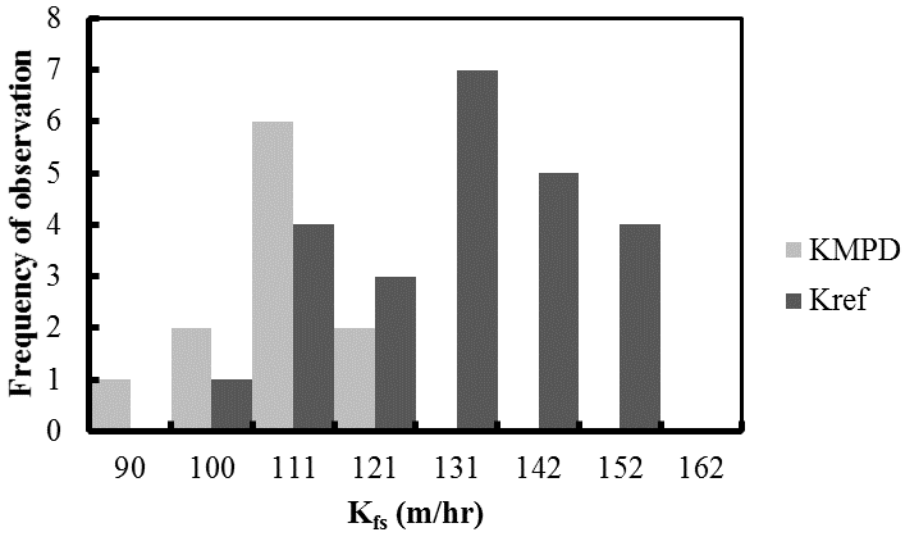
Frequency of observation
0
1
2
3
4
5
6
7
8
90
100
111
121
131
142
152
162
K_{fs} (m/hr)
KMPD
Kref

(a)

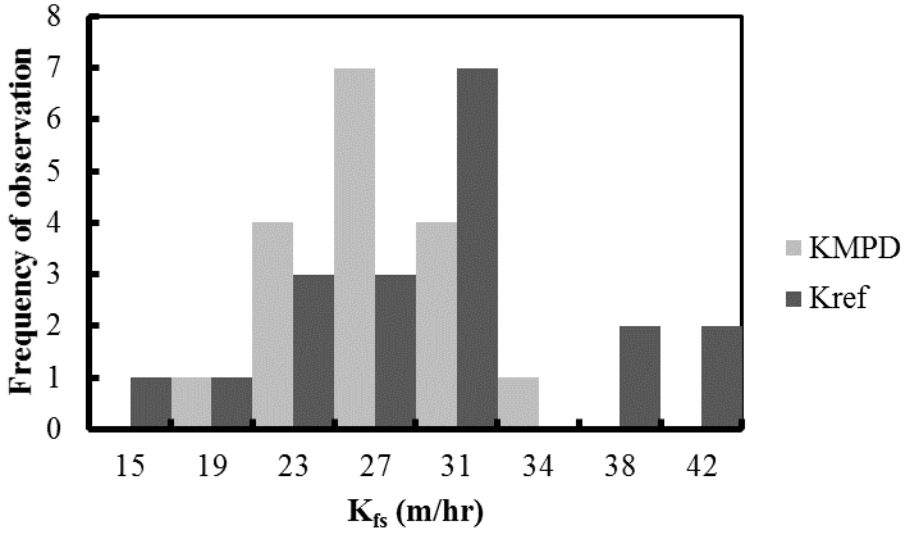
Frequency of observation
0
1
2
3
4
5
6
7
8
15
19
23
27
31
34
38
42
K_{fs} (m/hr)
KMPD
Kref

(b)

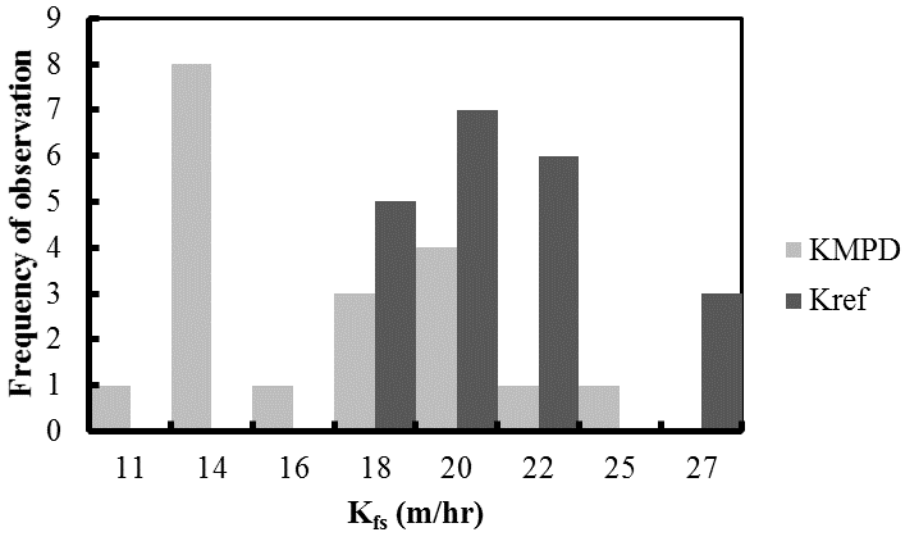

(c)

Figure 2-10. Histogram of K_{MPD} and K_{ref} measurement before removing outliers for (a) media 1, (b) media 2 and (c) media 3.

Comparison between falling head test and MPD test

The ratio of arithmetic mean of K_{MPD} and arithmetic mean of K_{ref} (excluding outliers) for the three sands measured with the MPD infiltrometer are presented in Figure 2-11Figure 2-11 with corresponding descriptive statistics in Table 2-4. The graph also shows the upper and lower limit of the ratio ($\frac{K_{MPD}}{K_{ref}}$) within 67% confidence interval around the ratio of mean K_{MPD} and mean K_{ref}. Equation 13 was used to calculate the upper and lower confidence interval of the ratio ($\frac{K_{MPD}}{K_{ref}}$) for each barrel.

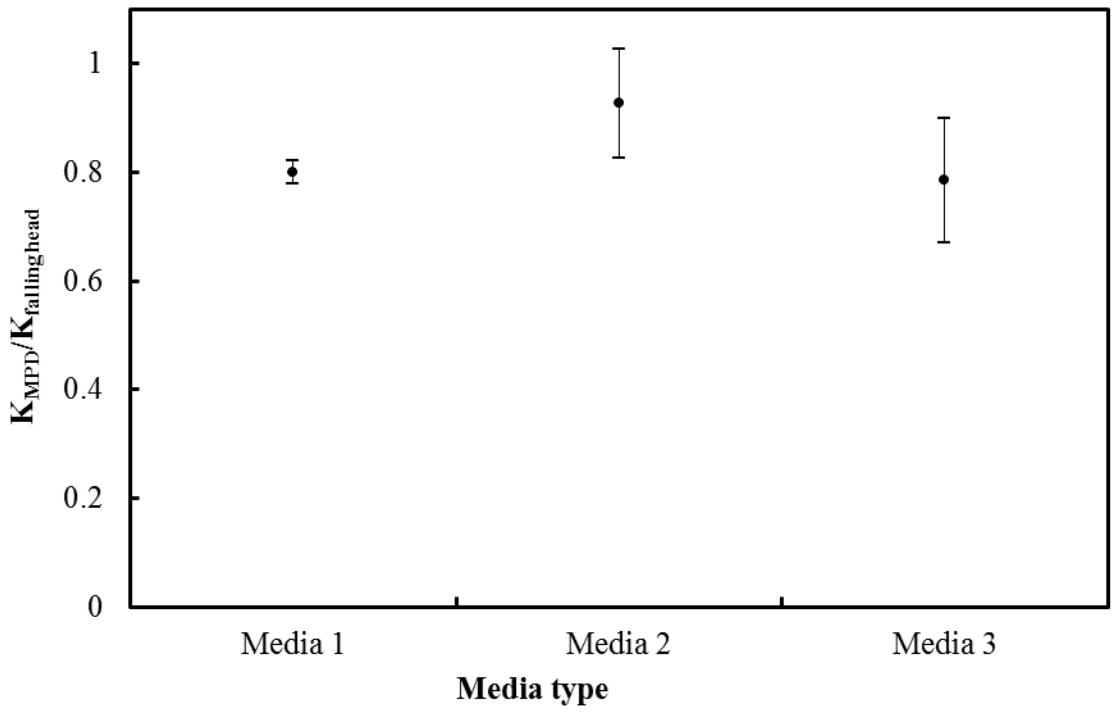

Figure 2-11. Comparison of ratio of arithmetic mean of KMPD and arithmetic mean of Kref for three different porous media. Error bars represent 67% confidence intervals.

Table 2-4. Descriptive statistics for hydraulic conductivity of three barrels. N represents the sample size, and CV indicates the coefficient of variation.

	Media type 1		Media type 2		Media type 3	
Statistic	**MPD**	**Falling Head**	**MPD**	**Falling Head**	**MPD**	**Falling Head**
Min.(m/s)	$2.7x10^{-4}$	$3x10^{-4}$	$5.8x10^{-5}$	$5.2x10^{-5}$	$3.1x10^{-5}$	$4.7x10^{-5}$
Max.(m/s)	$3x10^{-4}$	$4x10^{-4}$	$8x10^{-5}$	$1x10^{-4}$	$5.6x10^{-5}$	$6.1x10^{-5}$
Mean(m/s)	$2.9x10^{-4}$	$3.6x10^{-4}$	$6.8x10^{-5}$	$7.4x10^{-5}$	$4.2x10^{-5}$	$5.4x10^{-5}$
Median(m/s)	$2.9x10^{-4}$	$3.6x10^{-4}$	$6.8x10^{-5}$	$7.6x10^{-5}$	$3.9x10^{-5}$	$5.5x10^{-5}$
Std.Dev.(m/s)	$1.4x10^{-5}$	$3.1x10^{-5}$	$7x10^{-6}$	$1.4x10^{-5}$	$9x10^{-6}$	$4.4x10^{-6}$
CV	4.8%	8.6%	10.5%	19.1%	21.5%	8.2%
Skewness	-0.1648	-0.3177	0.31	0.71	0.27	-0.01
Kurtosis	-1.309	-0.7244	-0.85	0.61	-1.72	-1.30
N	8	20	15	16	18	18

Media 1 has the highest K_{sat} value and Media 2 and 3 have roughly equivalent K_{sat} values, which are because of the fines present that restrict passage of water, and the fines are similar in both media. The average initial moisture content for media 1, 2 and 3 are 6%, 10.5% and 7.6% respectively for the MPD Infiltrometer test. The coefficients of variation (CV) for all the tests are relatively low, ranging from 4.8% to 21.5%. *Munoz-Carpena et al. (2002)* reported CV values of 39% to 101% when comparing permeameter

results from field measurements. *Asleson et al. (2009)* reported CV values between 54 and 178% in an infiltration assessment of rain gardens with engineered soil. Lower CV values would be expected for a controlled laboratory comparison because the sand media is homogenous in comparison to field soils. The relatively low skewness and kurtosis values indicate that the datasets may be described as normally distributed. This could also be a consequence of the relatively homogenous sands used in the testing. Comparatively, it is typical for field measured hydraulic conductivity to be represented by a lognormal distribution (*Asleson et al., 2009*).

A Games and Howell procedure (*Toothaker, 1994*) was used to compare the mean K_{sat} values for each of the barrels with the K_{fs} values estimated with the MPD infiltrometer. The results showed that the mean K_{fs} values from the MPD infiltrometer measurements were statistically different at the 5% level from the mean reference falling head test K_{sat} values for barrels 1 and 3 but not for barrel 2. In general, the K_{fs} values from the MPD infiltrometer tests are in good agreement with the reference falling head tests. Nevertheless, there is a consistent bias in that the mean K_{fs} values were 80, 92 and 78 percent of the mean reference falling head tests for barrels 1, 2 and 3, respectively. One possible reason for this bias is the air entrapment or encapsulation by the downward advancing wetting front during the MPD measurements. MPD infiltrometer measures the field-saturated hydraulic conductivity (K_{fs}) which will generally be less than that of fully saturated media (K_{sat}). *Bouwer (2002)* showed that because of entrapped air the hydraulic conductivity in a wetted zone during infiltration is less than for the fully-

saturated value, and he indicated that for sandy soil this can cause up to a factor of 2 decreases in the measured K_{fs} value. Given that the barrels were wetted to saturation from the bottom up prior to the falling head tests, one could reasonably expect much less entrapped air in the sands during falling head tests, and hence a greater saturated hydraulic conductivity value. Fortunately, this amount of bias is relatively low in comparison to the amount of variability observed for MPD infiltrometer measurements at field sites (mean CV of 107%; *Asleson et al. 2009*).

CONCLUSIONS

Infiltration rate parameters, including field-saturated hydraulic conductivity, should be measured at the soil surface in stormwater infiltration practices because surface issues (e.g., compaction, particle accumulation) can severely limit infiltration and the overall performance of these stormwater management practices. The development of a novel and inexpensive device for surface infiltration rate measurements, called the Modified Philip-Dunne (MPD) infiltrometer, and the associated approximate data analysis method, was described herein. Such a device could be used to determine when and where to perform maintenance in stormwater infiltration practices. In addition, this device could also be used for evaluation of landscape altering practices, such as construction activities.

An MPD analysis method was developed based on the Green-Ampt model, which assumes a sharp spherical wetting front. The MPD analysis method produced a reasonably accurate estimate of hydraulic conductivity for simulated MPD tests of homogeneous and isotropic soil. The MPD analysis method, however, overestimated the

field-saturated hydraulic conductivity (10 to 36%) for low n values (n=1.1~2.3) and overestimated/ underestimated (-6 to 34%) for high n values (n=4), which was attributed to: 1) the value of the shape factor proposed by Philip (1993) which does not fully account for possible effects of capillarity on wetted volume shape, and 2) the wetting front is neither sharp nor necessarily spherical in shape, both of which are assumptions made with the Green-Ampt analysis. The accuracy of the infiltrometer was tested by comparison to reference falling head tests on three barrels containing sand media with different grain size distributions. The MPD infiltrometer K_{fs} values were, on average, 83.3 percent of the reference falling head test values. The error in K_{fs} values produced by the MPD infiltrometer is thought to be small compared to the orders of magnitude of variability in K_{fs} observed in the field.

3. Accuracy of Infiltration Measurements in Layered Soil and Containing Macropores

F. Ahmed, Department of Civil, Environmental and Geo-Engineering, University of Minnesota, Minneapolis, MN 55414; J. S. Gulliver, Department of Civil, Environmental and Geo-Engineering, University of Minnesota, Minneapolis, MN 55414; J. L. Nieber, Department of Bioproduct and Biosystem Engineering, University of Minnesota, St. Paul, MN 55108

EXECUTIVE SUMMARY

The Modified Philip Dunne Infiltrometer (MPD) is a falling head device for measurement of Green Ampt parameters (field saturated hydraulic conductivity and soil suction) as well as infiltration rate across the soil surface that uses the Green-Ampt assumptions for a semi-circular wetting front. The accuracy of MPD Infiltrometer has been investigated by laboratory tests and numerical simulations for uniform soil and by field tests. In this paper the Modified Philip Dunne formulation has been compared with numerical simulations of the Richards' equation for non-uniform soil. Non-uniformity of the soil is characterized by stratification of soil properties and the presence of macropores in uniform soil. For layered soil, the MPD infiltrometer results in a field saturated hydraulic conductivity (K_{fs}) that is 12% to 63% higher than the K_{fs} in uniform soil. When a single macropore is present directly below the MPD infiltrometer in uniform soil the K_{fs} values are between 4% to 29% of the uniform soil K_{fs} value. However, MPD Infiltrometer also overestimates K_{fs} value by 10 to 36% for the uniform soil. These differences are relatively small compared to the spatial order of magnitude variation in K_{fs}, indicating

that the MPD infiltrometer is a viable infiltration device to be used to characterize the infiltration rate of soil surface.

INTRODUCTION:

Infiltration is a primary means of reducing runoff volume and removing pollutants from surface runoff *(LeFevre et al. 2014, Kayhanian et al. 2012, 2007).* This is especially important in urban settings, where impervious surfaces can be disconnected from the storm sewer system by infiltration practices *(Asleson, et al. 2009, Paus et al. 2014*). Design variants on these practices include infiltration basins, infiltration trenches, dry wells, bioinfiltration practices, vegetated swales, porous pavement and underground infiltration systems (*EPA, 2010, Erickson et al. 2013*). Moreover, these stormwater control measures (SCMs) also include filtration, adsorption and precipitation to remove pollutants from the water as it percolates through the soil matrix.

It is important to characterize the infiltration capacity of the soils in stormwater infiltration practices to evaluate their performance and facilitate maintenance scheduling *(Weiss, et al. 2007; Erickson et al 2010, 2013).* The infiltration capacity can be characterized by either direct measurement or by measuring the hydraulic properties of the soil *in-situ*, which can then be related to the infiltration rates through infiltration capacity equations. A principal hydraulic property required for assessment of infiltration capacity of stormwater infiltration practices is the field saturated hydraulic conductivity (K_{fs}) of the soil. Common devices used to determine the field saturated hydraulic conductivity of the soil surface are disk infiltrometers, single ring infiltrometers or double ring infiltrometers *(ASTM, 2003),* most often applied for steady-state flow, but

occasionally for unsteady flow (*Reynolds and Elrick, 1990; Bagarello et al., 2004; Lassabatere et al. 2006; Reynolds, 2008; Nimmo et al., 2009*). Because of the time and water volume needed for a measurement, it is difficult to obtain more than a few measurements in one day, so it is not practical to characterize the spatial variability of field saturated hydraulic conductivity within the infiltration practice.

Recent research (*Asleson, et al. 2009*), has shown that K_{fs} will often vary spatially by two orders of magnitude in an infiltration practice, similar to field soils (*Olson et al., 2013*) even though the soil is engineered. One measurement in such a practice used to predict the mean value would have substantial uncertainty that is not quantified. Thus, to determine a representative K_{fs} of an infiltration practice, numerous measurements are needed. This means that a falling head technique is a more suitable method to take multiple infiltration measurements because of reduced time and volume of water required. The Modified Philip-Dunne (MPD) infiltrometer (*Nestingen, 2007, Ahmed et al., 2014*), is one such falling head device that can be used to measure the field saturated hydraulic conductivity of soil at multiple, simultaneously locations.

The MPD infiltrometer is similar to the Philip-Dunne Permeameter *(Philip, 1993)* except that it is modified to measure the field saturated hydraulic conductivity of the soil at its surface. The Green-Ampt assumption of a sharp wetting front, with the initial soil moisture ahead of the front and saturated soil behind the front is applied along with the assumption that the domain of wetting has a spherical shape. In the analysis by Philip, the permeameter is placed in an auger borehole and the field saturated hydraulic conductivity of the soil at that depth is determined from the analysis of the falling head versus time

data. In the modified form, the same type of analysis is applied, but the permeameter is inserted into the soil at the surface to a small depth without removing the soil from the interior of the permeameter. The boundary conditions and solution with the Green-Ampt assumption are adjusted accordingly.

For homogeneous soils, the migration of a wetting front originating from a point at the surface is initially spherical in shape due to the dominance of capillary forces. Once gravity effects become important the shape will be distorted in downward direction. Comparison of the MPD infiltrometer with solutions using the Richards equation were performed by *Ahmed et al., (2014).* They found that an upward adjustment of between 10 and 36 % was required to match the K_{fs} determined with the MPD infiltrometer to the computational solution of the Richards equation. However, soil is usually non-homogeneous in nature. It is generally assumed that the hydraulic properties of soil are more homogeneous in the horizontal direction than the vertical because of layering and weathering processes (*Beven, 1984*). In a fully developed soil profile, top soil often has a loose texture containing macropores, cracks and preferential paths which lead to an increase in the hydraulic conductivity (*Barontini et al., 2007*). The underlying soil layer, however, tends to have a lower permeability because of the presence of partially decayed organic matter, finer-grained particles and less weathering. The opposite is true of stormwater infiltration practices, where finer-grained particles are present at the soil surface due to deposition of suspended sediment, resulting in a less permeable layer at the surface (*Erickson et al., 2010, 2013*).

Macropore impacts include the rapid flow of water and solute along certain pathways, bypassing a large part of the porous medium (*Schaik, 2010*). Macropores can be formed by soil fauna, plant roots, natural soil piping or cracks and fissures resulting from the freeze/thaw cycle. Though macropores contribute very little to the total porosity of the soil matrix, the presence of macropores close to the surface has an important impact on the infiltration rate of a soil. *Peterson and Dixon* (*1971*), for example, reported that a 0.002% increase in pore space by a single macropore can increase the infiltration capacity by 65% (*Beven and Germann 1982*).

Wu L. et al. (1993) applied three models to evaluate the effect of macropores, cracks and layered soil on saturated hydraulic conductivity (K_{sat}) of soil estimated with a borehole permeameter. A finite element solution of the Richards equation was used to simulate infiltration from a borehole permeameter and thereby generate synthetic data for used with the three models. The three models included the Guelph model (Reynolds et al., 1985), the Philip model (Philip, 1985), and a Laplace model (Reynolds and Elrick, 1985). To estimate saturated hydraulic conductivity from the synthesized infiltration data the Guelph and Philip models were implemented using both the simultaneous equation approach (SEA) and the constant α approach. The Laplace model is similar to the Guelph model in form except that it is simplified by neglecting the effect of capillarity. For the case of homogeneous and isotropic soil the three methods yielded estimates of saturated hydraulic conductivity that ranged between 53% and 1200% of the value prescribed for the finite element solution. For the case of layered soil or soil with a vertical macropore intersecting the bottom of the borehole it was found that the Guelph

and the Philip models with SEA yielded very poor estimates of the saturated hydraulic conductivity, in some cases negative values which are unrealistic.

In this paper the effect of macropores and layering of soil on the infiltration rate of water at the soil surface is modeled with the intent of examining the accuracy of surface layer field saturated hydraulic conductivity derived using an analysis of falling head data based on a Green-Ampt equation formulation (i.e., the MPD infiltrometer). To avoid the measurement errors inherent in field and laboratory data, the falling head data are derived from numerical solutions of the Richards equation, where the properties of the "soil" matrix are prescribed. The numerical solution facilitates the examination of various soil types and soil geometric configurations (layering and macropore presence).

THEORY OF THE MODIFIED PHILLIP-DUNNE INFILTROMETER:

The MPD infiltrometer is a 0.1 m diameter cylinder that is driven 0.05 m into the soil, and has been used in Asleson, et al. *(2009)* and Olsen, et al. *(2013).* The initial moisture content of the soil near the surface is measured and is assumed to be uniform across the underlying soil profile. To perform the test the infiltrometer is filled with water to a specified level and the water level in the cylinder is monitored over time. The test continues until sufficient measurements of water surface elevation versus time have been taken to estimate K_{fs}, usually until the water has completely emptied out of the infiltrometer cylinder. After the test is performed the water level vs time data and initial and saturated soil moisture content are input in the MPD software to calculate the K_{fs} and capillary soil suction, (ψ). The

software is developed based on the Modified Philip Dunne Infiltrometer theory (Ahmed et al. 2014) which has been described briefly in following.

The mathematical model of the MPD infiltrometer is a modification of Philip's borehole permeameter model *(Philip 1993).* Assumptions that were made are: isotropic homogeneous

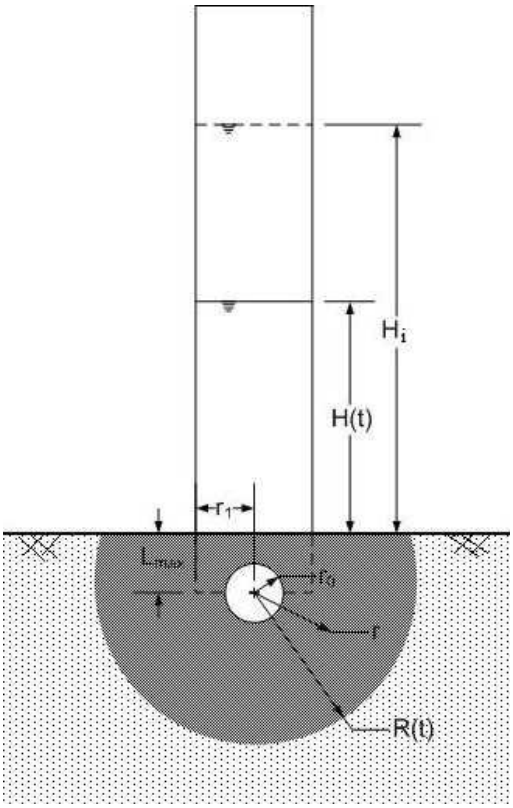

Figure 3-1. Important parameters of the MPD infiltrometer. H_i is the initial height of water; H(t) is the height of water at time t; L_{max} is the depth of insertion into the soil; r_0 is the equivalent source radius; r_1 is the radius of the cylinder; r, any radius within the wetted front; and *R(t)* is the radius to the sharp wetted front at time *t*.

media, a Green-Ampt sharp wetting front and a spherical geometry for the wetting front by subtracting the gravitational component of the flow. The equation for cumulative infiltration assuming capped sphere as shown in Figure 3-1, is:

$$[H_i - H(t)]\pi r_1^2 = \frac{(\theta_s - \theta_0)\pi}{3}[2[R(t)]^3 + 3[R(t)]^2 L_{max} - L_{max}^3 - 4r_0^3] \quad (1)$$

where θ_s and θ_0 are the saturated and initial moisture content of the soil. By equating the pressure capillary potential drop ΔP from the spherical source to the wetted front obtained by following same analysis procedure as Philip (1983) and the pressure capillary potential drop obtained by using Darcy's law and then discretizing it we get (Ahmed et al., 2014):

$$H^n - H^{n-1} = \frac{K_{fs}}{L_{max}}\left[\frac{\pi^2}{8}\left\{(\theta_s - \theta_0)\left(\frac{(R^n)^2 + R^n L_{max}}{K_{fs}}\frac{(R^n - R^{n-1})}{\Delta t}\right) - 2r_0^2\right\}\frac{\ln\left\{\frac{R^n(r_0+L_{max})}{r_0(R^n+L_{max})}\right\}}{L_{max}} - \psi + H^{n-1} + L_{max}\right]\Delta t$$

(2)

$$t^n - t^{n-1} = \frac{\frac{\pi^2}{8}(\theta_s - \theta_0)\frac{(R^n)^2 + R^n L_{max}}{K_{fs} L_{max}}\ln\left\{\frac{R^n(r_0+L_{max})}{r_0(R^n+L_{max})}\right\}(R^n - R^{n-1}) - \frac{L_{max}}{K_{fs}}\Delta H}{\psi - H^n - L_{max} + \frac{\pi^2}{8}\frac{2r_0^2}{L_{max}}\ln\left\{\frac{R^n(r_0+L_{max})}{r_0(R^n+L_{max})}\right\}} \quad (3)$$

where K_{fs} is the field saturated hydraulic conductivity and ψ is the wetting front suction. For more accuracy in the computation of K_{fs} and ψ the middle points between two consecutive observed head vs time data was interpolated using cubic spline approximation (*Hanna and Sandall, 1995*). The solution is achieved by minimizing the root mean square (rms) of the difference between interpolated head increment and predicted head increment (ΔH) and interpolated time increment and predicted time increment (Δt), by adjusting the values of field saturated hydraulic conductivity (K_{fs}) and capillary soil suction (ψ). The MPD software is developed based on Equation 1, 2 and 3. By using the MPD software the solution that gives lower rms error between ΔH and Δt optimization will be the optimal value of K_{fs} and ψ.

NUMERICAL EXPERIMENTS

Procedure

The water level vs. time data used as input in the MPD spreadsheet was generated by solving the Richards equation using the commercial software package COMSOL (Comsol, 2013), a flexible modeling software for solving coupled partial differential equations governing multi-physics phenomena. The numerical solutions are based on Galerkin finite element formulations, and can solve problems that are time-dependent or time-independent, in one-dimension, two dimensions, or three dimensions. Element basis function orders vary up to fifth order. The method uses an automatic time-step adjustment algorithm based on DASPK solver methodology. A number of direct and iterative matrix solver schemes are available to solve the discrete algebraic equations resulting from the Galerkin procedure. Newton iteration is used to solve the set of equations in the case where the algebraic equations are nonlinear.

The form of the Richards equation applicable to three-dimensional regions obeying axisymmetric geometry, similar to that of the MPD infiltrometer is :

$$\frac{\partial \theta}{\partial t} = \frac{1}{r}\frac{\partial}{\partial r}\left(Kr\frac{\partial h}{\partial r}\right) + \frac{\partial}{\partial z}\left(Kr\frac{\partial h}{\partial z}\right) + \frac{\partial K}{\partial z} \qquad (12)$$

where, K *is* unsaturated hydraulic conductivity (m/sec), h is soil water pressure head (m), θ is volumetric water content, r and z are the radial and vertical (positive upward) coordinates respectively, and t is time. The functions θ and K are determined by the using Modified Mualem-Van Ganuchten model (*Vogel et al., 2001)* with the following equations:

$$\theta = \begin{cases} \theta_r + \frac{\theta_m - \theta_r}{(1+|\alpha h|^n)^m} & h < h_s \\ \theta_s & h \geq h_s \end{cases} \quad (13)$$

$$K = \begin{cases} K_{sat} K_r & h<(h_s) \\ K_{sat} & h \geq h_s \end{cases} \quad (14)$$

and

$$S_e = \frac{\theta - \theta_r}{\theta_s - \theta_r} \quad (15)$$

where, S_e is the effective saturation, h_s is the minimum capillary height, θ_s and θ_r are the saturated and residual moisture content respectively, $\theta_m (\geq \theta_s)$ is an extrapolated parameter associated with h_s, α and n are the Van Ganuchten shape parameters (with $n>1$) and $m = 1-1/n$. K_{sat} is the saturated hydraulic conductivity and K_r is relative hydraulic conductivity. $K_r = \frac{K}{K_{sat}}$, where K is the unsaturated hydraulic conductivity. The parameter θ_m and the function K_r can be determined from the following expression:

$$\theta_m = \theta_r + (\theta_s - \theta_r)(1 - |\alpha h_s|^n)^m \quad (16)$$

$$K_r = S_e^l \left[\frac{1-F(S_e)}{1-F(1)}\right]^2 \quad (17)$$

$$F(S_e) = \left(1 - S_e^{*1/m}\right)^m \quad (18)$$

$$S_e^* = \frac{\theta_s - \theta_r}{\theta_m - \theta_r} S_e \quad (19)$$

where l is a pore connectivity parameter usually assumed to be 0.5 following *Mualem (1976).*

As explained by *Vogel et al. (2001),* the modified forms of the Van Genuchten relations have an advantage when $n \leq 2$, since for those values the unmodified K function becomes infinitely steep, leading to numerical convergence problems. In addition, the

predicted hydraulic conductivity using the unmodified equations does not fit actual unsaturated hydraulic conductivity well near saturation. In our analysis we chose the values of h_s = -0.04 m. This value was suggested by *Schaap (2006)* to be optimal.

The flow domain of interest in a layered soil and in a macropore containing soil for the Modified Philip-Dunne application is represented by the axisymmetric region illustrated in Figure 2(a) and 2(b) respectively**.** For both domains, all boundaries have been considered as impermeable except for the bottom boundary, which is treated as a unit gradient boundary, and the soil surface inside the tube, which has a time varying pressure calculated from the mass balance of the water stored inside the tube. The depth of water inside the tube decreases in time due to the infiltration derived from the numerical solution. The boundary conditions for the infiltrometer domain in the layered soil (Figure 3-2(a)) are the following. AB: $h = depth(t)$ BC = CD = DE = $\frac{\partial(h+z)}{\partial n} = 0$; EF = FG = IA: $h = h_{initial}$; GH = $\frac{\partial(h+z)}{\partial n} = -1$; HI= $\frac{\partial(h+z)}{\partial r} = 0$ due to axial symmetry, where n is the unit normal vector to the boundary, r and z represent radial and vertical direction respectively. The conditions for boundaries DE, EF and FG are sufficient as long as the wetting front does not reach the boundaries. The boundary conditions for the infiltrometer domain in the soil containing macropore (Figure 3-2(b)) are the following. AB: $h = depth(t)$ BC = CD = DE: $\frac{\partial(h+z)}{\partial n} = 0$; EF: $h = h_{initial}$; GF = $\frac{\partial(h+z)}{\partial n} = -1$; GH = HI= IA = $\frac{\partial(h+z)}{\partial r} = 0$ due to axial symmetry. IH is the macropore in the soil which is represents a porous media that has

a K_{sat} value of 0.5 m/s. The conditions for boundaries DE and EF are sufficient as long as the wetting front does not reach the boundaries.

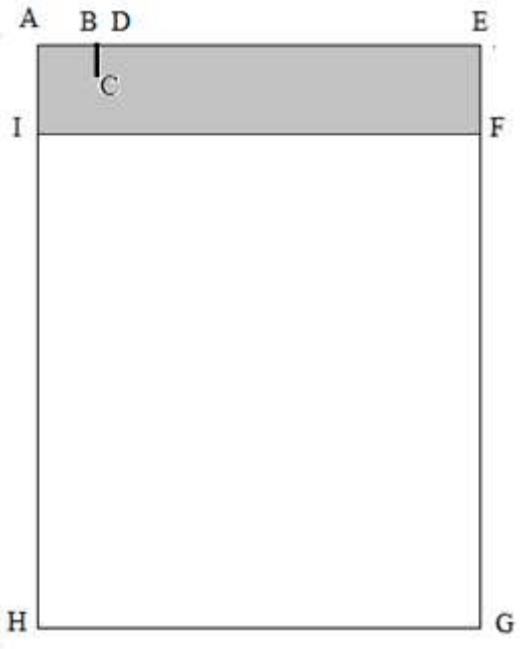

(a)

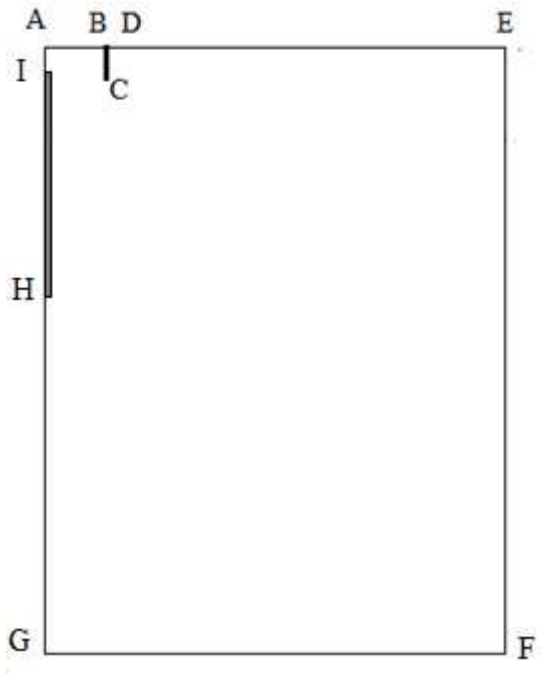

(b)

Figure 3-2. 2-D flow domain and axisymmetric mesh for (a) layered soil and (b) soil with macropore

Computations

Fifty-one simulations were performed as part of a test of the MPD infiltrometer methodology. Among these simulations, sixteen had layered soil with variations in hydraulic conductivity and the depth of the top layer. The axisymmetric boundaries were set such that the outer boundary does not affect the flow domain (width 0.5m and length 0.6m). The initial moisture content of the soil is determined by using equation (13), which is dependent upon α, n, θ_m and h. The soil water pressure depends on the suction head of the soil and the position of the water table, which was set to be 1.6 m below the soil surface. The initial water depth in the tube was set at 0.43m and the infiltration

simulation continued until the water depth in the tube decreased to within one time step of zero.

For the simulation of layered soil, five types of soil with different textures were chosen to be representative of loamy sand, sandy clay loam, silty loam, sandy clay and silty clay. These are the most common soil types in infiltration practices. The values of H_i, θ_r *and* θ_S are kept constant as 0.43m, 0.067 and 0.45 respectively, while values for van Ganuchten parameter α and K_{sat} were varied using linear scaling theory (*Vogel et al., 1991*), where a reduction in α by a factor γ has a corresponding reduction in K_{sat} by a factor γ^2. The factor γ was chosen so that the value of α and K_{sat} falls within one standard deviation around the mean value of these five soil types (*Carsel et. al., 1988*) and the corresponding value of van Genuchten parameter *n* was used for each soil type. The top soil property was always kept constant (α=2 and *n*=1.41), which is the property of silty loam (*Carsel et. al., 1988*). Silty loam with α = 2 and *n* = 1.41 was also used as a reference soil for the bottom soil parameters, which were varied using linear scaling. The bottom soil varied from loamy sand to silty clay. Since the α and *n* value of the top and bottom soil was not the same, the initial moisture content of the top soil was different from that of the bottom soil. The depth of the top soil (*T*) was varied from 0.025m to 0.1m. Figure 3-3 shows a schematic diagram of the layered soil numerical model. Table 3-1 shows the values of the parameters that determine the initial condition for the simulations.

MPD infiltrometer

L_{max} T

$K_t = K_{sat}$ of top soil

$K_b = K_{sat}$ of bottom soil

Figure 3-3. Schematic diagram of the numerical model for layered soil case

Table 3-1. Values of *α*, n and initial soil moisture content of top and bottom soil when top soil depth is 0.1m

Soil layer	**Soil type**	***A*** ***(m^{-1})***	***n***	***K_{sat}*** **(m/s)**	**Initial moisture content**
Top soil	Silty loam	2	1.4	$1.4x10^{-6}$	0.30
Bottom soil	Loamy sand	10	2.3	$3.47x10^{-5}$	0.079
	Sandy clay loam	4.48	1.5	$6.94x10^{-6}$	0.22
	Silty loam	2	1.4	$1.4x10^{-6}$	0.30
	Sandy clay	0.894	1.2	$2.78x10^{-7}$	0.40
	Silty clay	0.4	1.1	$5.56x10^{-8}$	0.44

Thirty-five simulations were also performed for uniform soil containing a macropore of 10 mm diameter, where in fifteen cases the macropore was not connected to the surface and in twenty simulations the macropore was connected to the surface. The macropore length was varied from 0.05m to 0.4m and the saturated hydraulic conductivity of the soil was varied from $5x10^{-4}$m/s (gravel) to $5x10^{-8}$m/s (silty clay). The macropore was represented by a coarse textured porous media with a saturated hydraulic conductivity of 0.5 m/s. The values of α, n, H_i, θ_0, θ_r *and* θ_S are kept constant as $2m^{-1}$(Silty loam), 1.41 (Silty loam), 0.43m, 0.322, 0.067 and 0.5 respectively.

Results

Figure 3-4(a) through Figure 3-4(e) show the Richards equation simulation of axi-symmetric distribution of the volumetric moisture content for layered soil, with a top layer thickness of 10cm, after complete draining to within one time step, of the MPD Infiltrometer. The red color indicates the wettest portion of the soil and the blue color is the driest. In Figure 3-4(a) and Figure 3-4(b), the bottom layer has higher α and n value than the top soil, which indicates that the bottom layer is coarser than the top layer. This is reversed in Figure 3-4(d) and (e), where the bottom layer is finer than the top layer. Figure 3-4(c) represents uniform soil. Figure 3-4(a), (b), (d) and (e) indicate that for this layered soil set up, if the bottom soil is coarser than the top soil, it will take less time to drain the MPD infiltrometer than the case where the bottom soil is finer than the top soil. With the soil texture combination shown in Figure 3-4(a) and (b) note that since the top layer is thick (0.1m) relative to the volume of water infiltrated, the bottom layer has less contribution in the infiltration. Thus, the time to drain the MPD infiltrometer in fine over

coarse soil layer (Figure 3-4(a) and Figure 3-4(b)) is close to similar to that for uniform soil (Figure 3-4(c)).

Also, the volume of water added during the simulations, given in Figure 3-4, indicate that, in most cases (except sandy clay loam), a larger volume of water is contained in the top layer than the bottom layer. With a bottom layer of loamy sand, the top soil has higher capillarity and lower hydraulic conductivity than the bottom soil, which leads most of the infiltrated water to move laterally in the top layer. With a bottom layer of sandy clay and silty clay, the bottom soil has higher capillarity but the moisture content of the bottom soil is close to saturation, such that the infiltrated water stays in the top layer and moves laterally. In this case water will not infiltrate into the bottom layer until the moisture content of top and bottom soils are similar. For these reasons a larger volume of infiltrated water is found in the top. With a bottom layer of sandy clay loam the volume of infiltrated water in the top layer is lower than that of bottom layer, it might be because the initial moisture content and K_{fs} value of the top and bottom layer are similar. It is apparent that, in many cases, stratification of the soil leads the infiltrated water to move laterally in the top layer. Figures of 0.025m, 0.05m and 0.075m top layers, provided in Appendix B, show similar trends.

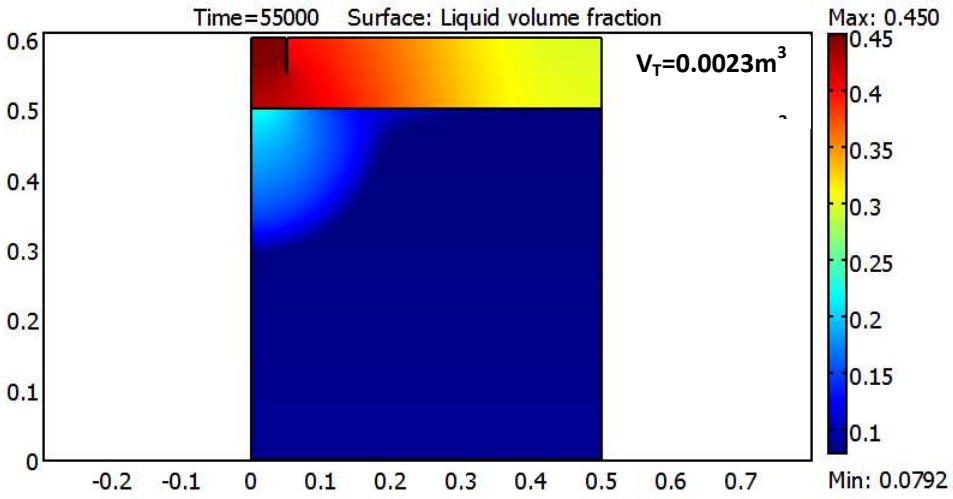
Time=55000 Surface: Liquid volume fraction
Max: 0.450
V_T=0.0023m^3
0.6
0.5
0.4
0.3
0.2
0.1
0
-0.2 -0.1 0 0.1 0.2 0.3 0.4 0.5 0.6 0.7
0.45
0.4
0.35
0.3
0.25
0.2
0.15
0.1
Min: 0.0792

(a)

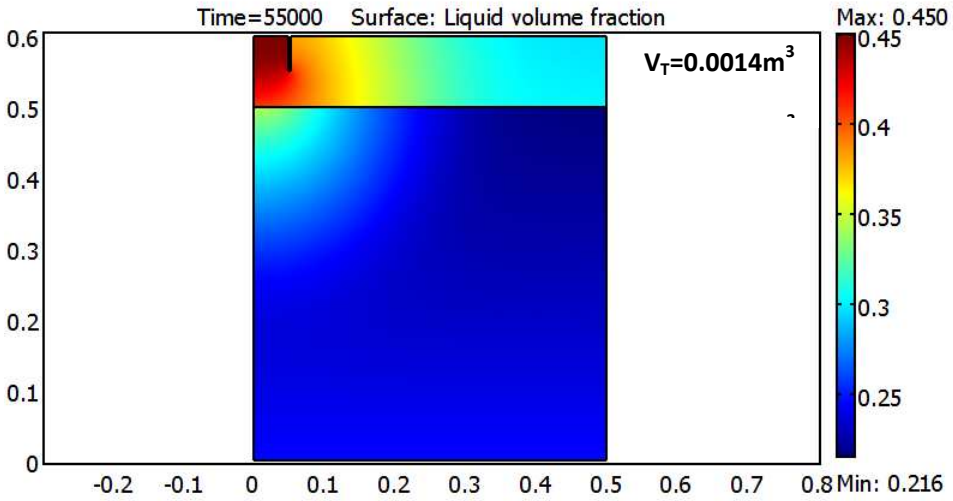
Time=55000 Surface: Liquid volume fraction
Max: 0.450
V_T=0.0014m^3
0.6
0.5
0.4
0.3
0.2
0.1
0
-0.2 -0.1 0 0.1 0.2 0.3 0.4 0.5 0.6 0.7 0.8
0.45
0.4
0.35
0.3
0.25
Min: 0.216

(b)

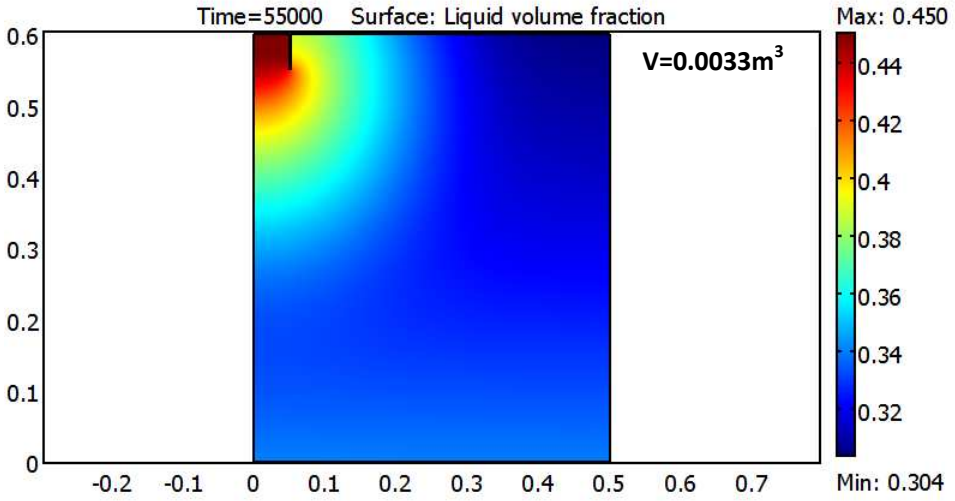
Time=55000 Surface: Liquid volume fraction
V=0.0033m3
Max: 0.450
0.44
0.42
0.4
0.38
0.36
0.34
0.32
Min: 0.304
0.6
0.5
0.4
0.3
0.2
0.1
0
-0.2
-0.1
0
0.1
0.2
0.3
0.4
0.5
0.6
0.7

(c)

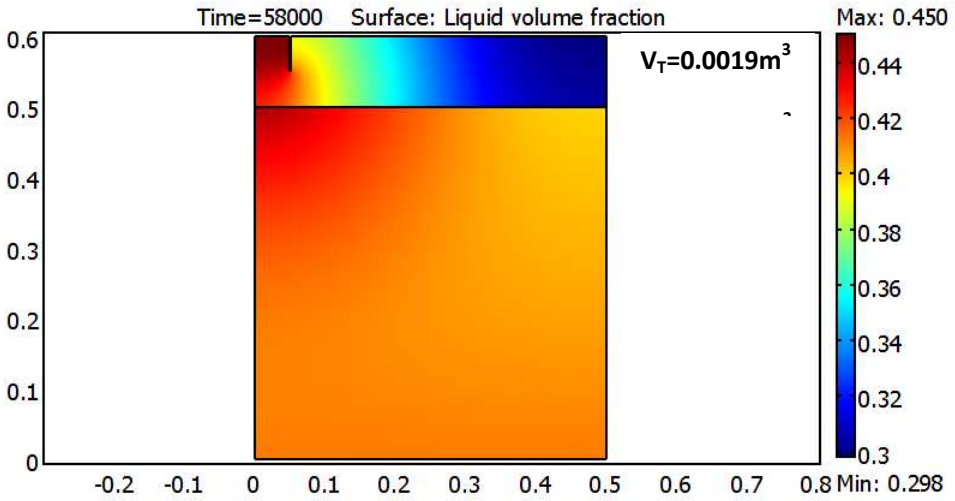
Time=58000 Surface: Liquid volume fraction
VT=0.0019m3
Max: 0.450
0.44
0.42
0.4
0.38
0.36
0.34
0.32
0.3
Min: 0.298
0.6
0.5
0.4
0.3
0.2
0.1
0
-0.2
-0.1
0
0.1
0.2
0.3
0.4
0.5
0.6
0.7
0.8

(d)

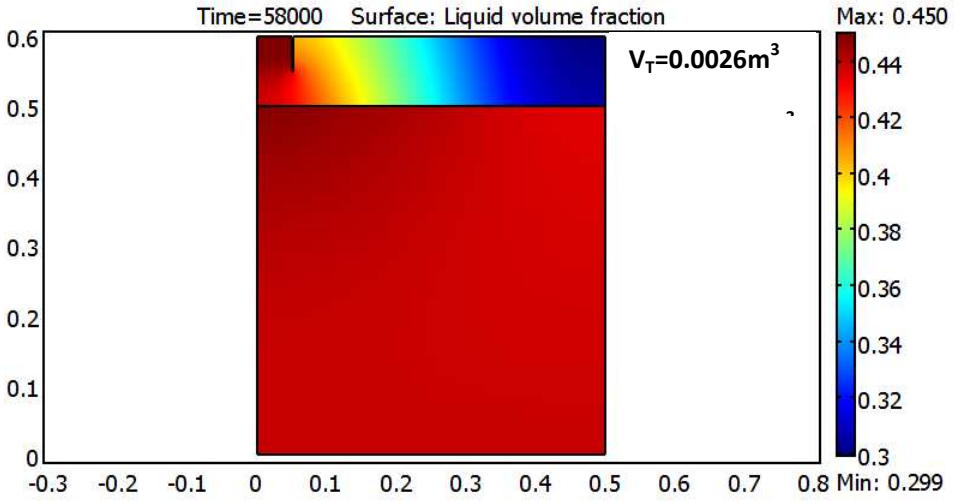

(e)

Figure 3-4. Simulated axi-symmetric distribution of the volumetric moisture content at the conclusion of the run for layered soil with a 0.1m thick top layer. The MPD infiltrometer is inserted to 0.05m depth in the top left corner. Moisture content scale is to the right of each figure and the time (sec) of drainage of MPD infiltrometer, within one time step being empty, is mentioned on top of each plot. The volume of water infiltrated at the top layer is termed as V_T, the volume of water infiltrated at the bottom layer is termed as V_B and the total volume of infiltrated water is termed as V. The top layer is silty loam and the bottom layer is (a) loamy sand, (b) sandy clay loam, (c) silty loam, (d) sandy clay, (e) silty clay.

When uniform soil contains a macropore at the center of the infiltration measurement device, the shape of the wetting front becomes elongated, depending upon the length of the macropore. Example simulations of uniform soil with a macropore are given in Figures 4a and 4b with macropores of 10 mm diameter and 0.2m in length. Figures for 0.05m, 0.1m, 0.3m and 0.4m for K_{sat}= 5x10^{-5} m/s are shown in supporting information. If

the macropore is connected to the surface (Figure 3-5a) water will first flow rapidly to the bottom of the macropore while also infiltrating through the boundary of the macropore into the surrounding soil matrix. When the macropore begins 0.025m below the surface (Figure 3-5b), water will enter into the macropore once the water pressure in the soil matrix adjacent to the macropore exceeds the water entry potential of the macropore, a value that is close to 0 m pressure head.

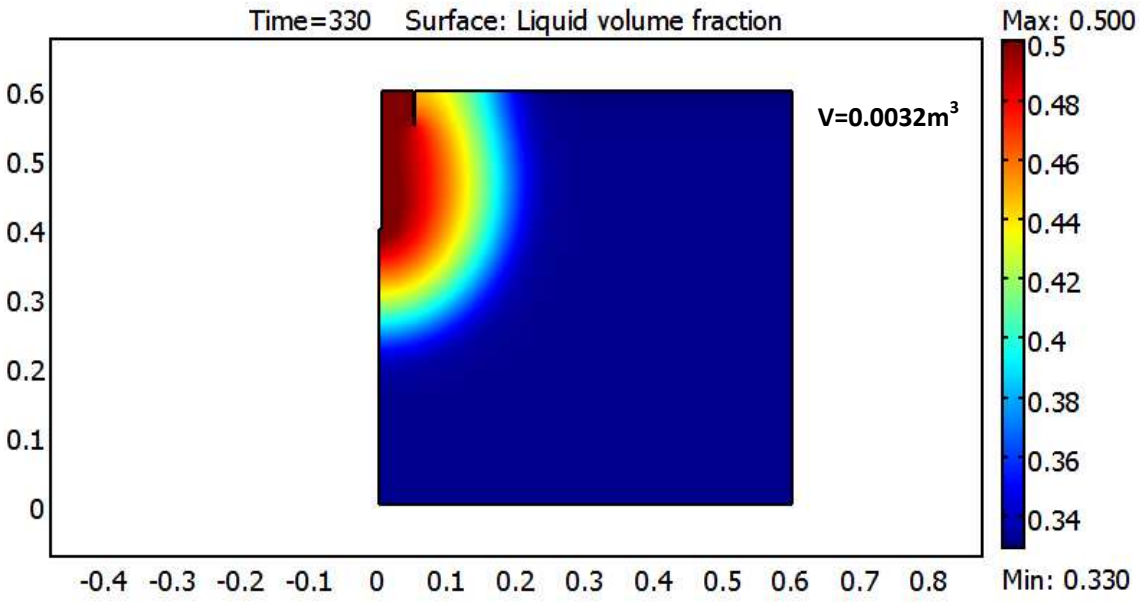

(a)

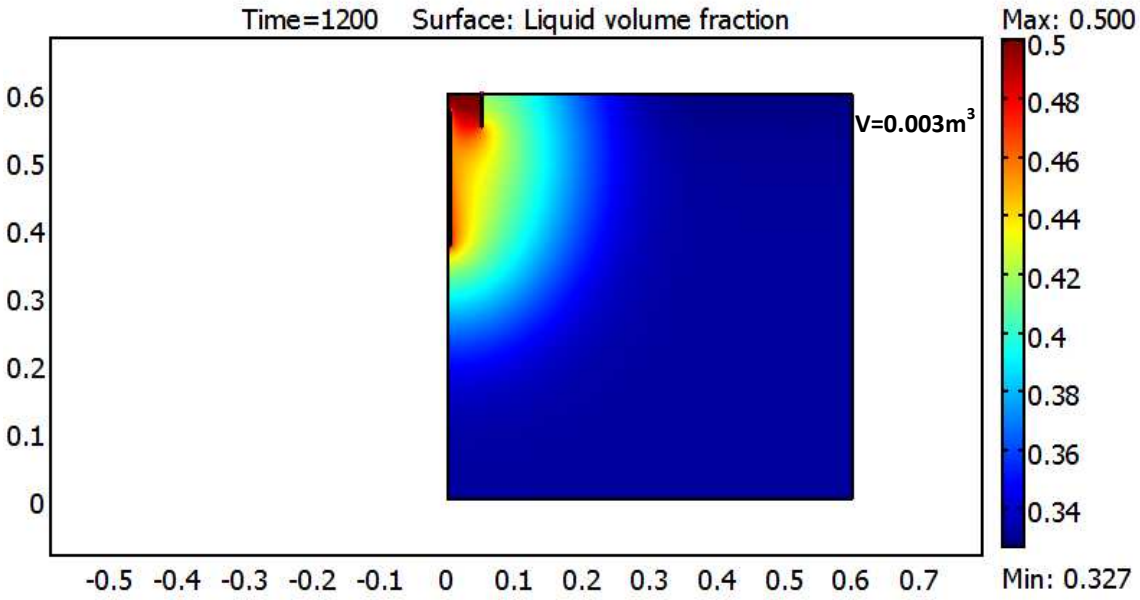

(b)

Figure 3-5. Simulated axi-symmetric distribution of the volumetric moisture content at the conclusion of the run for uniform soil containing a 10 mm diameter macropore at the time of infiltrometer drainage (sec) to within one time step. The MPD infiltrometer is inserted to 0.05m depth in the top left corner. Soil containing a macropore is given in plots (a) top of the macropore connected to the surface and (b) with the top of the macropore at 0.025m below the surface. K_{sat}= 5x10^{-5}m/s in the uniform soil and 0.5m/s in the macropore.

The mathematical model of MPD inifltrometer assumes a capped spherical shape wetting front. But stratification or presence of macropores distorts the shape of the wetting front. To investigate the effect of macropore length on the shape of the wetting front, the moment of inertia (M) of the wetting front about the vertical axis was calculated for the simulations where the macropore is connected to the soil surface ($M_{connected\_pore}$) , for the

simulations where macropore is not connected to soil surface ($M_{not\_connected\_pore}$) and for uniform soil ($M_{uniform}$).

The moment of inertia was calculated as a function of time using the following equation.

$$M(t) = \int_0^t 2\pi\theta(t) r\, dr\, dz \qquad (20)$$

The ratio of the moment of inertia of the wetting front of the soil matrix containing a macropore is compared to the moment of inertia of the wetting front of uniform soil. This ratio is proposed to represent the shape of the wetting front. The ratio of M values at the instant the infiltrometer has emptied is provided in Table 3-2.

Table 3-2. Comparison of the moment of inertia of the wetting front that contains a macropore and wetting front of uniform soil

Length of macropore(m)	$M_{connected\_pore}/M_{uniform}$	$M_{not\_connected\_pore}/M_{uniform}$
0.05	0.88	0.98
0.1	0.73	0.94
0.2	0.54	0.86
0.3	0.42	0.79
0.4	0.33	0.75

From Table 3-2 we can observe that the ratio is less than 1 which indicates that the wetted bulge with a macropore is narrower than the wetting front of a uniform soil. When the macropore is connected to the surface the wetting front is narrower than the cases where macropore is not connected to the surface. A macropore buried 0.025m below the soil surface does not have much effect on the shape of the wetting front until the length of the macropore is higher than 0.1m.

COMPARISON OF SIMULATIONS WITH MPD INFILTROMETER:

Each of the simulations generates synthetic data of water level vs. time to be used in the MPD infiltrometer analysis. These synthetic data are input into the MPD spreadsheet along with initial and final moisture content. The values of K_{fs} and ψ were then obtained from the spreadsheet for each simulation.

Effective saturated hydraulic conductivity (K_{eff}) for the Richards equation solution were determined by best fitting the computed synthetic head vs time data with the Richards equation solutions assuming homogeneous conditions with no macropores and no soil layers. The input parameters of the homogeneous soil were the same as the input parameters of the top layer (Silty loam). The equivalent K_{eff} obtained from the numerical experiments on the Richards equation can then be compared with the field saturated hydraulic conductivity (K_{MPD}) obtained from the MPD spreadsheet in order to determine the accuracy of the MPD calculation method for nonhomogeneous soil. However, the calculation of the effective wetting front suction in layered soil is complicated because of different initial condition as well as initial soil water pressure in top and bottom layer. For this reason the effective wetting front suction was not calculated and the wetting front suction calculated from MPD analysis are not reported in this manuscript.

The values of K_{eff} and K_{MPD} are compared in Table 3-3 for various types of layered soil, where K_t is the K_{sat} value of the top soil (constant at 1.4×10^{-6}m/s), K_b is the K_{sat} value of the bottom soil, T is the thickness of the top soil and L_{max} is the depth of insertion of the MPD infiltrometer. From Table 3-3 we see that K_{MPD} is always higher than K_{eff}. For

layered soil K_{MPD} is 12 to 63% higher than K_{eff} while for uniform soil this value was found to be 10 to 36% (*Ahmed et al., 2014*). Of the 16 runs made with these different soil characteristics, the mean value of K_{MPD} was 28% higher than K_{eff} with a standard deviation of 12%, which can be compared to 21.6% +/-10 % higher in uniform soil (*Ahmed et al., 2014*).

Table 3-3 also indicates that low permeable soil dominates in the determination of both K_{MPD} and K_{eff}. From these simulations it was observed that the bottom soil does not have a substantial effect on effective hydraulic conductivity (K_{eff}) unless the bottom layer lies 0.05m or less below the soil surface ($L_{max}/T \geq 1.0$). In these cases K_{eff} is high if the bottom soil is coarser than the top. Correspondingly, K_{eff} is lower when the bottom soil is finer than the top soil. For T greater than or equal to 0.075m ($L_{max}/T \leq 0.67$), K_{eff} is close to the K_{fs} of the top soil which is a silty loam. Note that slowing of the wetting front for the case of fine-over-coarse material could lead to unstable flow as described by *Raats (1973),* and fingering as described by *Hillel (1988)* and *Jury (2004).* This instability phenomenon is not investigated here.

Table 3-3. Comparison between K_{MPD} and K_{eff} for different thicknesses of top soil and different K_{fs} values of bottom soil. L_{max} is set at 0.05 m. K_t is constant at 1.4×10^{-6}m/s.

Soil type	K_b(m/s)	K_b/K_t	L_{max}/T	K_{MPD}(m/s)	K_{eff}	K_{MPD}/K_{eff}	K_{eff}/K_b	K_{eff}/K_t
Loamy sand	3.47×10^{-05}	25	0.5	1.51×10^{-06}	1.18×10^{-06}	1.28	0.03	0.85
			0.67	1.58×10^{-06}	1.20×10^{-06}	1.32	0.03	0.86
			1	2.05×10^{-06}	1.40×10^{-06}	1.46	0.04	1.01
			2	4.04×10^{-06}	2.48×10^{-06}	1.63	0.07	1.79
Sandy clay loam	6.94×10^{-06}	5	0.5	1.49×10^{-06}	1.22×10^{-06}	1.22	0.18	0.88
			0.67	1.55×10^{-06}	1.26×10^{-06}	1.23	0.18	0.91
			1	1.87×10^{-06}	1.46×10^{-06}	1.28	0.21	1.05
			2	3.23×10^{-06}	2.30×10^{-06}	1.40	0.33	1.66
Silty loam	1.4×10^{-6}	1	Uniform soil	1.47×10^{-6}	1.4×10^{-6}	1.05	1	1
Sandy clay	2.78×10^{-07}	0.2	0.5	1.42×10^{-06}	1.17×10^{-06}	1.21	4.21	0.84
			0.67	1.30×10^{-06}	1.08×10^{-06}	1.20	3.88	0.78
			1	6.71×10^{-07}	6.00×10^{-07}	1.12	2.16	0.43
			2	3.74×10^{-07}	3.13×10^{-07}	1.19	1.13	0.23
Silty clay	5.56×10^{-08}	0.04	0.5	1.40×10^{-06}	1.12×10^{-06}	1.25	20.14	0.81
			0.67	1.21×10^{-06}	9.67×10^{-07}	1.25	17.39	0.70
			1	2.07×10^{-07}	1.74×10^{-07}	1.19	3.13	0.13
			2	7.93×10^{-08}	6.17×10^{-08}	1.29	1.11	0.04

Figure 3-6 shows the effect of the ratio L_{max}/T on the K_{fs} obtained from the MPD software (K_{MPD}). Figure 3-6 indicates that when $L_{max}/T \leq 0.67$ (T≥0.075m), K_{MPD} does not depend on the K_{fs} of the bottom soil. When the opening between the MPD insertion

depth (L_{max}) and the soil interface (T) is 0.025 m and above, most of the water infiltrates vertically and laterally through the top soil, regardless of the K_{fs} of the bottom soil, and K_{MPD} is dominated by the top soil. Figure 3-6 also indicates that when $L_{max}/T \geq 1$ (T≤0.05m), K_{MPD} is dominated by the bottom soil. When $L_{max}/T \geq 1$, the bottom surface of the MPD is inserted into the bottom soil and water will infiltrate through the bottom soil. Thus, in this case ($L_{max}/T \geq 1$) the K_{fs} of the bottom soil has an effect on the K_{eff} but the less permeable between the top and bottom soil will still dominate.

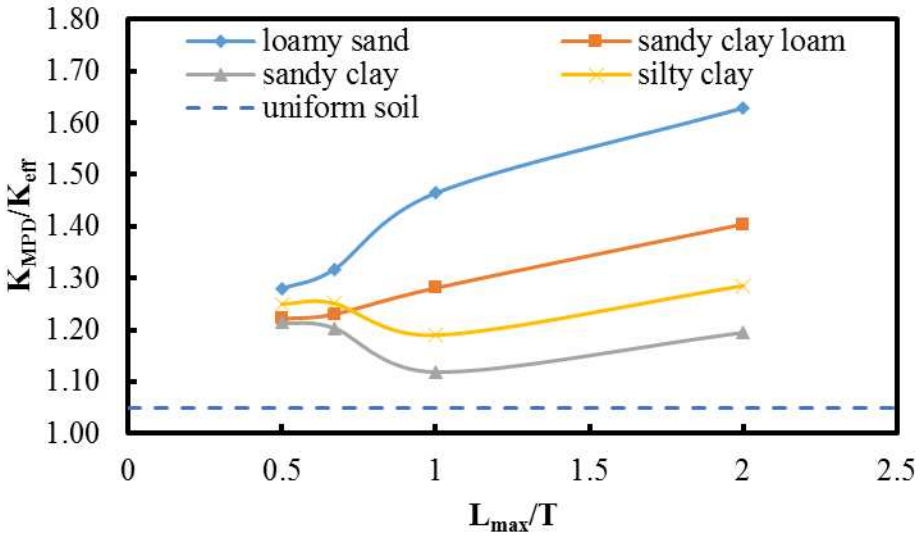

Figure 3-6. Effect of the bottom soil type on the K_{MPD} / K_{eff} ratio.

The K_{eff} and K_{MPD} determined with a 10 mm macropore, located in the center of the MPD Infiltrometer, connected and not connected to the surface are summarized in

Table 3-4 and Table 3-5, respectively. The MPD analysis with a macropore was within 4% and 29% of the effective field saturated hydraulic conductivity. Of the twenty runs with macropores, the mean value of K_{MPD} was 16% higher than K_{eff} with a standard deviation of 7%.

Figure 3-7 shows the effect of macropore length on K_{eff} for cases where the macropore is connected or not connected to the soil surface. Figure 3-7 indicates that the length of macropore does not have a substantial effect on K_{eff} if it begins 0.025m below the surface, but if the macropore is connected to the surface then K_{eff} can vary up to one order of magnitude as the macropore length increases from 0.05 to 0.4 m. The value of K_{eff} is thus substantially higher when the macropore is connected to the surface. Macropores not connected directly to the surface do not have a significant effect upon K_{eff}.

A comparison of

Table 3-4. K_{MPD} and K_{eff} with macropores of 10 mm diameter connected to the soil surface for various K_{fs} values and various pore lengths. and Table 3-5 indicate that when the length of the macropore is less than 0.2m the K_{MPD}/K_{eff} ratio is lower if the macropore is not connected to the surface than if it is connected. Previously from

Table 3-4 we can see that when macropore length is less than 0.2m, the $M_{not\_connected\_pore}/M_{uniform}$ is close to 1 (0.94~0.98), which indicates that, when macropore is not connected to surface, the shape of the wetting front is similar to that for uniform soil. So the assumption made for the mathematical model of MPD that the shape of the wetting front is capped spherical is more applicable in this case (macropore not connected) which leads a K_{MPD}/K_{eff} ratio closer to 1.

Table 3-4. K_{MPD} and K_{eff} with macropores of 10 mm diameter connected to the soil surface for various K_{fs} values and various pore lengths.

Length of macropore (m)	K_{sat}(m/s)	K_{MPD} (m/s)	K_{eff} (m/s)	K_{MPD}/K_{eff}	K_{eff}/K_{sat}
0.05	$5x10^{-04}$	$6.75x10^{-04}$	$5.30x10^{-04}$	1.27	1.06
	$5x10^{-05}$	$6.71x10^{-05}$	$5.53x10^{-05}$	1.21	1.11
	$5x10^{-06}$	$6.61x10^{-06}$	$5.60x10^{-06}$	1.18	1.12
	$5x10^{-07}$	$6.60x10^{-07}$	$5.63x10^{-07}$	1.17	1.13
0.1	$5x10^{-04}$	$1.14x10^{-03}$	$8.95x10^{-04}$	1.27	1.79
	$5x10^{-05}$	$1.12x10^{-04}$	$9.48x10^{-05}$	1.18	1.90
	$5x10^{-06}$	$1.12x10^{-05}$	$9.54x10^{-06}$	1.17	1.91
	$5x10^{-07}$	$1.12x10^{-06}$	$1.08x10^{-06}$	1.04	2.16
0.2	$5x10^{-04}$	$2.36x10^{-03}$	$2.02x10^{-03}$	1.17	4.04

	$5x10^{-05}$	$2.41x10^{-04}$	$2.04x10^{-04}$	1.18	4.08
	$5x10^{-06}$	$2.38x10^{-05}$	$2.07x10^{-05}$	1.15	4.14
	$5x10^{-07}$	$2.39x10^{-06}$	$2.11x10^{-06}$	1.13	4.22
0.3	$5x10^{-04}$	$3.86x10^{-03}$	$3.40x10^{-03}$	1.14	6.80
	$5x10^{-05}$	$4.48x10^{-04}$	$3.47x10^{-04}$	1.29	6.94
	$5x10^{-06}$	$4.04x10^{-05}$	$3.59x10^{-05}$	1.13	7.18
	$5x10^{-07}$	$4.04x10^{-06}$	$3.59x10^{-06}$	1.13	7.18
0.4	$5x10^{-04}$	$5.63x10^{-03}$	$5.08x10^{-03}$	1.11	10.16
	$5x10^{-05}$	$5.92x10^{-04}$	$5.15x10^{-04}$	1.15	10.30
	$5x10^{-06}$	$6.08x10^{-05}$	$5.43x10^{-05}$	1.12	10.86
	$5x10^{-07}$	$5.99x10^{-06}$	$5.45x10^{-06}$	1.10	10.90

Table 3-5. K_{MPD} and K_{eff} with macropores of 10 mm diameter beginning at 0.025m below soil surface for various K_{sat} values and various pore lengths.

Length of macropore(m)	K_{sat} **(m/s)**	K_{MPD} **(m/s)**	K_{eff} **(m/s)**	K_{MPD}/K_{eff}	K_{eff}/K_{sat}
0.05	$5x10^{-04}$	$5.66x10^{-04}$	$5.31x10^{-04}$	1.07	1.06
	$5x10^{-05}$	$5.66x10^{-05}$	$5.30x10^{-05}$	1.07	1.06
	$5x10^{-06}$	$5.69x10^{-06}$	$5.33x10^{-06}$	1.07	1.07
0.1	$5x10^{-04}$	$6.34x10^{-04}$	$5.81x10^{-04}$	1.09	1.16
	$5x10^{-05}$	$6.37x10^{-05}$	$5.84x10^{-05}$	1.09	1.17
	$5x10^{-06}$	$6.33x10^{-06}$	$5.85x10^{-06}$	1.08	1.17
0.2	$5x10^{-04}$	$6.91x10^{-04}$	$5.62x10^{-04}$	1.23	1.12
	$5x10^{-05}$	$6.91x10^{-05}$	$5.62x10^{-05}$	1.23	1.12
	$5x10^{-06}$	$7.02x10^{-06}$	$5.62x10^{-06}$	1.25	1.12
0.3	$5x10^{-04}$	$7.09x10^{-04}$	$5.82x10^{-04}$	1.22	1.16

	$5x10^{-05}$	$7.12x10^{-05}$	$5.81x10^{-05}$	1.23	1.16
	$5x10^{-06}$	$7.04x10^{-06}$	$5.78x10^{-06}$	1.22	1.16
0.4	$5x10^{-04}$	$7.21x10^{-04}$	$5.93x10^{-04}$	1.22	1.19
	$5x10^{-05}$	$7.17x10^{-05}$	$5.90x10^{-05}$	1.22	1.18
	$5x10^{-06}$	$7.22x10^{-06}$	$5.91x10^{-06}$	1.22	1.18

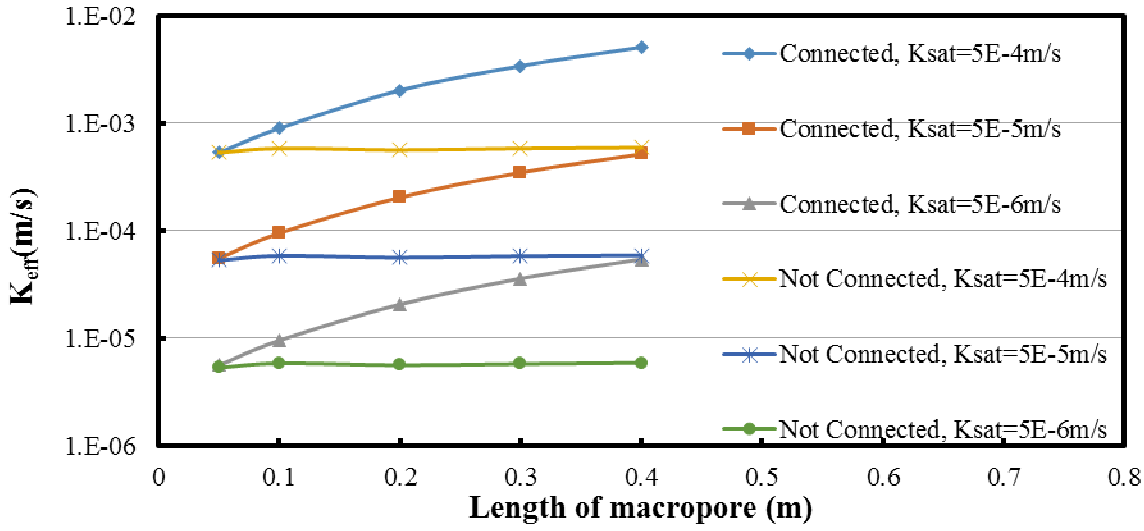

Figure 3-7. Effect of 10 mm diameter macropore length on K_{MPD} for saturated hydraulic conductivities of different orders of magnitude.

Similar to our analysis, *Wu et al. (1993)* used simultaneous equation approach (SEA) to estimate the K_{sat} of uniform soil containing macropore and layered soil. A finite element solution of the Richards equation was used to generate synthetic data to use in Philip, Guelph and Laplace model where K_{sat} of the upper and lower layers are prescribed. Then by using these data with SEA a new K_{sat} was estimated which is comparable to the K_{MPD} value in our analysis. But unlike to our analysis *Wu et al.* reported 3 times higher K_{sat} than the prescribed K_{sat} of the upper layer and 42 times higher effective K_{sat} than the prescribed K_{sat} of the lower layer while in our analysis the value of K_{MPD} and K_{eff} is

always between the K_{sat} value of top (K_t) and bottom (K_b) soil (Table 3-3). Also Wu et al. compared the K_{sat} obtained from SEA with prescribed K_{sat} value of top or bottom soil not with the effective K_{sat} value of the soil matrix. In our analysis we compared the K_{MPD} with K_{eff}. Again for the uniform soil containing macropore case, by using Richards' equation simulated generated data, the effective K_{sat} was estimated to be negative in Wu et al. analysis. These prove that MPD analysis provides better results for uniform soil containing and macropore and layered soil cases.

CONCLUSIONS

The MPD infiltrometer is suitable for infiltration practices because it can be performed relatively quickly to capture the large spatial variability that commonly occurs with infiltration rates. The MPD infiltrometer has been used at up to 20 locations simultaneously with a three-person team, allowing for up to 40 measurements per day. The results obtained from the MPD (K_{fs} and soil suction at the wetting front) has been compared with the numerical simulations for uniform soil (*Nestingen, 2007, Ahmed et al., 2014*) and with the double ring infiltrometer (*Ahmed et al., 2011*) in the field. But soil in the field is non-uniform in nature. The results obtained from the MPD infiltrometer for infiltration data synthesized with a computational solution of the Richards equation for axisymmetric flow in layered soil, and for a soil with a single vertical macropore. . The results are that the K_{fs} from MPD infiltrometer is an average of 28 +/- 12 % higher than the effective K_{fs} of the numerical solution for stratified soil and an average of 16 +/- 7 % for soil with a macropore. In a previous study by *Ahmed et al. (2014)* for homogeneous soils it was found that the MPD method a MPD over-prediction of 21.6 +/- 10 %. In

addition, a 28% overestimation is not large relative to the spatial variation of K_{fs} typically seen in the field. While neither stratified soil nor soil with a macropore develops a hemi-spherical wetting front, the model still estimates K_{fs} that is within 28+/-12% or 16+/-7% range for stratified soil or soil with a macropore, respectively, of the effective K_{fs} used in the simulations.

4. Field Infiltration Measurements in Grassed Swales

F. Ahmed, Department of Civil, Environmental and Geo-Engineering, University of Minnesota, Minneapolis, MN 55414; J. S. Gulliver, Department of Civil, Environmental and Geo-Engineering, University of Minnesota, Minneapolis, MN 55414; J. L. Nieber, Department of Bioproduct and Biosystem Engineering, University of Minnesota, St. Paul, MN 55108

EXECUTIVE SUMMARY:

Grassed swales or drainage ditches are an attractive BMP since they can reduce runoff volume by infiltrating water into the soil, filter sediments and associated pollutants out of the water, and settle solids onto the soil surface. In this study a total of 720 infiltration measurements were collected in five swales located in Twin-Cities, MN and one swale located in Madison, WI to characterize the field-saturated hydraulic conductivity (K_{fs}) derived from the infiltration measurements of these swales. Measurements were taken with a Modified Philip Dunne (MPD) infiltrometer, which allows collecting multiple measurements simultaneously. Field-saturated hydraulic conductivity was higher than expected. We hypothesize that this is due to plant roots creating macropores that break up the soil for infiltration. Statistical analysis was performed on the K_{fs} values to analyze the

effect of initial soil moisture content, season, soil texture class and distance in downstream direction on the geometric mean K_{fs} value of a swale. Because of high spatial variation of K_{fs} value in the same swale no effect of initial soil moisture content, season and soil texture class was observed on the geometric mean K_{fs} value. But the distance in downstream direction of the swale may have positive or negative effect on the K_{fs} value. An uncertainty analysis on the K_{fs} value indicated that approximately twenty infiltration measurements is the optimum number to obtain a representative geometric mean K_{fs} value of a swale.

Key words:

Field-saturated hydraulic conductivity, soil moisture content, infiltrometer, soil texture, statistical analysis, confidence interval.

INTRODUCTION:

Impervious surface areas, such as roads, parking lots and rooftops, lead to increased runoff volume which will increase the mass of pollutants that reach receiving water bodies (*Field 1975; Booth and Jackson 1997;. Kayhanian et al. 2007, 2012)* Stormwater control measures (SCMs) are designed to treat runoff to improve water quality before receiving water bodies (*National Research Council 2008*). Many conventional SCMs, such as catch basins, wetlands and retention ponds, are efficient in capturing suspended solids (e.g., *Wilson et al. 2009; Howard, et al. 2011, 2012)* but are not designed to treat for dissolved pollutants (*Van Buren et al. 1997; Lucas and Greenway; Erickson, et al. 2007, 2012; O'Neill and Davis 2012a, 2012b; LeFevre, et al. 2014*). Infiltration practices are believed to return the watershed towards a pre-development water balance and to

remove most pollutants, with the exception of chloride and nitrate, through filtering through and adsorption upon the soil matrix. (*National Research Council 2008; Davis et al. 2012*). These practices include permeable pavement, bioinfiltration, infiltration basins and grassed swales (*Erickson et al. 2013*).

Grassed swales are shallow, flat-bottomed, open vegetated channels with a 2 to 10 ft width that are designed to convey, filter and infiltrate stormwater runoff (*Barrett et al., 1998a; Deletic and Fletcher, 2005; NJ stormwater management technical manual, 2010*). They are often employed along highways, where highway medians and roadside drainage ditches may essentially act as grassed swales (*Barrett et al., 1998a; 1998b*). Figure 4-1 shows a roadside grassed swale on Hwy 51 in Arden Hills, Minnesota. They have the capability to reduce runoff volume and improve water quality. Volume reduction occurs primarily through infiltration into the soil, either as the water flows over the slide slope perpendicular to the roadway into the swale or down the length of the swale parallel to the roadway. Pollutant removal can occur by sedimentation of solid particles onto the soil surface, filtration of solid particles by vegetation, or infiltration of dissolved pollutants (with stormwater) into the soil (*Abida and Sabourin, 2006*).

Figure 4-1. The Roadside drainage ditch on Hwy 51 at off ramp to County Road E has been shown to infiltrate stormwater and act as a grassed swale

As with infiltration trenches and basins, grassed swales can become clogged with particles and debris in the absence of proper maintenance. Several studies have shown that a majority of stormwater pollutants are trapped in the upper soil layers (*Wigington et al., 1986; Mikkelsen et al., 1997; Dierkens and Geiger, 1999*), and in some cases the sediment deposits can begin to choke out the vegetated cover and create an erodible surface capable of contributing sediment and other pollutants directly downstream (*Erickson et al., 2010; 2013*).

The fraction of stormwater runoff that can be infiltrated by a grassed swale depends on many variables including rainfall intensity and total runoff volume, swale soil type, the maintenance history of the swale, vegetative cover in the swale, swale slope and other factors. Thus, reported swale performances have ranged from less than 10% to 100%

volume reduction. For example, using simulated runoff, *Yousef et al. (1987)* found that swales infiltrated between 9% (input rate of 0.079 *m/hr*) and 100% of the runoff (at 0.036 *m/hr*) with significant variability. Due to the wide range of performance *Yousef et al. (1987)* stated that in order to determine the performance of individual swales, each swale should be tested separately. Also because of this wide variability of infiltration rates, even within a single swale, multiple measurements should be made. New methods of measuring infiltration capacity have recently been developed (*Asleson et al., 2009; Olson et al., 2013; Paus et al., 2014; Ahmed et al., 2014*), where a rapid infiltration technique allows multiple measurements to be taken over a relatively large area. This is needed because the infiltration capacity at a given site will have substantial spatial variation (*Asleson et al., 2009; Olson et al., 2013*).

Despite the prevalence of grassed swales within roadway right-of-ways that convey and treat road runoff, data on the performance of swales with regards to infiltration and contaminant capture is relatively sparse. This research will document the infiltration parameters of five grassed swales/ drainage ditches located in the Twin Cities, MN and one swale located in Madison, WI.

METHODS

Site Selection

Sixteen highways were selected around the Twin-Cities metropolitan area in Minnesota where swales are located at the median or at the side of the highways. The texture analysis of the soil samples at the swales located near each of the highways was

characterized and one highway was selected for each soil texture classification. Soil samples were collected at the soil surface and at different depth below the surface up to 0.6m deep to investigate the soil profile with depth. For each highway three or four soil cores were collected from swales using a soil corer. These soil samples were brought into the lab for further analysis. The purpose of collecting soil cores is to perform textural analysis on the soil sample and identify the soil texture class of that swale. On each soil sample wet sieving analysis (*ASTM D6913*) and hydrometer analysis (*ASTM D422*) were performed. This combination is a standard method to determine % clay, % silt and % sand in a soil sample. Using these percentages in a textural triangle (*USDA, 2014*), the soil texture class was identified.

The lists of soil texture class for different swales are given in Table 4-1. In Table 4-1, if the same highway is addressed in two or more rows it indicates that the swale located in that highway contains all corresponding textural classes of soil (i.e. Hwy 35E, Hwy 35W near TH 10).

Table 4-1. Soil texture class of different swales located in Minnesota.

Swale locations	**Soil texture class**
Hwy 10, Hwy 35E, Hwy 35W near TH 10	Sand
Hwy 5, Hwy 47, Hwy 65, Hwy 96, Hwy 97, Hwy 77, Hwy 7, Hwy 35W Burnsville, Hwy 35E, Hwy 35W near TH 10	Loamy sand and Sandy loam
Hwy 51, Hwy 36	Loam and Sandy loam

Hwy 212	Silt loam and Loam
Hwy 13	Loam, Sandy clay loam and Silt

Based upon the soil texture class of the swales five highways were finally selected for this study for five types of soil combinations. At each swale, infiltration measurements were taken at the upstream and downstream reach using a Modified Philip Dunne (MPD) infiltrometer (*Ahmed et. al 2014*). At each reach 8 to 10 infiltration measurements were taken within a 7 *m* (20 *ft*) long stretch (Figure 4-2) in Fall 2011. A total of 17 to 20 infiltration measurements were collected at each swale. A brief description of the MPD Infiltrometer is presented in the next section. The infiltrometer was used to calculate the field-saturated hydraulic conductivity (K_{fs}) and capillary soil suction (ψ) of the soil at that location.

(a)

(b)

Figure 4-2. (a) Modified Philip Dunne (MPD) Infiltrometer, and (b) Collecting infiltration measurement at the swale located near Hwy 51, Arden Hills, MN using MPD Infiltrometer

Among these five swales three were chosen where repeated infiltration measurements were taken again in spring 2012 and summer 2012. For each swale a total of 20 infiltration measurements were taken at the upstream and downstream reach of the swale. The purpose of taking the measurements in Spring 2012 was to analyze the effect of season on the field-saturated hydraulic conductivity (K_{fs}) of the swale.

At each of these three swales infiltration measurements were further taken at the upstream, middle and downstream reaches in summer 2012 as shown in Figure 4-3. At each reach (upstream, middle and downstream) 18 to 21 infiltration measurements were taken repeatedly on three different days to maximize variation in the initial soil moisture content. The purpose was to analyze the effect of soil moisture content on geometric mean K_{fs} and distance from the outflow pipe downstream. The distance from the outflow

pipe was hypothesized to be important because sedimentation should increase as the pipe is approached, and the sedimentation could decrease the K_{fs}.

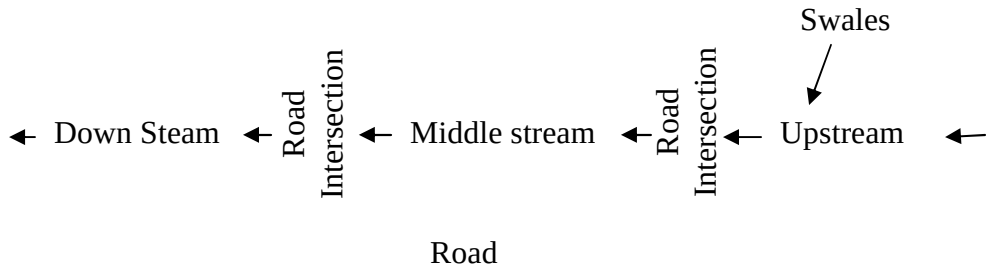

Figure 4-3. A schematic diagram of the reaches of grassed swales located next to road

In addition to the measurements taken at Minnesota's swale sites, a total of 108 infiltration measurements were taken in a swale located near Hwy 51 in Madison, WI, north of Hwy 12/18. The precipitation, inflow, and outflow monitoring data were available via the USGS National Water Information System (*U.S. Geological Survey, 2014*). The swale is 450 m long with an area of 4700 m^2. The area of the road that contributes to the runoff received by the swale is 14,500 m^2. This swale was divided into the upstream reach and the downstream reach where 83 and 25 infiltration measurements were taken respectively. Within a 330 m long stretch the swale was divided into 20 cross sections, 12.2 to 23.8 *m* apart and at each cross section 3 to 7 measurements were taken 1.2 *m* apart. Statistical analysis was performed on these field data, which is presented in the Results section.

Infiltrometer Operation

Ten soil samples from the soil surface were collected at each site on the test day by core method (*A.S.T.M. D 2937-04, 2004*) to determine the soil bulk density, porosity and

initial gravimetric soil moisture content (*Klute, 1986; ASTM, 2000, 2005*) of each soil sample. The mean initial soil moisture content was assumed to be uniform for the whole media. The mean porosity of the soil samples is assumed to be saturated soil moisture content. The MPD infiltrometer was inserted 5cm into the surface of the soil. The MPD infiltrometer was then filled to a certain height (usually between 30~40cm) with the water. The head of water over time during the test was recorded.

Infiltrometer Data Analysis

Background of MPD Infiltrometer

The mathematical model of the MPD infiltrometer is a modification of Philip's borehole permeameter model (*Philip 1993*). The assumptions that were made are: isotropic homogeneous

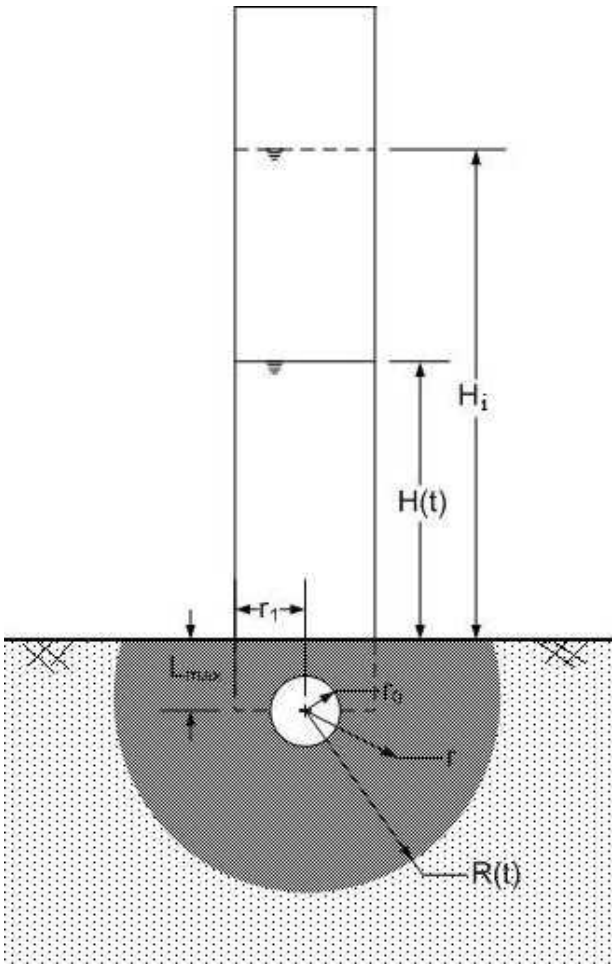

Figure 4-4. Important parameters of the MPD infiltrometer. H_i is the initial height of water; *H(t)* is the height of water at time *t;* Lmax is the depth of insertion into the soil; r_0 is the equivalent source radius; r_1 is the radius of the cylinder; *r*, any radius within the wetted front; and *R(t)* is the radius to the sharp wetted front at time *t*.

media, a Green-Ampt sharp wetting front and a spherical geometry for the wetting front. The equation for cumulative infiltration assuming capped sphere geometry as shown in Figure 4-4, is:

$$[H_i - H(t)]\pi r_1^2 = \frac{(\theta_s - \theta_i)\pi}{3}[2[R(t)]^3 + 3[R(t)]^2 L_{max} - L_{max}^3 - 4r_0^3] \quad (1)$$

Where H_i is the initial height of water; *H(t)* is the height of water at time *t;* L_{max} is the depth of insertion into the soil; r_0 is the equivalent source radius; r_1 is the radius of the

cylinder; r is any radius within the wetted front; and $R(t)$ is the radius to the sharp wetted front at time t; θ_s and θ_i are the saturated and initial moisture content of the soil. Equation (1) is valid when R(t) $\geq \sqrt{r_1^2 + L_{\max}^2}$. Following the analysis procedure by *Philip (1993)*, the pressure capillary potential drop ΔP from the spherical source to the wetting front becomes (*Ahmed et al., 2014*):

$$\Delta P = \psi - H(t) - L_{max} + \frac{L_{max}}{K_{fs}} \frac{dH}{dt} \tag{2}$$

The pressure capillary potential drop from the spherical source to the wetting front using Darcy's law would be (*Ahmed et al., 2014*):

$$\Delta P = \frac{\pi^2}{8} \int_{r_0}^{R} \frac{v_c(r)}{K_{fs}} dr$$

$$= \frac{\pi^2}{8} \left\{ (\theta_s - \theta_i) \frac{[R(t)]^2 + [R(t)] L_{max}}{K_{fs}} \frac{dR}{dt} - 2r_0^2 \right\} \left\{ \frac{\ln[R(t)[r_0 + L_{max}]/r_0[R(t) + L_{max}]}{L_{max}} \right\} \tag{3}$$

where K_{fs} is the field-saturated hydraulic conductivity and ψ is the wetting front suction. From equation (2) and (3) we develop the following equations; given in discretized form:

$$\Delta H = \frac{K_{fs}}{L_{max}} \left[\frac{\pi^2}{8} \left\{ (\theta_s - \theta_i) \left(\frac{(R^n)^2 + R^n L_{max}}{K_{fs}} \frac{(R^n - R^{n-1})}{\Delta t} \right) - 2r_0^2 \right\} \frac{\ln\left\{ \frac{R^n (r_0 + L_{max})}{r_0 (R^n + L_{max})} \right\}}{L_{max}} - \psi + H^{n-1} + L_{max} \right] \Delta t \tag{4}$$

$$\Delta t = \frac{\frac{\pi^2}{8} (\theta_s - \theta_i) \frac{(R^n)^2 + R^n L_{max}}{K_{fs} L_{max}} \ln\left\{ \frac{R^n (r_0 + L_{max})}{r_0 (R^n + L_{max})} \right\} (R^n - R^{n-1}) - \frac{L_{max}}{K_{fs}} \Delta H}{\psi - H^n - L_{max} + \frac{\pi^2}{8} \frac{2r_0^2}{L_{max}} \ln\left\{ \frac{R^n (r_0 + L_{max})}{r_0 (R^n + L_{max})} \right\}} \tag{5}$$

Two equations are provided in case the optimization procedure of either Eq. (4) or (5) does not converge. For more accuracy in the computation of K_{fs} and ψ the middle points between two consecutive observed head vs time data was interpolated using cubic spline approximation (*Hanna and Sandall, 1995*). Equation (1), (4) and the interpolated midpoint head difference were used to determine the value of K_{fs} and ψ. Likewise,

equation (1), (5) and the interpolated midpoint time difference were also used to determine the value of K_{fs} and ψ. The optimum solution for either case is achieved by minimizing the root mean square (rms) of the difference between interpolated head increment and predicted head increment (ΔH) and interpolated time increment and predicted time increment (Δt), by adjusting the values of field-saturated hydraulic conductivity (K_{fs}) and soil suction (ψ). The better of the two curve fits is used as the optimized K_{fs} and wetting front suction ψ. A computational spreadsheet procedure in MS Excel with the solver add-in and visual basic application (MPD spreadsheet) was developed to find solutions to equations (1), (4) and (5) and obtain optimal values of K_{fs} and ψ.

Procedure to run MPD spreadsheet

The general procedure of using the MPD spreadsheet for finding values of K_{fs} and ψ from the head versus time data is as follows:

1. Input all variables, including the arithmetic mean of initial and saturated soil moisture content, initial height of water inside the infiltrometer and the head versus time data.

2. For each measurement of head use the relationship in Equation (1) to find the corresponding distance of the sharp wetting front (SOLVER in Microsoft Excel 2010 and a macro were used to automate this step).

3. Estimate the change in head with respect to time and the change in wetting front distance with respect to time by using the forward finite difference method for all values of *R(t)* equal to or greater than the distance $\sqrt{r_1^2 + L_{\max}^2}$.

4. Make initial guesses for the values of K_{fs} and ψ. By default the initial guess for K_{fs} and ψ are set as $1x10^{-3}$cm/s and 100 cm, respectively. For a finer soil that has a K_{fs} value of less than $1x10^{-5}$cm/s, the initial guess of ψ might need to be changed to improve the convergence rate.

5. Solve Equations (4) and (5) for ΔH and Δt at each incremental value of *R(t)*.

6. Minimize the absolute difference between ΔH found in step 5 and change in measured head; and between Δt and the measured time interval by iterating the values of K_{fs} and ψ. Between these two optimization procedures (ΔH and Δt), the one with the minimum rms error between measured data and estimated data was chosen to calculate K_{fs} and ψ.

RESULTS AND DISCUSSION

Distribution of the derived field-saturated hydraulic conductivity (K_{fs})

The K_{fs} values of swales were observed to be log-normally distributed. As an example, the K_{fs} values of the Hwy 51, Madison swale are plotted in a histogram, showing the frequencies of occurrence in given intervals for the values of K_{fs} (Figure 4-5). To obtain a distribution that better fits a normal distribution, a logarithmic transformation was performed for all of the derived field-saturated hydraulic conductivity values. The

histogram of $log_{10}(K_{fs})$ for the Madison swale (Figure 4-6) indicates that the data is closer to a normal distribution in log space (a log-normal distribution). The statistical analyses on the derived field-saturated hydraulic conductivity values were therefore performed on the log-transformed distribution for all swales. The mean of a normal distribution in log space is the geometric mean, which will be reported for all K_{fs} values derived herein.

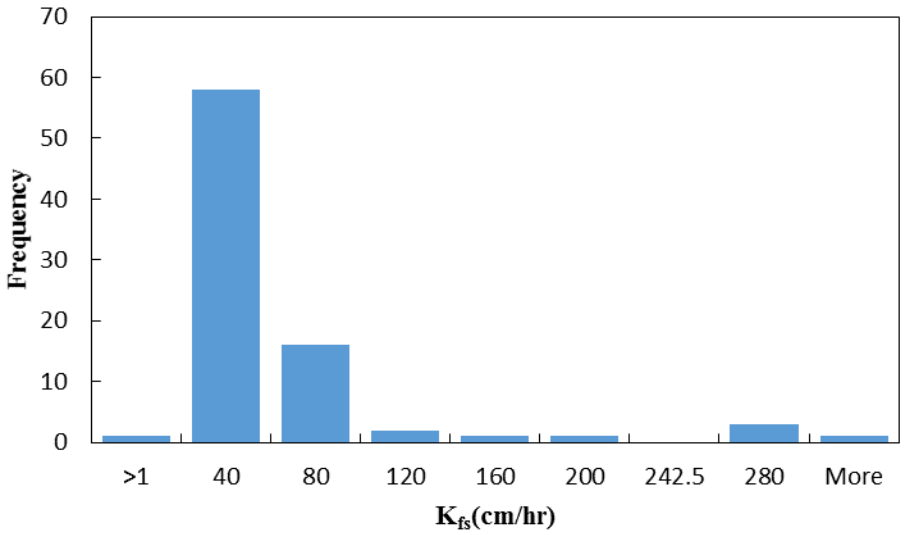

Figure 4-5. Histogram of actual K_{fs} values of Madison swale

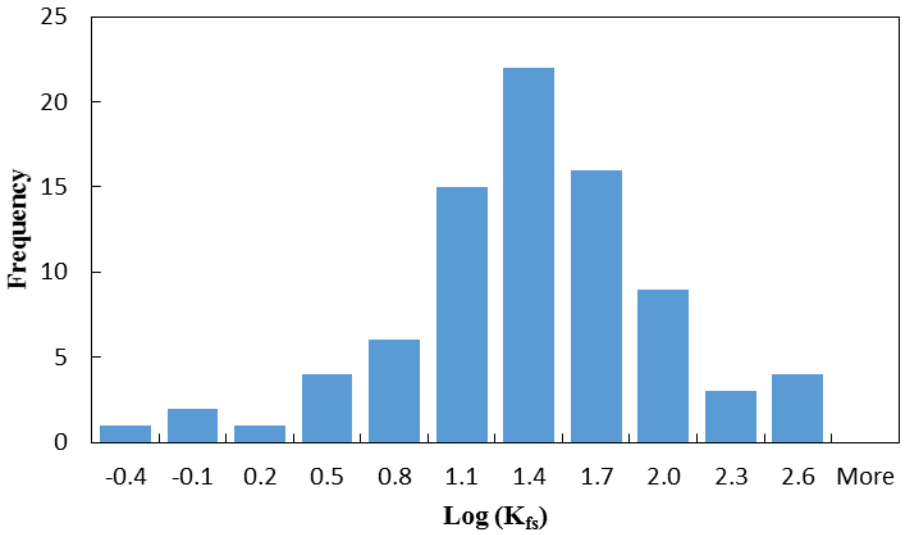

Figure 4-6. Histogram of log transformed K_{fs} values of Madison swale

Measurement Uncertainty Analysis

An uncertainty analysis was conducted on the 83, 42, 52 and 63 infiltration measurements on the Hwy 51, Madison swale, Hwy 47 swale, Hwy 51, Arden Hills swale and Hwy 212 swale respectively. The bootstrap nonparametric method (*Moore et al., 2009; Carpenter et al., 2000*) was used to develop confidence intervals around the geometric mean of each data set mentioned above. In the implementation of the bootstrap method, sampling was done with replacement and for 95% confidence interval the process was repeated 1000 times as recommended by *Carpenter et al. (2000)*. Figure 4-7 shows the 95% confidence interval around the geometric mean. The X-axis represents the number of measurements and Y axis represents the 95% confidence interval normalized by the geometric mean.

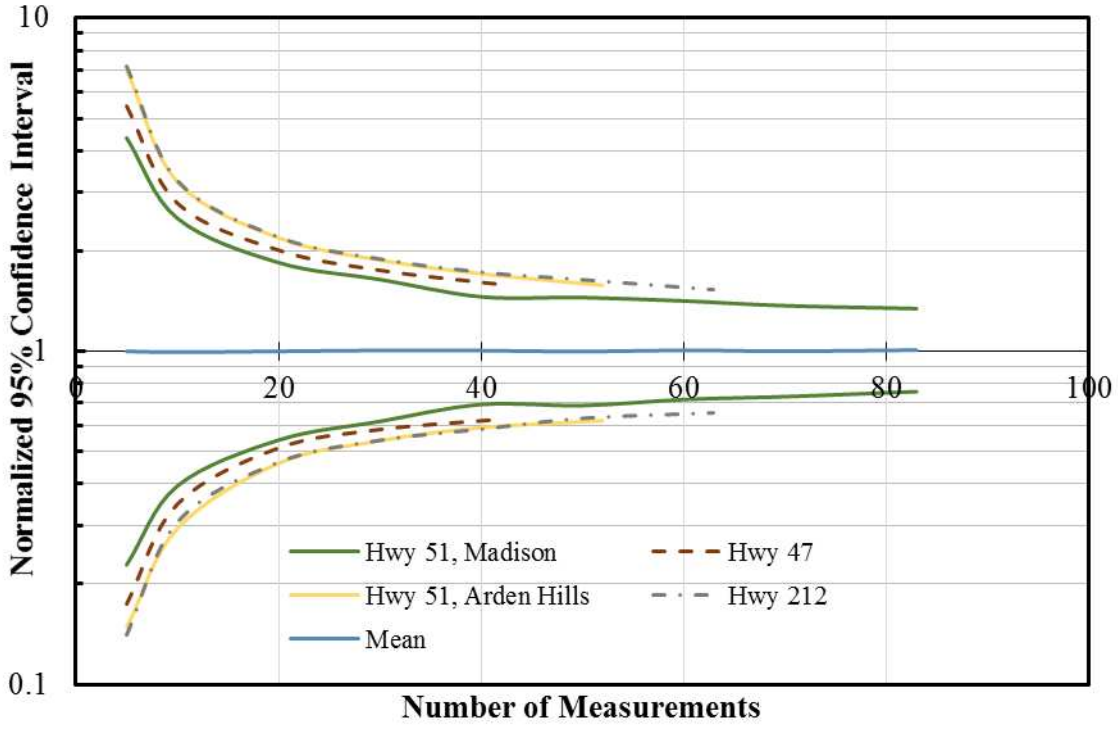

Figure 4-7. 95% confidence interval normalized by geometric mean

From Figure 4-7 we can conclude that

- Uncertainty of greater than a factor of 4 is associated with five or fewer measurements,
- With 10 measurements the uncertainty decreases to a factor of 2.5 ~ 3.25.
- With 20 measurements the uncertainty decreases to a factor of 1.8~2.8.
- Between 40 to 83 measurements uncertainty decreases to a factor of 1.7 (for 40 measurements) to 1.3 (for 83 measurements).

The uncertainty of the geometric mean does not decrease as rapidly beyond 20 measurements as it did below 20 measurements. This is roughly at the “knee” of the upper confidence interval curve. It indicates that based on the infiltration measurements

of the swales approximately 20 infiltration measurements is a balance between effort and accuracy of K_{fs} measurements.

Summary of infiltration measurements in swales

As discussed in the methods section, after collecting a soil sample from the swales located near sixteen highways, soil textural analysis was performed on the soil samples. For each soil texture class given in Table 4-1 one swale was selected for infiltration measurement and the number of swales was narrowed down to five on which infiltration measurements were taken in Fall of 2011. Table 4-2 shows the soil texture class, number of measurements and the mean initial soil moisture content on the day of measurement for these five swales that was taken in in Fall 2011, Spring 2012 and Summer 2012.

Table 4-2. Summary of infiltration measurements in Fall 2011, Spring 2012 and Summer 2012

Season	**Swale location**	**Soil texture class**	**# of measurement**	**Initial soil moisture content(%)**
Fall 2011*	Hwy 77	Loamy sand	17	18
	Hwy 47	Loamy sand/ Sandy loam	20	32
	Hwy 51	Loam/ Sandy loam	20	26
	Hwy 212	Silt loam/ Loam	20	29
	Hwy 13	Loam/ Sandy clay loam/ Silt	19	24

Spring 2012*	Hwy 47	Loamy sand/ Sandy loam	20	28
	Hwy 51	Loam/ Sandy loam	20	15
	Hwy 212	Silt loam/ Loam	20	20
Summer 2012*	Hwy 47 (upstream)	Loamy sand/ Sandy loam	21	22
			21	23
	Hwy 47 (middle)		21	31
			21	37
			19	43
	Hwy 47 (downstream)		21	23
			21	10
	Hwy 51 (upstream)	Loam/ Sandy loam	18	27
			18	30
			18	32
	Hwy 51 (middle)		21	33
			21	30
			18	15
	Hwy 51 (downstream)		21	29
			21	38
	Hwy 212 (upstream)	Silt loam/ Loam	21	24
			21	26

			21	25
	Hwy 212 (middle)		21	18
			12	39
			21	19
	Hwy 212 (downstream)		21	12
			21	29

*All measurements taken in the middle reach of the swale

Statistical Analysis on the derived K_{fs} values in Swales

The impact of soil texture class, location of the measurement (side slope/ center of the channel), season, soil moisture content and distance from outflow pipe downstream were observed for the swales. A summary of the statistical analysis is provided in this section.

Effect of Soil Texture Classes

Measurements were taken at five swales with different soil texture classes in Fall 2011, given in Table 4-3. The geometric mean value of K_{fs} varied from 0.75 to 3.9 cm/hr, a fairly small range given the variation in soil types. These swales are up to 50 years old, and it is possible that the macropores created by the grass in the swale provides them with a higher K_{fs} than would normally be expected. Since the number of measurements was not the same, a Tukey-Kramer method was used to determine differences in geometric mean K_{fs} value for different soil types. No significant difference was observed among geometric mean K_{fs} values within the 90, 95 and 99% confidence interval. The reason for this might be the high coefficient of variation (COV), which is the ratio between standard

deviation and arithmetic mean of log transformed K_{fs} data, between 1.09 and 14.4. A high COV value represents higher spatial variability of data, which is substantial in this case, thus making out any difference that might exist between soil textural classes. However, the factor of five variation in geometric mean K_{fs} is well below the expected variation of a factor of 20 (*Rawls et al., 1983*). This could be caused by plant root macropores in these swales.

Table 4-3. Geometric mean K_{fs} values in swales for different soil texture classes taken in Fall 2011.

Location	**Soil texture class**	**Number of measurements**	**Geometric mean of K_{fs}, (*cm/hr*)**	**Coefficient of variation (COV)* of K_{fs}**
Hwy 47	Loamy sand &	20	2	3.55
Hwy 51,	Loam &	20	2	3.34
Hwy 212	Silt loam &	20	0.75	14.38
Hwy 13	Loam, Sandy clay	19	3.9	5.60
Hwy 77	Loamy sand	17	2	1.09

*$COV = standard\ deviation\ of\ log transformed\ data / mean\ of\ log\ transformed\ data$

Derived K_{fs} values in Side Slope vs in Center of the Swale

A Tukey-Kramer test (*Kleinbaum et al., 2007*) was performed between K_{fs} values of the side slopes and K_{fs} values of center of the swales located in Minnesota and Madison, WI. A significant difference between geometric mean K_{fs} values of the side slopes and the center of the swale was observed for swales located in Minnesota and Madison, WI, at a

95% confidence interval with the exception of one swale in Hwy 212. This indicates that care should be taken to separately measure infiltration rates at the side slope and center of the swale. The geometric mean of K_{fs} from the side slopes and the center of the swales, shown in Table 4-4, indicate that there is no strong trend. At Hwy 212 and Hwy 47, the side slopes had a higher K_{fs} than the center of the swale, and at Hwy 51 in Minnesota and Madison, the side slopes had a lower K_{fs} than the center of the swale. Thus, while the side slopes are different than the center of the swale, there is no indication that either will have a higher K_{fs}. There is, therefore, no observed evidence that sedimentation in the center of the swale causes a reduction in infiltration. This is a different result than postulated by *Barrett (1998a).* One reason could be that the growth of plant roots in the center of the swale creates macropores that alleviate sedimentation-induced reduction of infiltration rates.

Table 4-4. Comparison between geometric mean K_{fs} at the center and side slope of the swales. K_{fs} = Geo-mean x $10^{\pm w}$

Location	Center of the swale			Side slope of the swale		
	# of meas.	Geo-mean K_{fs} (*cm/hr*)	95% C.I. of Log K_{fs} *(w)*	# of meas.	Geo-mean K_{fs} (*cm/hr*)	95% C.I. of Log K_{fs} *(w)*
Hwy 212, Chaska, MN	78	0.8	0.2	90	1.31	0.16
Hwy 47, Fridley, MN	63	2.9	0.2	87	6.5	0.2
Hwy 51, Arden Hills, MN	78	4.8	0.16	81	2.2	0.16
Hwy 51, Madison, WI	13	45.7	0.25	70	16	0.14

Effect of Season

A summary of the analysis using the infiltration measurements that were taken at three swales (Hwy 212, Hwy 47 and Hwy 51) of different soil texture classes for two seasons are given in Table 4-5. The geometric mean of K_{fs} was higher in Spring 2012 for Hwy 51 and lower for Hwys 47 and 212. The differences, however, were not great compared to the COV of each data set. Since the number of measurements is the same for each treatment, two factor ANOVA tests were performed on season. No significant difference was observed between the geometric mean K_{fs} values of fall and spring with 50 to 95% confidence intervals, partially due to the high COV (1.92~14.38).

Table 4-5. Summary of the analysis using infiltration measurements in Fall 2011 and Spring 2012.

Location	Fall 2011			Spring 2012		
	Number of measurements	**Geometric mean of K_{fs}, (cm/hr)**	**COV* of K_{fs}**	**Number of measurements**	**Geometric mean of K_{fs}, (cm/hr)**	**COV* of K_{fs}**
Hwy 47	20	2	3.55	20	1.5	4.94
Hwy 51, Arden Hills	20	2	3.34	20	2.8	1.92
Hwy 212	20	0.75	14.38	20	0.45	2.66

*$COV = standard\ deviation\ of\ log\ transformed\ data / mean\ of\ log\ transformed\ data$

Effect of Moisture Content

Initial moisture content should not affect the measurement of K_{fs}. To test this assumption infiltration measurements were repeated at each reach (upstream, middle and downstream) of each swale (Hwy 47, Hwy 51 and Hwy 212) in order to result in different initial moisture contents. The results, of this investigation shown in Table 4-6 are mixed. At Hwy 51 (downstream), K_{fs} went up with an increase in initial moisture content. At Hwy 47(downstream) and Hwy 212 (downstream), K_{fs} went down with an increase in initial moisture content. At Hwy 47 (middle), Hwy 51 (upstream), Hwy 51 (middle) and Hwy 212 (middle), K_{fs} went both up and down with an increase in initial moisture content. It appears that initial moisture content does not substantially affect K_{fs} in any consistent manner, as was expected for the Green-Ampt analysis technique.

The Tukey-Kramer test for significant differences confirms the above result. The test resulted in no significant difference among geometric mean K_{fs} value in the same swale for different moisture content within 90, 95 and 99% confidence interval, with the exception of one swale (Hwy 47, middle). In this swale the geometric mean K_{fs} for moisture content of 37% was statistically significantly different than the geometric mean K_{fs} for moisture content of 43% at the 90, 95 and 99% confidence interval. These statistical tests confirm that field-saturated hydraulic conductivity is a soil property that, with the Green-Ampt analysis, is relatively unchanged with the change of initial moisture content.

Table 4-6. Summary of the analysis using infiltration measurements with different moisture content

Location	Initial moisture content (%)	Number of measurements	Geometric mean of K_{fs} (*cm/hr*)	COV* of K_{fs}
Hwy 47 (middle)	31	21	1.7	4.16
	37	21	3.85	1.49
	43	19	0.85	15.21
Hwy 47 (downstream)	23	21	11.5	0.58
	10	21	17	0.24
Hwy 51 , Arden Hills(upstream)	27	18	6.5	0.78
	30	18	5.7	0.87
	32	18	2.1	2.58
Hwy51, Arden Hills (middle)	33	21	1.75	3.36
	30	21	4.45	0.8
	15	18	2.8	1.87
Hwy 51 , Arden Hills(downstream)	29	21	2	2.85
	38	21	4	1.23
Hwy 212 (middle)	18	21	0.45	2.39
	39	12	0.3	0.93
	19	21	1.05	32.41
Hwy 212 (downstream)	12	21	6.53	1.06
	29	21	2.03	2.80

*$COV = standard\ deviation\ of\ log\ transformed\ data / mean\ of\ log\ transformed\ data$

Effect of Distance from Downstream Outflow Pipe

At each of the three swales three reaches were selected where 41 to 61 infiltration measurements were taken at different distances from the outflow pipe. The purpose was

to test whether sediment that would be eroded in the swale during a large storm could settle near the outlet pipe. The geometric mean value of each reach was calculated and a Tukey-Kramer test was performed to see if there are significant differences among geometric mean K_{fs} for three different reaches of the same swale for 90, 95 and 99% confidence intervals. From this test it was observed that in some cases there is a significant difference among the geometric mean K_{fs} of the same swale and in some cases there is no significant difference. For further investigation, regression analysis was performed on these data. For all three highways it was found that there is significant difference in at least one of the geometric mean K_{fs} values among three reaches. The regression equations for all three swales are as follows:

$$\text{Hwy 47: } K_{fs} = 10^{1.82-0.96x} \tag{6}$$

$$\text{Hwy 212: } K_{fs} = 10^{1.52-1.16x} \tag{7}$$

$$\text{Hwy 51: } K_{fs} = 10^{-0.57+0.85x} \tag{8}$$

where, x is the distance from upstream (*km*), and K_{fs} is the field-saturated hydraulic conductivity (*cm/hr*). Over the length of each swale in the downstream direction (approximately a quarter km), the geometric mean K_{fs} of Hwy 47 decreased by a factor of 1.73, the geometric mean K_{fs} of Hwy 212 decreased by a factor of 2.0 and the geometric mean K_{fs} of Hwy 51 increased by a factor of 1.6.

We can conclude that in some cases geometric mean K_{fs} will increase and in some cases geometric mean K_{fs} will decrease with distance downstream. In general, one might expect to have lower K_{fs} value downstream because of increased sedimentation as the pipe is approached. However, vegetation density, erosion, the presence of macropores, soil bulk

density and soil compaction can have an effect on the K_{fs} values which might increase or decrease the geometric mean K_{fs} value downstream. As a result, there was no consistent trend for K_{fs} to decrease with distance in the downstream direction, and thus no evidence of sedimentation reducing K_{fs} in the sedimentation zones. It is possible that the grass growth and associated macropores kept the soil permeable to water, such that the effects of sedimentation on infiltration rates would be reduced.

CONCLUSION

Six roadside swales were selected for analysis of infiltration rates, chosen to represent the range of soil samples found in Minnesota and Wisconsin, USA. The near-surface (upper 20cm) K_{fs} values of the six swales varied from 0.75 *cm/hr* to 15.5 *cm/hr*, and were roughly a factor of 2.8 (mean) or 1.5 (median) greater than the published mean values (*Rawls et al., 1983*) for the soil texture classes. This may be due to roots creating macropores in the near-surface soil, which is normally not taken into consideration in laboratory soil permeability tests.

For these measurements we found that there is no statistically significant evidence that soil texture class has an effect on the mean field-saturated hydraulic conductivity of a swale. One reason for this might be the high coefficient of variation (COV), but the variation in K_{fs} were lower than those expected for these soil type from the literature (*Rawls et al., 1983*). In addition soil moisture content and season has no statistically significant effect on the mean field-saturated hydraulic conductivity of a swale. This is expected, because K_{fs} values should not be dependent upon soil moisture and should not change significantly with season, within the high spatial variation of K_{fs}. This observation

is a verification of the validity of the MPD infiltrometer in measuring highly spatially variable K_{fs} values. Finally the number of measurements of K_{fs} is recommended to be obtained from Figure 4-7 to capture the spatial variability and estimate a geometric mean K_{fs} value with a sufficiently low uncertainty.

The K_{fs} values at the side slope are observed to be different than in the center of the swale, but not necessarily higher. This could be attributed to sedimentation in the center of the swale causing a reduction in K_{fs} values, but also result of roots in the vegetated swale creating macropores which will help to increase K_{fs}. Distance from the downstream may or may not have an effect on the geometric mean K_{fs} of the swale similar to what was found in the literature (*Yonge 2000, Barrett 2004a, 2004b, Ahearn and Tveten 2008*). The swale located in Madison did not show any evidence of the effect of the distance from downstream on geometric mean K_{fs} of the swale. On the other hand, the swales located in Minnesota showed evidence that the distances from downstream can have a positive or negative effect on the cross-sectional geometric mean K_{fs}. This result implies that infiltration measurements should be spread over the swales of interest to obtain accurate results. Deposition at the lower reaches of the swale did not appear to cause a lower K_{fs} in that region, possibly because the grass roots broke up the sedimentation and created macropores in the near-surface soil or because sedimentation did not favor the lower reaches of the swale.

5. Overall Summary and Conclusion

Soil compaction and particle accumulation can severely reduce the infiltration rate of stormwater infiltration practices. The MPD infiltrometer can be used to determine when and where to perform maintenance in stormwater infiltration practices. Infiltration data synthesized with a computational solution of the Richards equation for uniform soil, layered soil and soil containing a macropore were analyzed with the MPD theory and compared with an infiltration parameter (K_{fs}) obtained from Richards' equation. Though neither layered soil nor soil with a macropore develop a hemi-spherical wetting front, which is the assumption of MPD analysis, the MPD model provides an acceptable estimate of K_{fs}. The MPD analysis overestimated the results obtained from Richards equation by 10 to 36% for uniform soil, which could be considered a calibration, 12 to 63% for layered soil and 4 to 29% for uniform soil containing macropore. The possible reasons of this overestimation are 1) the value of the shape factor proposed by Philip (1993) which does not fully account for the possible effects of capillary soil suction on wetted volume shape, and 2) the wetting front is neither sharp nor necessarily spherical in shape. Nevertheless, the error in K_{fs} values produced by the MPD infiltrometer is small compared to the orders of magnitude of variability in K_{fs} observed in the field.

Grassed swales are capabile of reducing runoff volume and improving water quality, but data on the performance of swales with regards to infiltration is limited. The MPD infiltrometer was applied on six roadside swales selected in Minnesota and Wisconsin, USA to characterize their infiltration property. No statistically significant difference was observed on geometric mean K_{fs} values of the same swale for different initial soil

moisture content, season and soil texture class. But in some cases significant difference was observed on geometric mean K_{fs} value with the variation of distance from the downstream. Co-efficient of variation of K_{fs} values were between 1 and 14, which is a verification of the necessity of the MPD infiltrometer (or another minimal volume infiltrometer) in measuring spatially variable K_{fs} values.

FUTURE STUDY

One reason of the overestimation of K_{fs} in MPD analysis might be due to the distortion of the actual flow path lines caused by the no-flow boundaries of the infiltrometer. This distortion should increase with increasing capillarity and should effect the β value. In MPD analysis $\beta = \frac{\pi^2}{8}$ was used as assigned by Philip (1993); but it is not clear if this constant value of β is correct, or whether it would be better to assign a value of β that accounts for capillarity. Reynolds (2011) suggested this coefficient to be 1 and in his analysis by using β = 1 the measured K_{fs} value was consistently more accurate (≤20% difference). In future studies this effect should be examined further.

6. Bibliography

Abernethy R.B., R.P. Benedict, R.B. Dowdell, 1985, "ASME measurement uncertainty", Journal of Fluids Engineering, 107(2), P 161-164.

Abida H. and Sabourin, J. F., 2006. Grass swale-perforated pipe systems for stormwater management. *Journal of Irrigation and Drainage Engineering*, 132(1), 55-63.

Ahearn, D., and Tveten, R., 2008. Legacy LID: Stormwater treatment in unimproved embankments along highway shoulders in Western Washington, *International Low Impact Development Conference*, November 16-19, 2008, Seattle, Washington.

Ahmed F., J. Gulliver, and J. Nieber, 2011, "Rapid Infiltration Measurement of LID Best Management Practices", *EWRI Conference Proceedings*, Palm Spring, CA

Ahmed F., J.S. Gulliver, J.L. Nieber, 2011, "A New Technique to Measure Infiltration rate for Assessing Infiltration of BMPs", *International Conference on Urban Drainage*, Porto Alegre, Brazil, September.

Ahmed F., R.S. Nestingen, , J. L Nieber, J.S. Gulliver and R. M. Hozalski, 2014 "Modifications to the Philip-Dunne Permeameter for Assessment of Surface Infiltration Rates," *Vadose zone journal*, accepted.

Asleson, B.C., R.S. Nestingen, J.S. Gulliver, R.M. Hozalski, and J.L. Nieber, 2009. "Assessment of Rain Gardens by Visual Inspection and Controlled Testing," *Journal of the American Water Resources Association*, 45(4), 1019-1031.

A.S.T.M. C136, 2006. Standard test method for sieve analysis of fine and coarse aggregates., *Annual Book of ASTM Standards*, 04.02. Amer. Soc. Testing Materials, West Conshohocken, PA.

A.S.T.M. D2216-05, 2005. Standard Test Method for Laboratory Determination of Water (Moisture) Content of Soil and Rock by Mass. *Annual Book of ASTM Standards*, 04.08. Amer. Soc. Testing Materials, West Conshohocken, PA.

ASTM. D3385-03, 2003. Standard test method for infiltration rate of soils in field using double-ring infiltrometer. *Annual Book of ASTM Standards* 04.08. Amer. Soc. Testing Materials, West Conshohocken, PA

A.S.T.M. D 4643-00, 2000. Standard Test Method for Determination of Water (Moisture) Content of Soil by the Microwave Oven Method. *Annual Book of ASTM Standards*, Amer. Soc. Testing Materials, West Conshohocken, PA.

A.S.T.M. D 2937-04, 2004. Standard Test Method for Density of Soil in Place by the

Drive-Cylinder Method. *Annual Book of ASTM Standards, 04.08. Amer. Soc. Testing Materials*, West Conshohocken, PA

A.S.T.M. D422-63, 2007. Standard test method for particle size analysis. *Annual Book of ASTM Standards, D18.03 Amer. Soc. Testing Materials*, West Conshohocken, PA

A.S.T.M. D6913-04, 2009. Standard test methods for particle size distribution (Gradation) of soils using sieve analysis, D18.03. *Annual Book of ASTM Standards, Amer. Soc. Testing Materials*, West Conshohocken, PA

Bagarello V., Iovino M., Elrick D., 2004, A simplified falling head technique for rapid determination of field saturated hydraulic conductivity, Soil Sci. Soc. Am. J., 68:66-73.

Barontini S., Ranzi R., Bacchi B., 2007 ,"Water Dynamic in a Gradually Nonhomogeneous Soil Described by the Linearized Richards Equation", *Water Resource Research*, Vol 43(8), W08411, doi:10.1029/2006WR005126.

Barrett, M.E., Walsh, P.M., Malina, J.F., and Charbeneau, R.B., 1998a. Performance of vegetative controls for treating highway runoff, *Journal of Environmental Engineering*, 124(11), 1121-1128.

Barrett, M.E., Keblin, M.V., Walsh, P.M., Malina, J.F., and Charbeneau, R.B., 1998b. Evaluation of the performance of permanent runoff controls: summary and conclusions, *Center for Transportation Research*, University of Texas at Austin, Report #: 2954-3F, Available online at: <http://www.utexas.edu/research/ctr/pdf_reports/2954_3F.pdf>

Barrett, M.E., 2004a. Performance and design of vegetated BMPs in the highway environment, *Critical Transitions In Water And Environmental Resources Management, Proceedings of The 2004 World Water and Environmental Resources Congress*, June 27-July 1, 2004, Salt Lake City, Utah.

Barrett, M.E. 2004b. Performance and design of vegetated BMPs in the highway environment. *Center for Research in Water Resources*, University of Texas, Austin, TX, USA.

Beven K., Germann P. 1982, "Macropores and Water Flow in Soils", *Water Resources Resaerch*, Vol. 18, No. 5, P 1311-1325.

Beven K., 1984 ,"Infiltration Into a Class of Vertically Nonuniform Soils", *Hydrological Sciences Journal*, 29(4): 425-434.

Buower H., (2002), Artificial recharge of groundwater: hydrogeology and engineering, Hydrogeology Journal, Vol. 10, iss. 1, 121-142

Booth, D. B., and Jackson, C. R. (1997). "Urbanization of aquatic Systems: Degradation thresholds, stormwater detention, and the limits of mitigation." *J.Am.Water Resour.Assoc.*, 33(5), 1077-1090.

Carpenter, J. and J. Bithell (2000). Bootstrap Confidence Intervals: when, which, what? A practical Guide for Medical Statisticians." *Statistics in Medicine* 19: 1141-164.

Carsel R.F. and R.S. Parrish ,1988. Developing joint probability distributions of soil water retention characteristics, *Water Resour. Res.*, 24, 5, 755-769.

Celia, M.A, E.T. Bouloutos, and R.L. Zarba, 1990. A general mass conservative numerical solution for the unsaturated flow equation, *Water Resour. Res*., 26: 1483-1496.

Cheng, Q., X. Chen, X. Chen, Z. Zhang, and M. Ling, 2011. Water infiltration underneath single-ring permeameters and hydraulic conductivity determination, *J. Hydrol*., 398: 135-143.

COMSOL, 2013. COMSOL Multiphysics Users Guide. Version 3.5a Documentation.

Davis, A. P., Traver, R. G., Hunt, W. F., Lee, R., Brown, R. A., and Olszewski, J. M. (2012). "Hydrologic Performance of Bioretention Storm-Water Control Measures." *J.Hydrol.Eng.*, 17(5), 604-614.

Deletic, A., and Fletcher, T. D., 2005. Performance of grass filters used for stormwater treatment- A field and modelling study, *Journal of Hydrology*, 317(3-4), 261-275.

Dierkes, C., Geiger, W. 1999. Pollution retention capabilities of roadside soils, *Water Science & Technology*, 39, 201-208.

Erickson, A.J., J.S. Gulliver and P.T. Weiss, 2007. "Enhanced Sand Filtration for Storm Water Phosphorus Removal," *Journal of Environmental Engineering*, 133(5), 485-497

Erickson, A.J., J.S. Gulliver, J.H. Kang, P.T. Weiss, and C.B. Wilson, 2010, "Maintenance of Stormwater Treatment Practices," *Journal of Contemporary Water Research and Education*, 146, pp. 75-82.

Erickson, A.J., J.S. Gulliver and P.T. Weiss, 2012, Capturing Dissolved Phosphorus with Iron Enhanced Sand Filtration, *Water Research*, 46**(**9), 6601–6608.

Erickson, A.J., Weiss, P.T. and Gulliver, J.S., 2013, *Optimizing Stormwater Treatment Practices: A Handbook of Assessment and Maintenance*, Springer, New York, NY, Field, R. (1975). "Coping with urban runoff in the United States." *Water Res.,* 9(5-6), 499-505.

.

Hanna O. T., Sandall O.C. 1995. Computational Methods in Chemical Engineering, *Prentice Hall PTR*

Hillel J., Baker R.S., 1988, "A Descriptive Theory of Fingering During Infiltration into Layered Soil", *Soil Science*, 146(1): 51-56.

Howard, A., O. Mohseni, J.S. Gulliver and H.G. Stefan, SAFL Baffle Retrofit for Suspended Sediment Removal in Storm Sewer Sumps, *Water Research*, 45: 5895-5904, 2011.

Howard, A., O. Mohseni, J.S. Gulliver and H.G. Stefan, Use of Standard Sumps for Suspended Sediment Removal from Stormwater, *Journal of Hydraulic Engineering*, 138(6), 491-502, 2012.

Jury W.A., Horton R. 2004, Soil Physics, John Wiley & Sons, Inc.

Kayhanian, M., Suverkropp, C., Ruby, A., and Tsay, K. 2007. "Characterization and prediction of highway runoff constituent event mean concentration." *J. Environ. Manage.*, 85(2), 279–295.

Kayhanian, M., B. Fruchtman, J. S. Gulliver, C. Montanaro, E. Raniere and S. Wuertz, 2012 Review of Highway Runoff Characteristics: Comparative Analysis and Universal Implications, *Water Research*, 46(9), 6609 -6624.

Kleinbaum D. G., Kupper L. L., Nizam A., Muller K. E. 2007. Applied regression analysis and other multivariable methods, *Duxbury Press*, Belmont, CA.

Klute, A., 1986. Methods of Soil Analysis, Part I. Physical and Mineralogical Methods, 2nd edition. *Soil Science Society of America*, Inc. Publisher, Madison, WI.

Lassabatere L., Angulo-Jaramillo R., Soria Ugalde J. M., Cuenca R., Braud I., Haverkamp R., 2006, Beerkan estimation of soil transfer parameter through infiltration experiments- BEST, Soil Sci. Soc. Am. J., 70:521-532.

LeFevre, G.H., K.H. Paus, P. Natarajan; J.S. Gulliver, P.J. Novak, and R.M. Hozalski, 2014, A Review of Dissolved Pollutants in Urban Stormwater and their Removal and Fate in Bioretention Cells, *Journal of Environmental Engineering*, In Press.

Lucas, W.C., Greenway, M. 2008. “Nutrient retention in vegetated and nonvegetated bioretention mesocosms.” *J. Irrig. Drain Eng.*, 134(5), 613-623.

Mikkelsen, P., Häfliger, M., Ochs, M., Jacobsen, P., Tjell, J. 1997. Pollution of soil and groundwater from infiltration of highly contaminated stormwater-a case study, *Water Science & Technology*, 36 (8-9), 325-330.

Moore D., McCabe G. P., Craig B. A., 2009, Introduction to the practice of statistics, sixth edition, *W. H. Freeman and Company*, New York ,NY.

Mualem Y., 1976, “A New Model for Predicting the Hydraulic Conductivity of Unsaturated Porous Media”. *Water Resource Research*, 12(3): 513-522.

Munoz-Carpena, R., C. M. Regalado, J. Alvarez-Benedi, and F. Bartoli, 2002. Field evaluation of the new Philip-Dunne permeameter for measuring saturated hydraulic conductivity. *Soil Sci.*, 167:9-24.

Nestingen, R. S., 2007. The comparison of infiltation devices and modificaiton of the Philip-Dunne Permeameter for the Assessment of Rain Gardens, M.S. Thesis, University of Minnesota, Minneapolis, Minnesota.

Nimmo J. R., Schimdt K. M., Perkins K. S., Stock J. D., “Rapid Measurement of Field Saturated Hydraulic Conductivity for Area Characterization”, *Vadose Zone Journal*, 8, 142-149

National Research Council. (2008). "Urban Stormwater Management in the United States." *Rep. No. Committee on Reducing Stormwater Discharge Contributions to Water Pollution, Water Science and Technology Board, Division on Earth and Life Studies.*, ,The National Academies Press, Washington, D.C.

Olson, N., 2010. “Quantifying stormwater infiltration rates on developed soils amended with tillage and compost ,” M.S. Thesis, University of Minnesota, Minneapolis, MN.

Olson, N.C., J.S. Gulliver, J.L. Nieber, and M. Kayhanian, 2013. Remediation to Improve Infiltration into Compact Soils, *Journal of Environmental Management*, 117, 85-95.

O’Neill, S. W., and Davis, A. P. (2012a). “Water treatment residual as a bioretention amendment for phosphorus. I: Evaluation studies.” *J. Environ. Eng.*, 138(3), 318-327.

O’Neill, S. and Davis, A. (2012b). “Water treatment residual as a bioretention amendment for phosphorus. II: Long-term column studies.” *J. Environ. Eng.*,138(3), 328-336.

Parr, J.R., Bertrand, A.R., 1960. Water infiltration into soils. Advances in Agronomy, 12, 311-363.

Paus, K.H., J. Morgan, J.S. Gulliver, T. Leiknes and R.M. Hozalski, Assessment of the Hydraulic and Toxic Removal Capacities of Bioretention Cells after 2 to 8 Years of Service, *Water, Soil and Air Pollution*, 225 (1803), 2013.

Peterson A.E., R.M.Dixon, 1971,"Water Movement in Large Soil Pore", Res. Rep. 75, pp, 1-8, Res. Div. Collage of Agricultural Life Science. University of Wisconsin, Madison, WI.

Philip, J.R., 1969. Theory of infiltration, *Adv. Hydrosci., 5: 215-296.*

Philip, J. R., 1992. Falling head ponded infiltration, *Water Resour. Res.*, 28:2147-2148.

Philip, J. R. 1993. Approximate analysis of falling-head lined borehole permeameter. *Water Resour. Res.*, 29:3763-3768.

Raats P.A.C., 1973 ,"Unstable Wetting Fronts in Uniform and Nonuniform Soils", *Soil Science Society of America Proceedings*, 37(5):681-685.

Rawls, J.W., D. L Brakensiek, N. Miller, 1983. Green-Ampt infiltration parameters from soils data. *J.f Hydraul. Eng.* 109: 62-70.

Reynolds W. D. and D.E. Elrick, 1990, Ponded infiltration from a single ring: I. Analysis of steady flow, *Soil Sci. Soc. Am. J*., 54:1233-1241.

Reynolds, W.D., 2008. Unsaturated hydraulic properties: Field tension infiltrometer. p. 1107–1127. In M.R. Carter and E.G. Gregorich (ed.) Soil sampling and methods of analysis. 2nd ed. CRC Press, Boca Raton, FL.

Reynolds W. D., 2011. Measuring soil hydraulic properties using a cased borehole permeameter: falling head analysis, *Vadose Zone J*., Vol. 10, P:999-1015.

Richards, L.A., 1931. "Capillary conduction of liquids through porous mediums". *Physics* **1** (5): 318–333.

Rousseeuw, P.J., 1990. Robust Estimation and Identifying Outliers, in *Handbook of Statistical Methods for Engineers and Scientists*, edited by H.M. Wadsworth, New York: McGraw-Hill, pgs. 16.1–16.24.

Schaap M.G., Genuchten M. Th., 2006 , "A Modified Mualem-van Genuchten Formulation for Improved Description of the Hydraulic Conductivity Near Saturation", *Vadose Zone Journal*, 5(1):27- 34.

Schaik N.L.M.B.V, Hendriks R.F.A., Dam J.C.V., 2010 , "Parameterization of Macropore Flow Using Dye-tracer Infiltration Pattern in the SWAP Model", *Vadose Zone Journal*, 9(1):95-106.

Toothaker, L. E., 1994. Multiple Comparison Procedures, *Quantitative Applications in the Social Sciences*. Newbury Park, California: Sage.

U.S. Geological Survey, 2014, National Water Information System data available on the World Wide Web (USGS Water Data for the Nation), accessed August 7, 2013, at URLhttp://waterdata.usgs.gov/nwis/inventory?agency_code=USGS&site_no=430356089183501.

van Genuchten, M.Th., 1980. A closed-form equation for predicting the hydraulic conductivity for unsaturated soils. *Soil Sci. Soc. Am. J.*. 44:892-898.

Vogel, T., M. Cislerova, and J. W. Hopmans, 1991. Porous Media With Linearly Variable Hydraulic Properties, *Water Resources Research.*, 27(10): 2735–2741.

Vogel T., Van Genuchten M. Th., Cislerova M, 2001,"Effect of the Shape of the soil Hydraulic Functions Near Saturation on Variably Saturated Flow Prediction", *Advances in Water Resources*, 24(2): 133-144.

Weiss, P.T., A.J. Erickson and J.S. Gulliver, 2007, Cost and pollutant removal of storm-water treatment practices, *Journal of Water Resources Planning and Management*, 133(3), 218-229.

Wigington, P.L., Jr., Randall, C.W. and Grizzard, T.J. (1986). Accumulation of selected trace metals in soils of urban runoff swale drains. *Water Resources Bulletin*, 22(1), 73–79.

Winogradoff, D. A., 2002. Bioretention Manual. Programs and Planning Division, Department of Environmental Resources, Prince George's County, Maryland.

Yonge, D.R., 2000. Contaminant detention in highway grass filter strips. Report No. WA-RD 474.1, *Washington State Department of Transportation*, Olympia, Washington, USA.

Yousef, Y.A., Hvitvedjacobsen, T., Wanielista, M.P., and H.H. Harper, 1987. Removal of contaminants in highway runoff flowing through swales, *Science of the Total Environment*, 59, 391-399.

7. Appendix A

The Philip-Dunne permeameter (Philip, 1993) consists of an open-ended solid wall tube placed into a vertical borehole of the soil. If the soil hydraulic conductivity is isotropic this situation can be represented as an axi-symmetric system. The pressure based form of the Richards' equation for this system is expressed as

$$C\frac{\partial h}{\partial t} = \frac{1}{r}\frac{\partial}{\partial r}\left(Kr\frac{\partial h}{\partial r}\right) + \frac{\partial}{\partial z}\left(K\frac{\partial h}{\partial z}\right) + \frac{\partial K}{\partial z} \qquad (1)$$

where, $C = \frac{d\theta}{dh} =$ specific moisture capacity, $\theta =$ volumetric water content, $K =$ unsaturated hydraulic conductivity, assumed to be isotropic, $h =$ water pressure head, $r, z =$ radial and vertical coordinates, and $t =$ time.

The COMSOL-MP software provides solutions to partial differential equations of the elliptic, parabolic or hyperbolic type commonly found in physics applications. The software is flexible and one is able to solve customized equations as well as the more standard type. COMSOL-MP solves Richards' equation directly through the Earth Science module. The equation is solved with finite element spatial discretization with basis function ranging from linear to quantic elements. The formulation leads to a set of differential-algebraic equations (DAEs), which COMSOL-MP solves using either a Backward Difference Formula (BDF) or the Generalized-alpha method. The BDF procedure provides up to fifth-order accuracy, while the Generalized-alpha procedure provide second order accuracy. The BDF procedure has the advantage that it can handle 'stiffer' equations than the generalized-alpha procedure.

The finite element discretization of equation (1) yields a set of ordinary differential equations represented by the matrix system,

$$[A]\left\{\frac{dh}{dt}\right\}+[B]\{h\}-\{f\}=0 \qquad (2)$$

Here the matrix $[A]$ is the capacitance (or mass) matrix and the matrix $[B]$ is the conductivity or stiffness matrix. The vector $\{f\}$ is the 'force' vector that contains the terms representing the boundary fluxes and these are the terms for specifying flux when that flux is known.

In the COMSOL-MP formulation the capacitance matrix is formulated using a consistent approach, leading to a distributed mass matrix, in contrast to a lumped mass matrix. It is well-known that the distributed mass matrix formulation leads to less smoothing of sharp fronts, however for certain timestep/grid-size combinations it can lead to a violation of the principle of the maximum (Celia et al., 1990), commonly manifested as overshoot or undershoot of a solution near high gradient regions.

In COMSOL-MP the Dirichlet boundary conditions, that is, the condition of specified pressure head is specified and on the same boundary the resulting boundary flux can be solved for simultaneously by representing the flux by a Lagrange multiplier term.

The time derivative terms in equation (2) are discretized in time using the BDF scheme. For a given node i the time derivative of the pressure head is given at (forward) time level n by

$$\left.\frac{dh_i}{dt}\right|_n \approx \frac{1}{\beta_o \Delta t}\sum_{j=0}^{k}\delta_j h_{n-j} \qquad (3)$$

where β_o, and δ_j are coefficients of the BDF method, and k is the order of the integration. With COMSOL-MP the value of k can take on any value between 1 and 5 inclusive, and this is automatically determined by the program to provide the required accuracy.

The spatial discretization leads to a system of DAEs represented by

$$F = F\left(x, r, t, h, \theta\right) \tag{4a}$$

$$0 = g\left(h, \theta\right) \tag{4b}$$

where the first equation is the spatially and temporally transformed Richards' equation, and the second equations represent the initial conditions, Dirichlet boundary conditions, and any other algebraic constraints set on the system. Due to the fact that equations (4) are implicit equations, besides the fact that they are nonlinear, the equations are solved with the Newton iterative procedure.

While it has been shown previously that mass conservative solutions of Richards' equation are best derived by using a mixed form of the differential equation (Celia et al., 1990), the DAE formulation of the pressure-based form described by equation (1) provides the constraints (Tocci et al., 1997) that facilitate mass conservative solutions even though the pressure-based form of Richards' equation is not itself the mass conservative form.

It is well-known that numerical solutions of Richards' equation for soils with values of van Genuchten n in the range $(1 < n < 2)$ can have difficulty in numerical convergence because of the behavior of the steepness of the unsaturated hydraulic conductivity function for this range of n. To address this problem we implemented the method of Vogel et al. (2001) into the COMSOL solution. This method has been shown to be very effective at

overcoming the associated numerical difficulties by modifying the van Genuchten moisture retention and hydraulic conductivity relation such that the relations are smoothed. Note that the unsaturated hydraulic conductivity relation is changed by the procedure and this was taken into account when determining the wetting front suction with equation (7) of Chapter 2.

SOLUTION STEPS WITH COMSOL-MP

The problem is set up within the COMSOL-MP GUI by first selecting Richards' equation as the governing equation, and then drawing the problem domain to be analyzed. Properties such as saturated hydraulic conductivity, moisture retention curve, and fluid density are assigned. The finite element grid is then constructed by specifying a gradation of element sizes starting with the smallest elements near the infiltration boundary, and gradually increasing element size with distance from that boundary.

The system of DAEs resulting from the spatial discretization and initial and boundary conditions can be solved with either the BFD procedure or the generalized-alpha procedure. We selected to use the BFD with a variable integration order, up to order five. The solver code automatically determines the time step to control the truncation error in the time solution. The resulting algebraic equations are solved using a Newton iterative procedure to resolve the nonlinearities in the system of equations, and the GMRES iterative matrix procedure to solve the system of matrix equations intermediate to the Newton iterations. The tolerance level for the GMRES solver and the Newton solver were set low enough to make the mass balances errors small (<0.1%).

The time-dependent boundary condition associated with the water depth in the infiltrometer tube, specified as was determined by mass balance on the volume of water stored in the tube as water leaves by infiltration through boundary AB. The mass balance was implemented through COMSOL-MP by specifying the following integration of the infiltration rate to give a cumulative infiltration amount,

$$I(t) = \int_0^t i(t)\,dt \qquad (5)$$

where $I(t)$ is the cumulative infiltration and $i(t)$ is the infiltration rate through boundary AB.

To calculate the depth of water remaining in the infiltration tube at any instant of time, that is,

$$H(t) = H_i - \frac{I(t)}{\pi r_1^2} \qquad (6)$$

where r_1 is the radius of the infiltration tube, $H(t)$ is the depth of water at t and H_i is the initial depth of water in the tube.

8. Appendix B

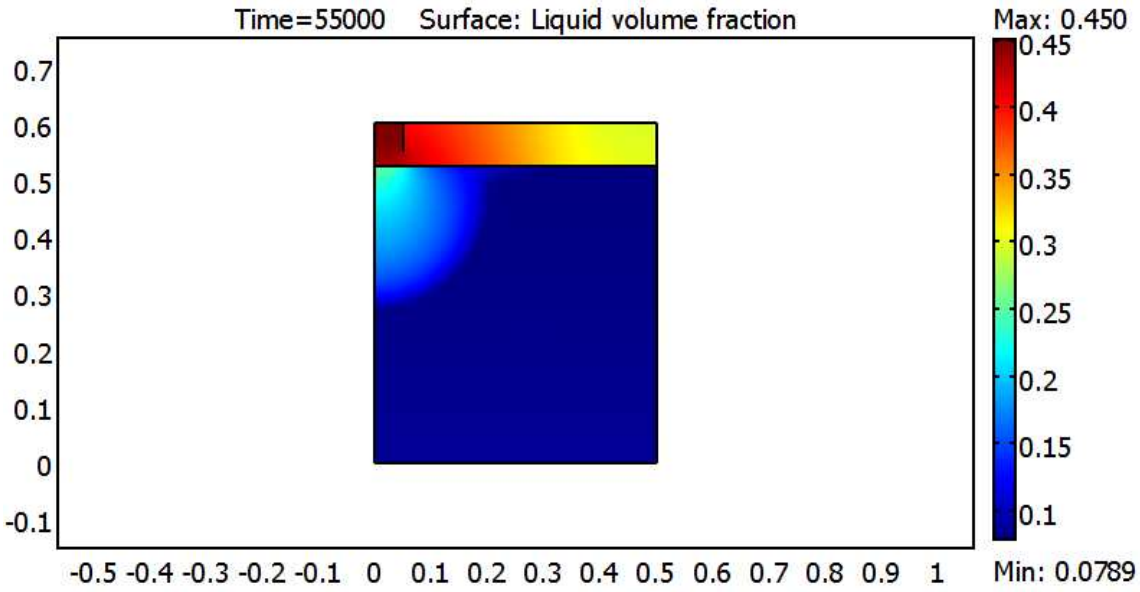

(a)

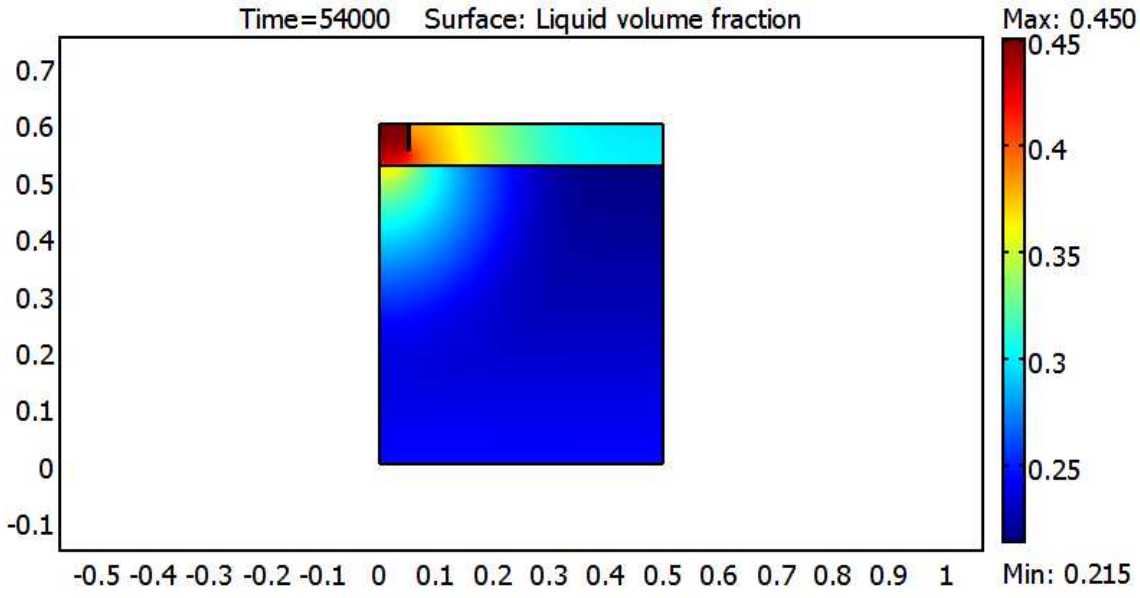
Time=54000 Surface: Liquid volume fraction
Max: 0.450
0.45
0.4
0.35
0.3
0.25
Min: 0.215
0.7
0.6
0.5
0.4
0.3
0.2
0.1
0
-0.1
-0.5 -0.4 -0.3 -0.2 -0.1 0 0.1 0.2 0.3 0.4 0.5 0.6 0.7 0.8 0.9 1

(b)

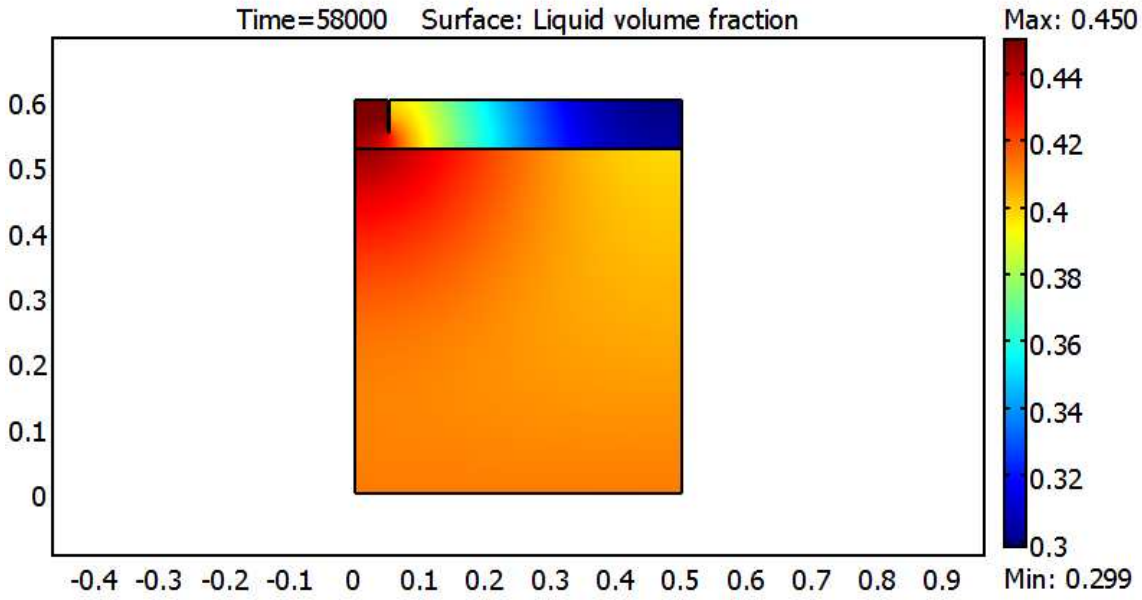
Time=58000 Surface: Liquid volume fraction
Max: 0.450
0.44
0.42
0.4
0.38
0.36
0.34
0.32
0.3
Min: 0.299
0.6
0.5
0.4
0.3
0.2
0.1
0
-0.4 -0.3 -0.2 -0.1 0 0.1 0.2 0.3 0.4 0.5 0.6 0.7 0.8 0.9

(c)

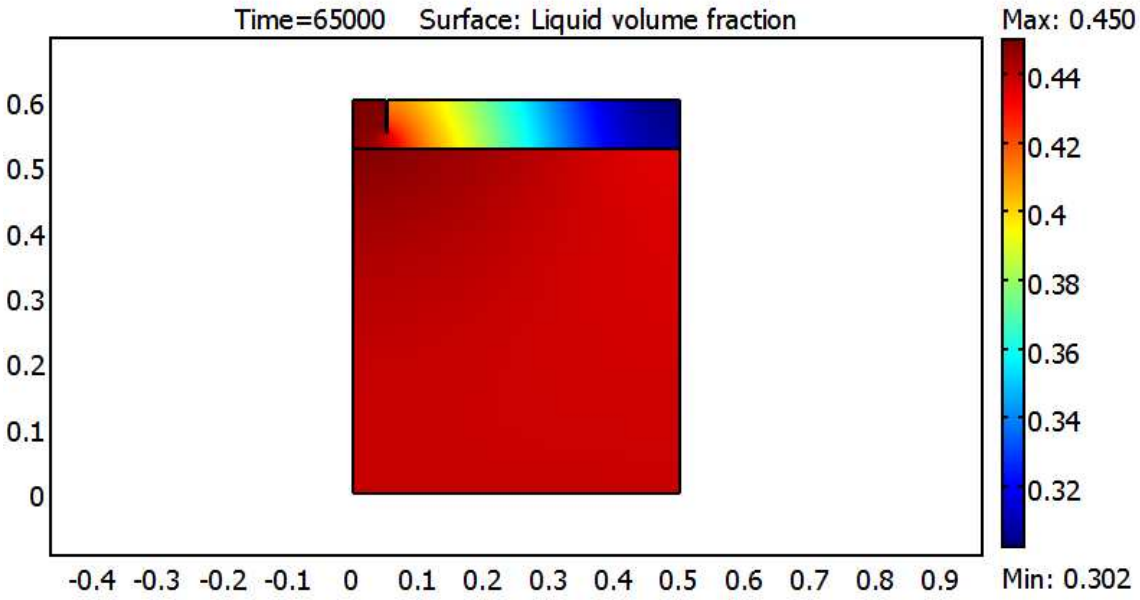
Time=65000 Surface: Liquid volume fraction
Max: 0.450
0.44
0.42
0.4
0.38
0.36
0.34
0.32
Min: 0.302
0.6
0.5
0.4
0.3
0.2
0.1
0
-0.4 -0.3 -0.2 -0.1 0 0.1 0.2 0.3 0.4 0.5 0.6 0.7 0.8 0.9

(d)

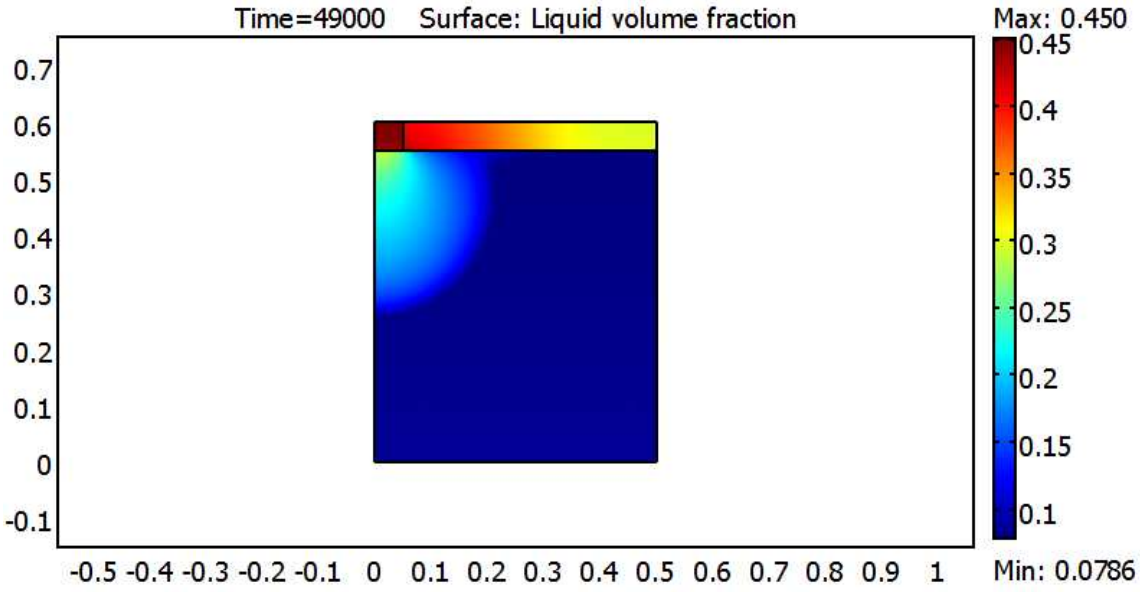
Time=49000 Surface: Liquid volume fraction
Max: 0.450
0.45
0.4
0.35
0.3
0.25
0.2
0.15
0.1
Min: 0.0786
0.7
0.6
0.5
0.4
0.3
0.2
0.1
0
-0.1
-0.5 -0.4 -0.3 -0.2 -0.1 0 0.1 0.2 0.3 0.4 0.5 0.6 0.7 0.8 0.9 1

(e)

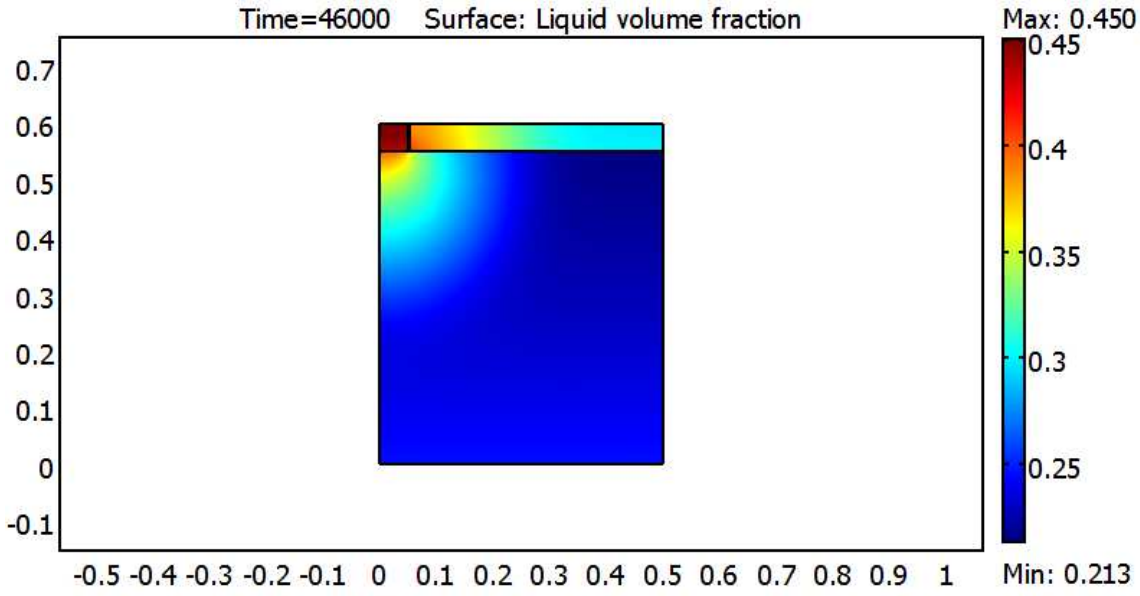
Time=46000 Surface: Liquid volume fraction
Max: 0.450
0.45
0.4
0.35
0.3
0.25
Min: 0.213
0.7
0.6
0.5
0.4
0.3
0.2
0.1
0
-0.1
-0.5 -0.4 -0.3 -0.2 -0.1 0 0.1 0.2 0.3 0.4 0.5 0.6 0.7 0.8 0.9 1

(f)

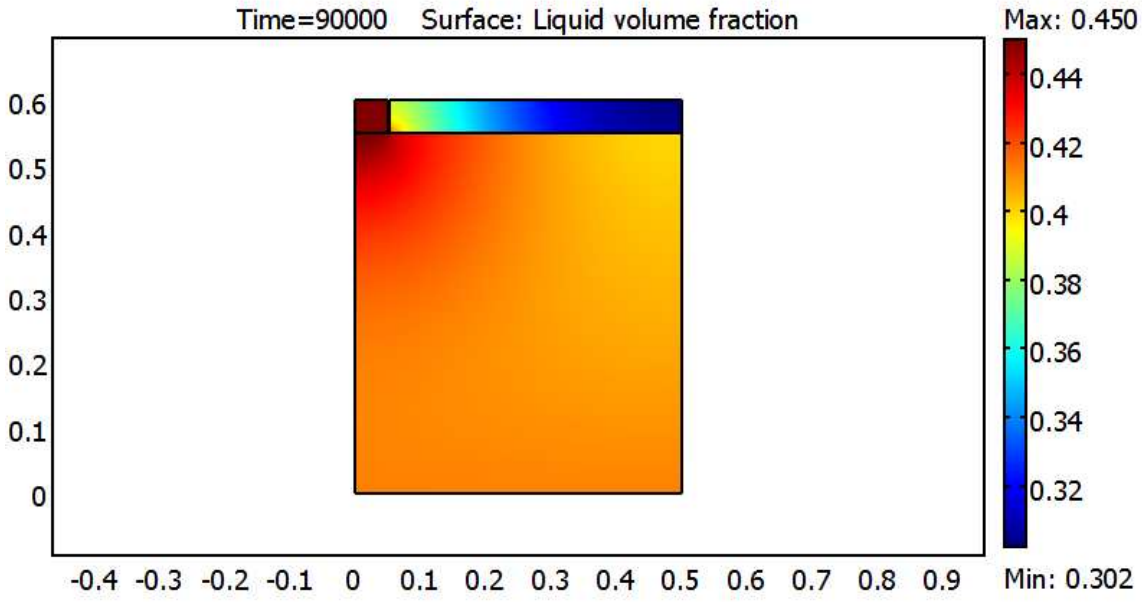
Time=90000 Surface: Liquid volume fraction
Max: 0.450
0.44
0.42
0.4
0.38
0.36
0.34
0.32
Min: 0.302
0.6
0.5
0.4
0.3
0.2
0.1
0
-0.4 -0.3 -0.2 -0.1 0 0.1 0.2 0.3 0.4 0.5 0.6 0.7 0.8 0.9

(g)

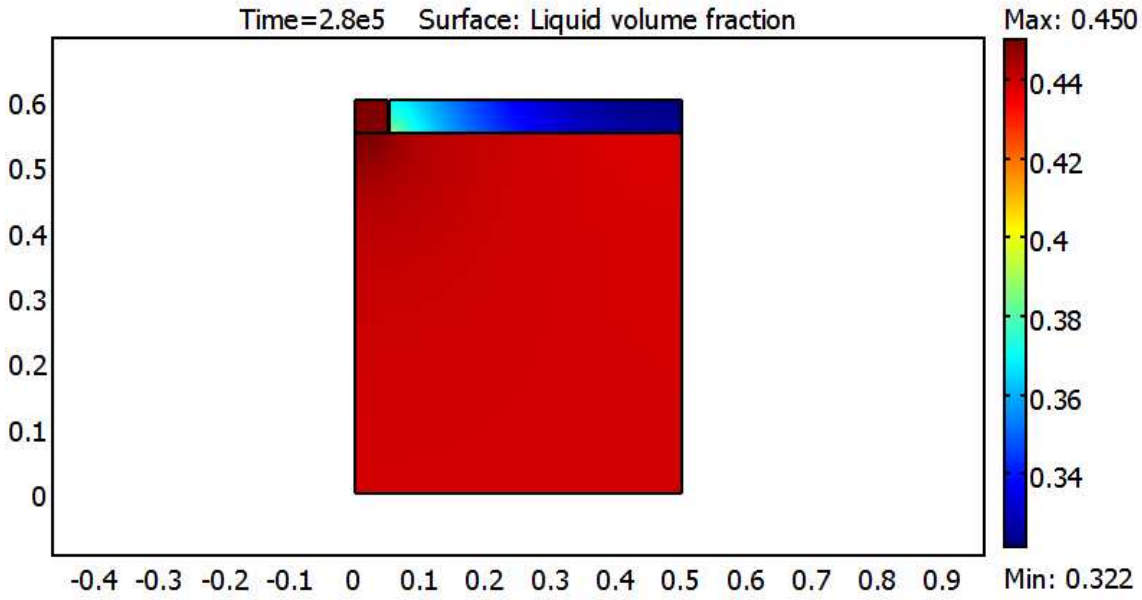
Time=2.8e5 Surface: Liquid volume fraction
Max: 0.450
0.44
0.42
0.4
0.38
0.36
0.34
Min: 0.322
0.6
0.5
0.4
0.3
0.2
0.1
0
-0.4 -0.3 -0.2 -0.1 0 0.1 0.2 0.3 0.4 0.5 0.6 0.7 0.8 0.9

(h)

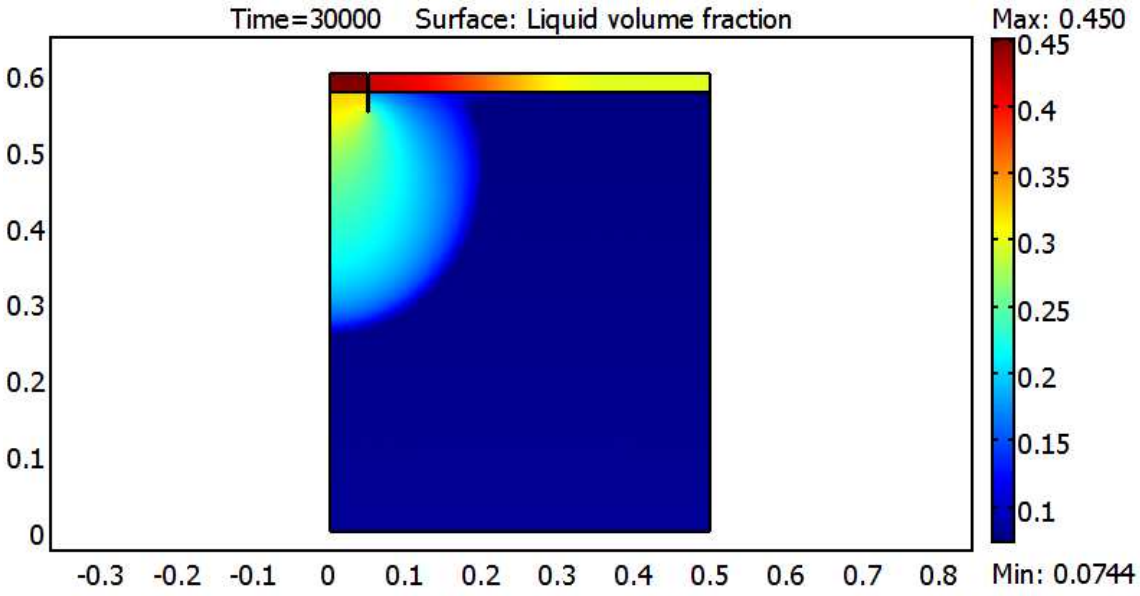
Time=30000 Surface: Liquid volume fraction
Max: 0.450
0.45
0.4
0.35
0.3
0.25
0.2
0.15
0.1
Min: 0.0744
0.6
0.5
0.4
0.3
0.2
0.1
0
-0.3 -0.2 -0.1 0 0.1 0.2 0.3 0.4 0.5 0.6 0.7 0.8

(i)

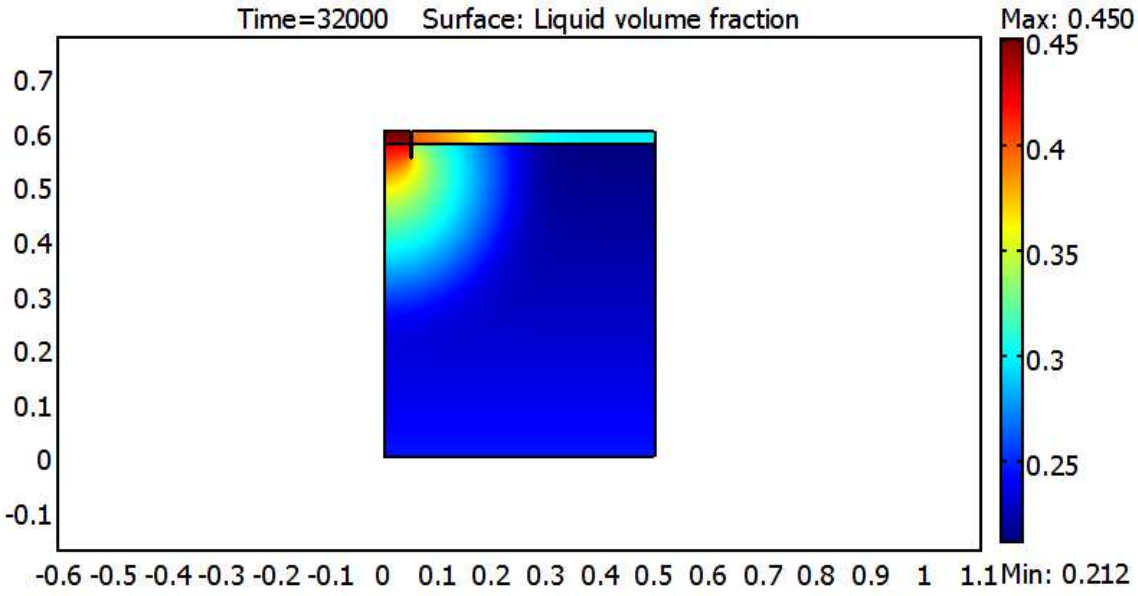
Time=32000 Surface: Liquid volume fraction
Max: 0.450
0.45
0.4
0.35
0.3
0.25
Min: 0.212
0.7
0.6
0.5
0.4
0.3
0.2
0.1
0
-0.1
-0.6 -0.5 -0.4 -0.3 -0.2 -0.1 0 0.1 0.2 0.3 0.4 0.5 0.6 0.7 0.8 0.9 1 1.1

(j)

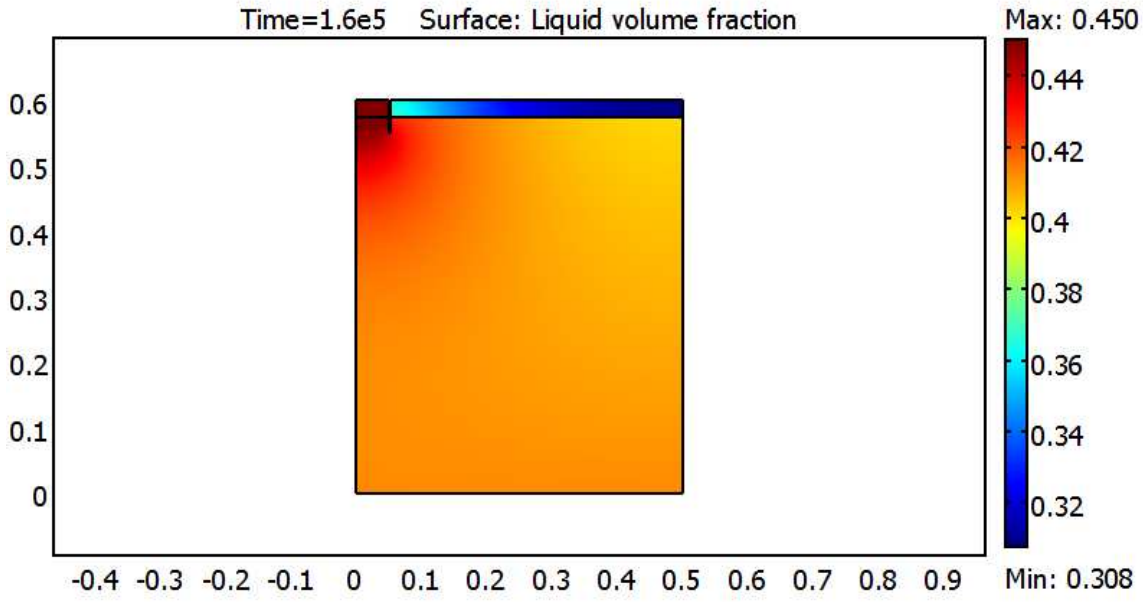
Time=1.6e5 Surface: Liquid volume fraction
Max: 0.450
0.44
0.42
0.4
0.38
0.36
0.34
0.32
Min: 0.308
0.6
0.5
0.4
0.3
0.2
0.1
0
-0.4 -0.3 -0.2 -0.1 0 0.1 0.2 0.3 0.4 0.5 0.6 0.7 0.8 0.9

(k)

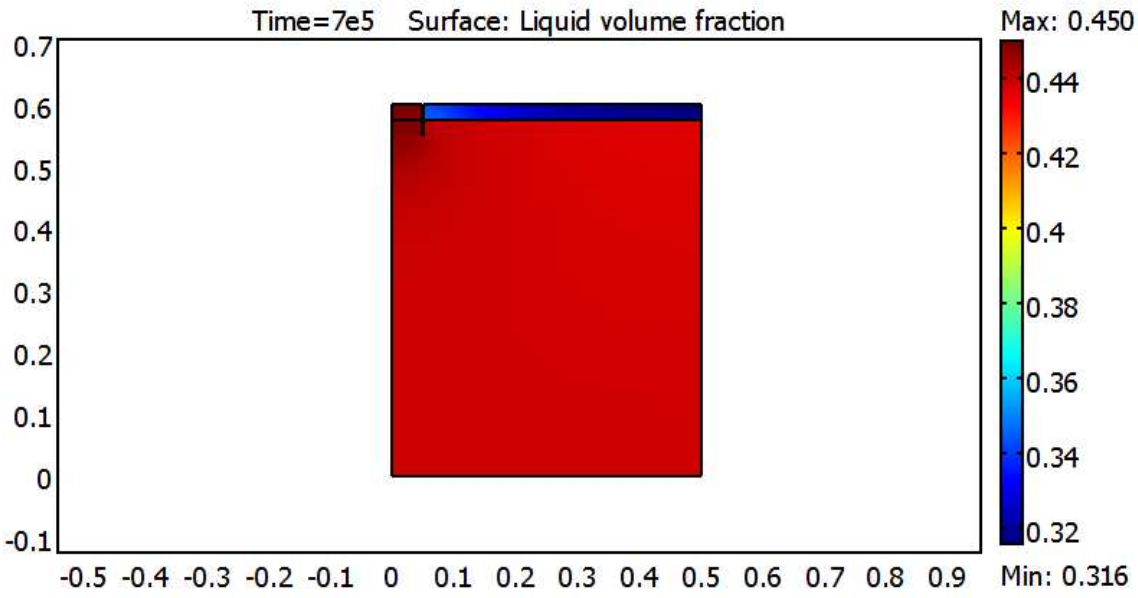

(l)

Figure 8-1. Simulated axi-symmetric distribution of the volumetric moisture content at the conclusion of the run for layered soil. The MPD infiltrometer is inserted to 5 cm depth in the top left corner. Moisture content scale is to the right of each figure and the time (sec) of complete drainage of MPD Infiltrometer, within one time step being empty, is mentioned on top of each plot. The top layer is 7.5cm thick silty loam and bottom layer is (a) loamy sand, (b) sandy clay loam, (c) sandy clay and (d) silty clay, the top layer is 5cm thick silty loam and bottom layer is (e) loamy sand, (f) sandy clay loam, (g) sandy clay and (h) silty clay, the top layer is 2.5cm thick silty loam and bottom layer is (i) loamy sand, (j) sandy clay loam, (k) sandy clay and (l) silty clay.

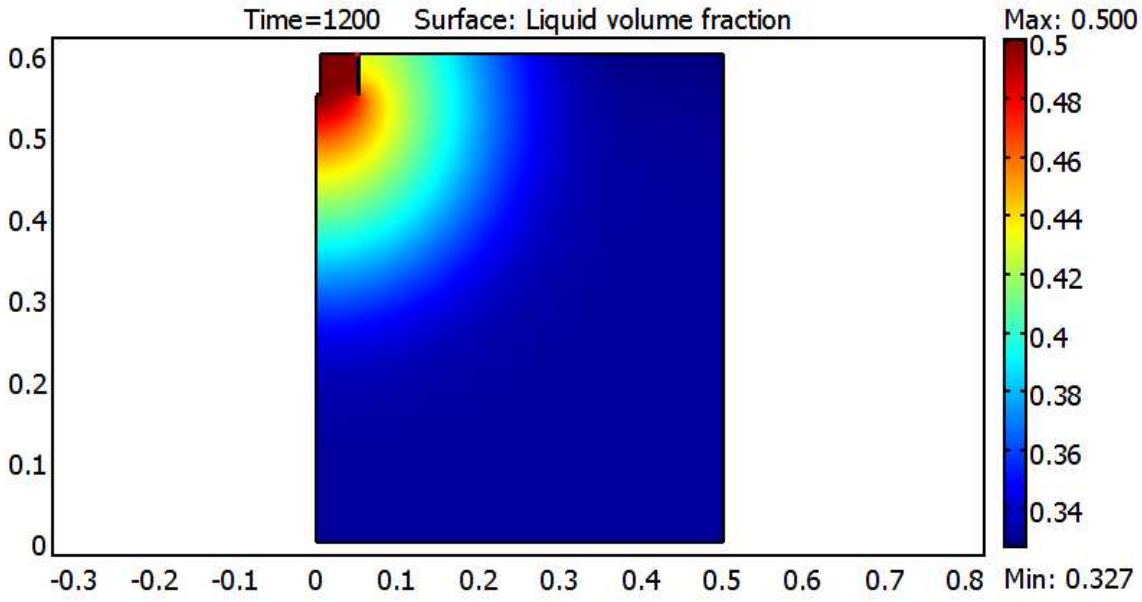
Time=1200 Surface: Liquid volume fraction
Max: 0.500
0.5
0.48
0.46
0.44
0.42
0.4
0.38
0.36
0.34
Min: 0.327
0.6
0.5
0.4
0.3
0.2
0.1
0
-0.3
-0.2
-0.1
0
0.1
0.2
0.3
0.4
0.5
0.6
0.7
0.8

(a)

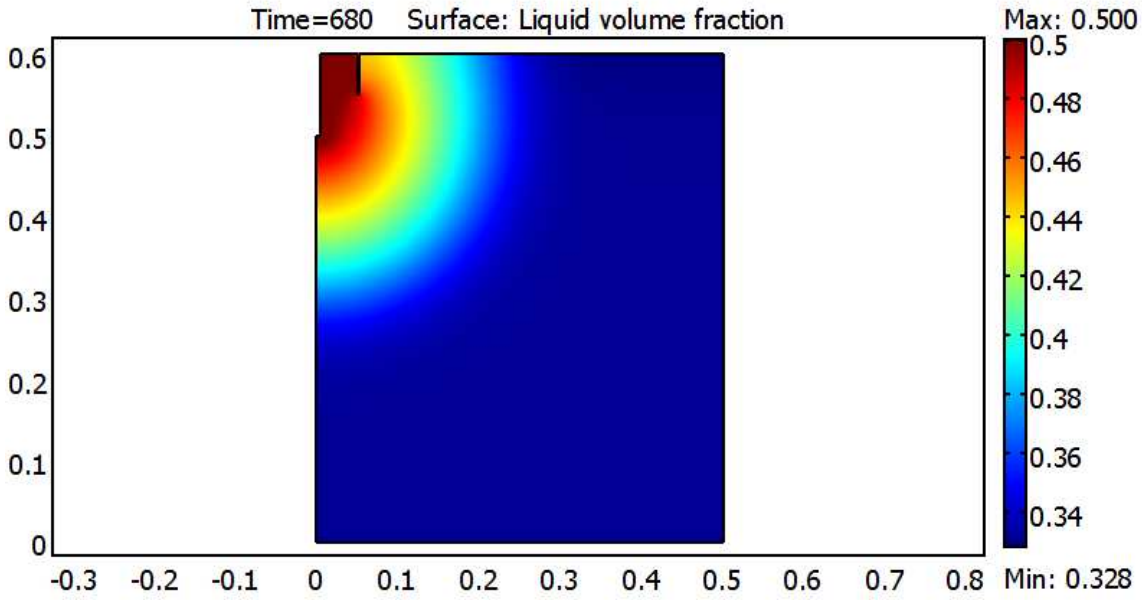
Time=680 Surface: Liquid volume fraction
Max: 0.500
0.5
0.48
0.46
0.44
0.42
0.4
0.38
0.36
0.34
Min: 0.328
0.6
0.5
0.4
0.3
0.2
0.1
0
-0.3 -0.2 -0.1 0 0.1 0.2 0.3 0.4 0.5 0.6 0.7 0.8

(b)

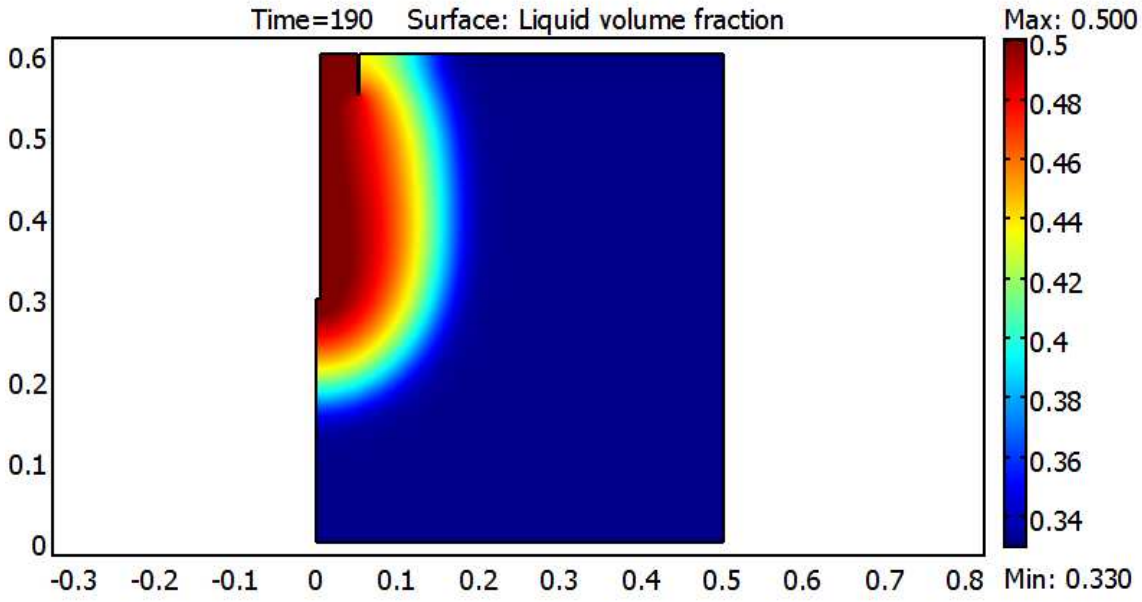
Time=190 Surface: Liquid volume fraction
Max: 0.500
0.5
0.48
0.46
0.44
0.42
0.4
0.38
0.36
0.34
Min: 0.330
0.6
0.5
0.4
0.3
0.2
0.1
0
-0.3
-0.2
-0.1
0
0.1
0.2
0.3
0.4
0.5
0.6
0.7
0.8

(c)

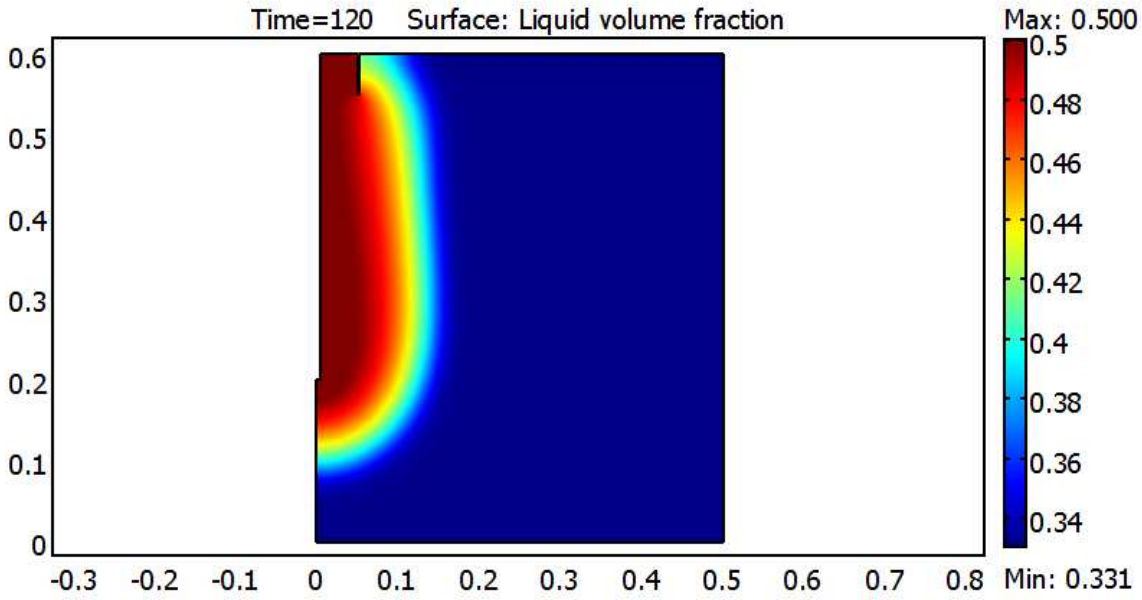
Time=120 Surface: Liquid volume fraction
Max: 0.500
0.5
0.48
0.46
0.44
0.42
0.4
0.38
0.36
0.34
Min: 0.331
0.6
0.5
0.4
0.3
0.2
0.1
0
-0.3
-0.2
-0.1
0
0.1
0.2
0.3
0.4
0.5
0.6
0.7
0.8

(d)

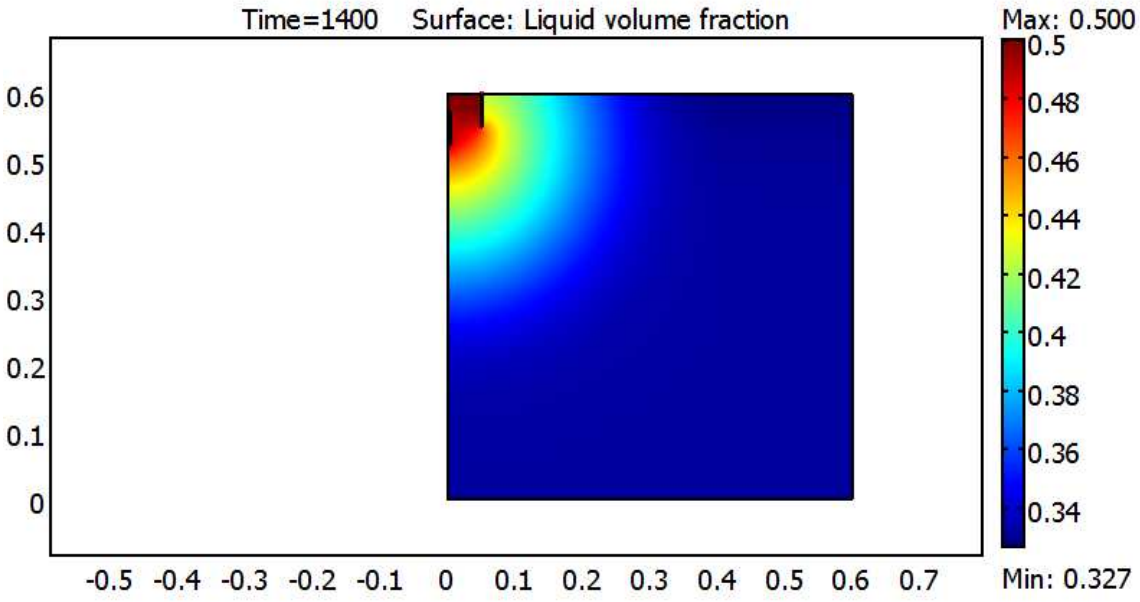
Time=1400 Surface: Liquid volume fraction
Max: 0.500
0.5
0.48
0.46
0.44
0.42
0.4
0.38
0.36
0.34
Min: 0.327
0.6
0.5
0.4
0.3
0.2
0.1
0
-0.5 -0.4 -0.3 -0.2 -0.1 0 0.1 0.2 0.3 0.4 0.5 0.6 0.7

(e)

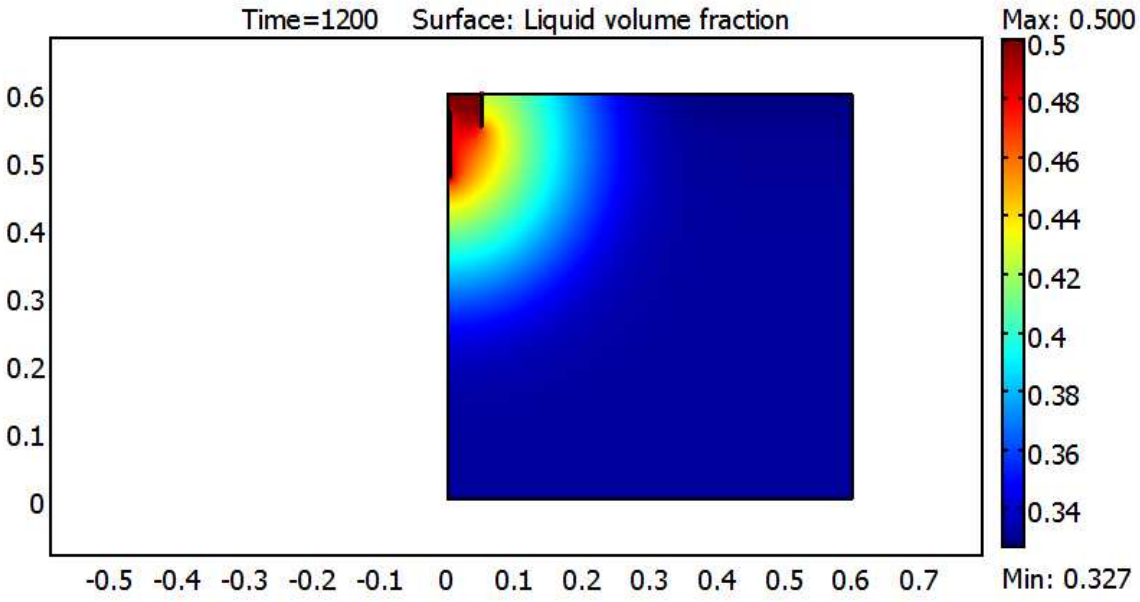
Time=1200 Surface: Liquid volume fraction
Max: 0.500
0.5
0.48
0.46
0.44
0.42
0.4
0.38
0.36
0.34
Min: 0.327
0.6
0.5
0.4
0.3
0.2
0.1
0
-0.5 -0.4 -0.3 -0.2 -0.1 0 0.1 0.2 0.3 0.4 0.5 0.6 0.7

(f)

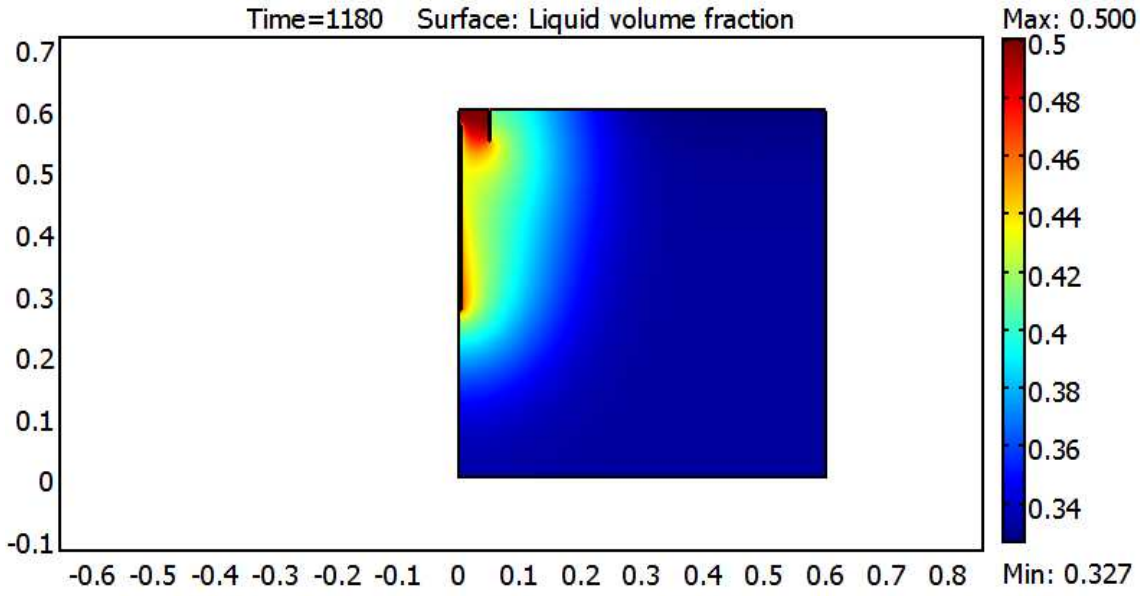
Time=1180 Surface: Liquid volume fraction
Max: 0.500
0.5
0.48
0.46
0.44
0.42
0.4
0.38
0.36
0.34
Min: 0.327
0.7
0.6
0.5
0.4
0.3
0.2
0.1
0
-0.1
-0.6 -0.5 -0.4 -0.3 -0.2 -0.1 0 0.1 0.2 0.3 0.4 0.5 0.6 0.7 0.8

(g)

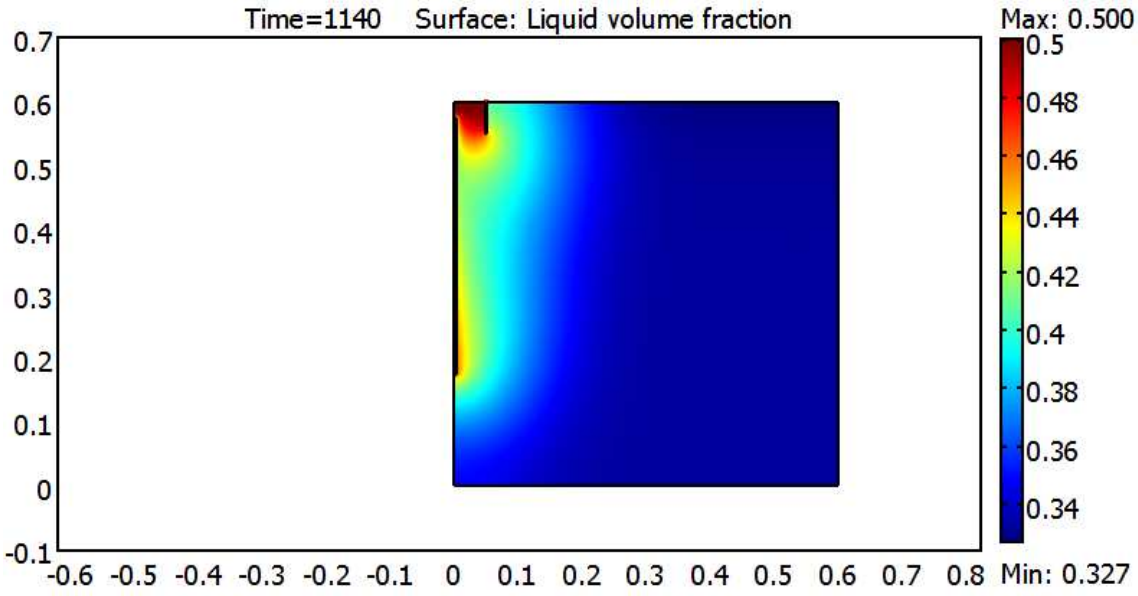

(h)

Figure 8-2. Simulated axi-symmetric distribution of the volumetric moisture content at the conclusion of the run for uniform soil containing a 10 mm diameter macropore at the time of infiltrometer drainage (sec) to within one time step. The MPD infiltrometer is inserted to 5 cm depth in the top left corner. Soil containing a macropore connected to surface is given in plots (a) 5cm long macropore, (b) 10cm long macropore, (c) 30cm long macropore, (d) 40cm long macropore, and soil containing macropore 2.5cm below surface is given in plot (e) 5cm long macropore, (f) 10cm long macropore, (g) 30cm long macropore, (h) 40cm long macropore. K_{fs}= 5x10^{-5}m/s in the uniform soil and 0.5 m/s in the macropore.